

THE EVOLUTION AND EXPLOSION OF MASSIVE STARS. II. EXPLOSIVE HYDRODYNAMICS AND NUCLEOSYNTHESIS

S. E. WOOSLEY^{1,2} AND THOMAS A. WEAVER²

Received 1995 January 24; accepted 1995 April 21

ABSTRACT

The nucleosynthetic yield of isotopes lighter than $A = 66$ (zinc) is determined for a grid of stellar masses and metallicities including stars of 11, 12, 13, 15, 18, 19, 20, 22, 25, 30, 35, and $40 M_{\odot}$ and metallicities $Z = 0, 10^{-4}, 0.01, 0.1,$ and 1 times solar (a slightly reduced mass grid is employed for nonsolar metallicities). Altogether 78 different model supernova explosions are calculated. In each case nucleosynthesis has already been determined for 200 isotopes in each of 600 to 1200 zones of the presupernova star, including the effects of time dependent convection. Here each star is exploded using a piston to give a specified final kinetic energy at infinity (typically 1.2×10^{51} ergs), and the explosive modifications to the nucleosynthesis, including the effects of neutrino irradiation, determined. A single value of the critical $^{12}\text{C}(\alpha, \gamma)^{16}\text{O}$ reaction rate corresponding to $S(300 \text{ keV}) = 170$ keV barns is used in all calculations. The synthesis of each isotope is discussed along with its sensitivity to model parameters. In each case, the final mass of the collapsed remnant is also determined and often found not to correspond to the location of the piston (typically the edge of the iron core), but to a “mass cut” farther out. This mass cut is sensitive not only to the explosion energy, but also to the presupernova structure, stellar mass, and the metallicity. Unless the explosion mechanism, for unknown reasons, provides a much larger characteristic energy in more massive stars, it appears likely that stars larger than about $30 M_{\odot}$ will experience considerable reimplosion of heavy elements following the initial launch of a successful shock. While such explosions will produce a viable, bright Type II supernova light curve, lacking perhaps the radioactive tail, they will have dramatically reduced yields of heavy elements and may leave black hole remnants of up to 10 and more solar masses. The production of black holes may be particularly favored for stars of low metallicity, both because of their more compact structure and reduced mass loss.

Subject headings: hydrodynamics — nuclear reactions, nucleosynthesis, abundances — stars: evolution — stars: interiors — stars: supernovae: general

1. INTRODUCTION

In Paper I (Weaver & Woosley 1995), we presented the evolution of stars of various metallicities and masses in the range $11\text{--}40 M_{\odot}$ to the point where their iron cores were collapsing and a supernova explosion was imminent. In this paper, we simulate explosions in a subset of these and examine the propagation of the resulting shock wave. We also study the mass reimplosion that occurs in some stars, especially the more massive ones. Our chief result is a grid of isotopic yields as a function of metallicity and mass for stars in the range $11\text{--}40 M_{\odot}$. (§ 5). This should be the most relevant mass range for producing the intermediate mass elements. Stars between 8 and $11 M_{\odot}$ have very thin shells of heavy elements when they die and contribute little to these elements (though there may be exceptions, e.g., ^{14}N , the s -process, and the r -process). Stars heavier than $40 M_{\odot}$ are rare. As we shall see they may collapse to black holes and their evolution is likely to depend on mass loss which has not been included here. See Woosley, Langer, & Weaver (1993, 1995) for a treatment of massive stars that lose appreciable mass.

¹University of California Observatories/Lick Observatory, Board of Studies in Astronomy and Astrophysics, University of California, Santa Cruz, CA 95064.

²General Studies Division, University of California, Lawrence Livermore National Laboratory, Livermore, CA 94550.

At the outset, we must acknowledge that it is impossible to predict with accuracy the abundances of certain isotopes whose production is sensitive to the still controversial explosion mechanism. However, we shall enumerate these isotopes and show that their number is small. Our results are also only so reliable as the nuclear physics and stellar physics that are employed, especially the model for convection. The nuclear data set used here is briefly summarized in § 2.2 (see also Hoffman 1994). The convective theory and its effects are reviewed in Paper I (see also Woosley & Weaver 1988).

Section 2 describes how the explosion of the stars is simulated, the critical choices being the location of the piston, its time history, and, of course, the obvious and necessary choice of doing our calculations in one spatial dimension. Having produced a shock, § 3 describes its propagation. Regions of increasing ρr^3 lead to the slowing of the shock. Early on, material in the deep interior communicates with the shock by sound waves. Later, communication is by a “reverse shock.” Depending upon the initial energy of the shock and the density structure of the star, amounts of material ranging from a few thousandths to many solar masses fall back onto the collapsed remnant. Even in those cases where large amounts of mass fall back, the shock emerges successfully from the stellar surface and gives rise to a typical Type IIp light curve. The fallback has important implications, however, both for nucleosynthesis and for the nature of the collapsed remnant, be it a black hole or neutron star.

Sections 4 and 5 give the major results of this paper. Yields are presented for all the stable isotopes (and their radioactive progenitors) lighter than germanium ($Z = 32$) ejected from stars having metallicities 0, 10^{-4} , 10^{-2} , 0.1, and 1 times the solar value. The site where each isotope originates is discussed using 15 and $25 M_{\odot}$ solar metallicity stars as examples. The metallicity dependence of the nucleosynthesis is also briefly described, though a more detailed comparison of the results of this paper both to solar abundances and to stellar observations pertinent to Galactic chemical evolution is given in Paper III (Timmes, Woosley, & Weaver 1995a).

2. THE CALCULATIONS

2.1. Overview

During the presupernova evolution described in detail in Paper I, a nuclear reaction network of 200 isotopes (Table 1) was carried in every stellar zone of each star throughout its evolution. While energy generation and stellar structure were determined using a set of smaller networks that were called several times during each iteration of a converged model, the large network of abundances was updated only once at the end of each time step (although this often required several matrix inversions in a zone experiencing considerable nuclear activity—i.e., subcycling). In zones where the changes in temperature and density were smaller than some prescribed value, the 200 isotopes were updated infrequently in order to save computer time. Still, during the course of one star's evolution the 200 by 200 matrix generated by this network was typically inverted 5 to 10 million times, accounting for a substantial fraction of the total cpu requirements of the calculation. For those zones experiencing convection or semiconvection, the 200 isotopes were mixed with the appropriate diffusion coefficient following each time step. This coupling of convection to the nuclear network was carried out in an explicit rather than implicit fashion, but using sufficiently small time steps to assure the stability and accuracy of the procedure.

At the end of the star's life, a shock wave propagates through all the material outside of the iron core, briefly raising its temperature to a high value. This explosive nucleosynthesis, along with the nucleosynthesis caused by the flood of neutrinos passing through the mantle and helium core (Woosley et al. 1990) is followed with the same network in each zone, though convective mixing was turned off. The explosion hydrodynamics was followed using the Kepler code (Weaver, Zimmerman, & Woosley 1978). Final abundances of all stable species, as well

as those having significant lifetimes, were extracted when the temperature fell to such low values that all (strong and electromagnetic) nuclear reactions had ceased. In each case, 78 models in all, a light curve was calculated for the supernova out to an age of 3×10^7 s. These will be discussed elsewhere.

In all the tables that follow it should be noted that the stars actually evolved and exploded had a mass that was given by an integer multiple of 2.00×10^{33} g, i.e., not exactly one solar mass (1.9891×10^{33} gm). Thus, what we call a $25 M_{\odot}$ star, for example, is actually a star of $25.14 M_{\odot}$. This notation has been used ever since Weaver et al. (1978) and we retain it here for consistency with our previous work. Yields will be quoted in solar masses.

For calibration, we also considered the evolution of two of our models, S15A and S25A, from start to finish using a much more extended network of 476 isotopes. Following precisely the same stellar model gave the same nucleosynthesis for isotopes lighter than (and including) ^{66}Zn to an accuracy of better than 7%, except in the one case of ^{19}F where inclusion of ^{19}Ne in the network led to an enhanced production of 10%. In most cases, and for all the most abundant elements, the difference was less than 1%.

2.2. Initial Composition and Nuclear Physics

The procedure for generating the initial composition of each star is discussed in Paper III. Briefly, zero metallicity stars were given a big bang composition and evolved to supernovae. Solar metallicity stars used initial abundances given by Anders & Grevesse (1989; Table 2) and were also evolved to supernovae. A Galactic chemical evolution model was then used to generate abundances appropriate to the intermediate metallicities studied -10^{-4} , 0.01, and 0.1 Z_{\odot} .

The cross section for the critically important $^{12}\text{C}(\alpha, \gamma)^{16}\text{O}$ reaction rate was the value given at each temperature by Caughlan & Fowler (1988) multiplied by a constant, 1.7. This is equivalent to $S(300 \text{ keV}) = 170 \text{ keV barns}$, a value that has been determined to be optimal for producing the solar abundance set (Weaver & Woosley 1993). This same value is also supported by recent measurements, $S(300 \text{ keV}) = 79 \pm 21$ or $82 \pm 26 \text{ keV barn}$ (R - and K -matrix fits, respectively) for the E1 part of this rate (Azuma et al. 1994), and the experimental and theoretical expectation that E2 be approximately $70 \pm 50 \text{ keV barn}$ (Barnes 1995; Okabe 1994; Mohr et al. 1995). Other resonances also contribute to the S -factor at 300 keV at the level of approximately 19 keV barn, so that the best current

TABLE 1
NUCLEAR REACTION NETWORK EMPLOYED

Element	A_{min}	A_{max}	Element	A_{min}	A_{max}	Element	A_{min}	A_{max}
H	1	3	Mg	23	27	V	45	52
He	3	4	Al	25	28	Cr	48	55
Li	6	8	Si	27	32	Mn	51	57
Be	7	9	P	29	34	Fe	52	61
B	8	11	S	31	37	Co	55	62
C	11	14	Cl	33	38	Ni	56	65
N	13	15	Ar	36	41	Cu	57	66
O	15	18	K	37	42	Zn	60	69
F	17	19	Ca	40	49	Ga	61	70
Ne	19	23	Sc	41	50	Ge	64	71
Na	22	24	Ti	44	51			

TABLE 2
SOLAR MASS FRACTIONS (ANDERS & GREVESSE 1989)

Isotope	Mass Fraction	Isotope	Mass Fraction	Isotope	Mass Fraction
¹ H	7.06(-1)	³⁰ Si	2.35(-5)	⁵¹ V	3.77(-7)
² H	4.80(-5)	³¹ P	8.16(-6)	⁵⁰ Cr	7.42(-7)
³ He	2.93(-5)	³² S	3.96(-4)	⁵² Cr	1.49(-5)
⁴ He	2.75(-1)	³³ S	3.22(-6)	⁵³ Cr	1.72(-6)
⁶ Li	6.50(-10)	³⁴ S	1.87(-5)	⁵⁴ Cr	4.36(-7)
⁷ Li	9.35(-9)	³⁶ S	9.38(-8)	⁵⁵ Mn	1.33(-5)
⁹ Be	1.66(-10)	³⁵ Cl	2.53(-6)	⁵⁴ Fe	7.13(-5)
¹⁰ B	1.07(-9)	³⁷ Cl	8.55(-7)	⁵⁶ Fe	1.17(-3)
¹¹ B	4.73(-9)	³⁶ Ar	7.74(-5)	⁵⁷ Fe	2.86(-5)
¹² C	3.03(-3)	³⁸ Ar	1.54(-5)	⁵⁸ Fe	3.70(-6)
¹³ C	3.65(-5)	⁴⁰ Ar	2.53(-8)	⁵⁹ Co	3.36(-6)
¹⁴ N	1.11(-3)	³⁹ K	3.47(-6)	⁵⁸ Ni	4.94(-5)
¹⁵ N	4.36(-6)	⁴⁰ K	5.54(-9)	⁶⁰ Ni	1.96(-5)
¹⁶ O	9.59(-3)	⁴¹ K	2.63(-7)	⁶¹ Ni	8.60(-7)
¹⁷ O	3.89(-6)	⁴⁰ Ca	5.99(-5)	⁶² Ni	2.78(-6)
¹⁸ O	2.17(-5)	⁴² Ca	4.20(-7)	⁶⁴ Ni	7.27(-7)
¹⁹ F	4.05(-7)	⁴³ Ca	8.97(-8)	⁶³ Cu	5.75(-7)
²⁰ Ne	1.62(-3)	⁴⁴ Ca	1.43(-6)	⁶⁵ Cu	2.65(-7)
²¹ Ne	4.13(-6)	⁴⁶ Ca	2.79(-9)	⁶⁴ Zn	9.92(-7)
²² Ne	1.30(-4)	⁴⁸ Ca	1.38(-7)	⁶⁶ Zn	5.88(-7)
²³ Na	3.34(-5)	⁴⁵ Sc	3.89(-8)	⁶⁷ Zn	8.76(-8)
²⁴ Mg	5.15(-4)	⁴⁶ Ti	2.23(-7)	⁶⁸ Zn	4.06(-7)
²⁵ Mg	6.77(-5)	⁴⁷ Ti	2.08(-7)	⁷⁰ Zn	1.38(-8)
²⁶ Mg	7.76(-5)	⁴⁸ Ti	2.15(-6)	⁶⁹ Ga	3.96(-8)
²⁷ Al	5.81(-5)	⁴⁹ Ti	1.64(-7)	⁷¹ Ga	2.71(-8)
²⁸ Si	6.53(-4)	⁵⁰ Ti	1.64(-7)	⁷⁰ Ge	4.32(-8)
²⁹ Si	3.43(-5)	⁵⁰ V	9.26(-10)		

combined experimental and theoretical estimate is 169 ± 55 keV barn (Barnes 1995). Thus, no further variation of $^{12}\text{C}(\alpha, \gamma)^{16}\text{O}$ was attempted in this study.

Rates for other strong interactions were taken chiefly from Caughlan et al. (1985), Caughlan & Fowler (1988), Woosley et al. (1978), Sargood (1982), and Bao & Käppeler (1986), though there have been numerous revisions to individual rates until 1992 when our rates for this study were frozen. A complete bibliography and tabulation of rates used in this study are available from Hoffman (1994). Cross sections for neutrino interactions (neutral current inelastic scattering and charged current) were computed by Wick Haxton and were the same values discussed in Woosley et al. (1990). Rates for electron capture, beta decay, and positron decay as a function of temperature and density were taken from Fuller, Fowler, & Newman (1980, 1982, 1985), though they were not of importance in these explosive studies. (They were of course very important in the presupernova nucleosynthesis). Below 10^5 g cm⁻³ or 2×10^9 K, whichever occurs first, unstable nuclei were presumed to decay at their zero temperature laboratory rates (Hoffman 1994).

The neutrino irradiation was parameterized as in Woosley et al. (1990) with an e -folding time scale for neutrino emission of 3 s and a total energy in neutrinos of 3×10^{53} ergs. This emission was assumed to commence at the time the presupernova model collapsed ($v_{\text{in}} = 1000$ km s⁻¹) and persisted, at an exponentially declining rate for 100 s. This included a typical period of 0.45 s during which the piston was moved *inward*, (§ 2.3) as well as the subsequent explosion. The effects of neutrino irradiation were followed in zones ahead of the shock as well as behind. That is, “forced updates” were carried out in zones well ahead of the shock where the local temperature and density were not changing, but where the composition evolved

due to neutrino interaction. The neutrinos were assumed to have a thermal spectrum with a temperature of 4 MeV for the electron neutrinos and antineutrinos. These participated chiefly through charged current reactions (though they were allowed to contribute to inelastic neutral current processes as well), and were not very important. The μ and τ neutrinos and antineutrinos were given a temperature of 8 MeV except in one case where the effect of a lower value (6 MeV) was explored. These neutrinos had a major effect on the nucleosynthesis. Calculations of a 20 M_{\odot} supernova by Jim Wilson (as reported in Woosley et al. 1994; their Fig. 3) show the (energy-weighted) mean energy of the μ and τ neutrinos rises rapidly during the first second of the supernova from less than 20 MeV to between 30 and 35 MeV. Representing the actual spectrum of the supernova by a thermal one (as was done in Woosley et al. 1990) is very approximate, but thermally averaged rates are the only ones currently available. In any case, it does not seem that 8 MeV is a gross overestimate of the effective temperature at which most of the neutrinos are emitted.

2.3. Simulation of the Explosion

For each star a piston was located at the outer edge of the iron core (Table 3), more precisely at the large discontinuous change in Y_e which marks the outer extent of the last stage of convective silicon shell burning. Typically Y_e inside this boundary was 0.475, while outside it was 0.498. If nothing else, nucleosynthetic restrictions suggest that the mass cut in the explosion should not be substantially interior to this (Weaver et al. 1978). Usually this boundary also corresponded to the place where the composition switched from one of iron to silicon and sulfur. This was not always the case though. For example, in S15A the Y_e discontinuity was at 1.29 M_{\odot} while the

TABLE 3
EXPLOSION CHARACTERISTICS OF ALL MODELS

Mass /Model	Z (/Z _⊙)	Fe Core (M _⊙)	Piston (M _⊙)	M ₉ (M _⊙)	BE ₉ (10 ⁵⁰ erg)	α	v _o (10 ⁴ km/s)	Remnant (M _⊙)	KE _∞ (10 ⁵¹ erg)	M(⁵⁶ Ni) (M _⊙)
S11A	1	1.32	1.32	1.52	0.18	2.52	2.90	1.32	1.29	0.069
S12A	1	1.32	1.32	1.53	0.37	4.04	3.67	1.32	1.17	0.043
S13A	1	1.41	1.41	1.86	0.56	1.06	1.94	1.46	1.31	0.133
S15A	1	1.32	1.29	1.99	1.48	1.09	1.88	1.43	1.22	0.115
S18A	1	1.46	1.42	2.34	2.84	0.46	1.28	1.76	1.17	0.066
S19A	1	1.66	1.66	2.86	4.14	0.35	1.22	1.98	1.19	0.100
S20A	1	1.74	1.74	2.93	5.16	0.35	1.24	2.06	1.17	0.088
S22A	1	1.82	1.82	3.10	7.12	0.50	1.51	2.02	1.47	0.205
S25A	1	1.78	1.78	3.14	9.78	0.47	1.45	2.07	1.18	0.129
S30A	1	1.83	1.83	3.13	10.7	0.35	1.27	4.24	1.13	0
S30B	1	1.83	1.83	3.13	10.7	0.71	1.81	1.94	2.01	0.440
S35A	1	2.03	2.03	3.63	15.9	0.50	1.60	7.38	1.23	0
S35B	1	2.03	2.03	3.63	15.9	0.81	2.04	3.86	1.88	0
S35C	1	2.03	2.03	3.63	15.9	0.95	2.20	2.03	2.22	0.568
S40A	1	1.98	1.98	3.90	20.1	0.64	1.79	10.34	1.19	0
S40B	1	1.98	1.98	3.90	20.1	1.04	2.28	5.45	1.93	0
S40C	1	1.98	1.98	3.90	20.1	1.34	2.59	1.98	2.57	0.691
P12A	0.1	1.35	1.35	1.75	0.33	1.01	1.85	1.38	1.26	0.177
P13A	0.1	1.32	1.30	1.82	0.71	1.26	2.03	1.31	1.10	0.180
P15A	0.1	1.38	1.38	2.08	1.34	0.76	1.62	1.49	1.27	0.195
P18A	0.1	1.47	1.43	2.33	2.91	0.61	1.48	1.69	1.31	0.137
P20A	0.1	1.64	1.64	2.87	4.81	0.42	1.32	1.97	1.25	0.122
P22A	0.1	1.80	1.80	3.11	6.64	0.41	1.36	2.12	1.31	0.124
P25A	0.1	1.84	1.84	3.00	8.29	0.59	1.65	1.99	1.34	0.203
P30A	0.1	1.61	1.60	2.74	8.77	0.46	1.36	2.76	1.24	0
P30B	0.1	1.61	1.60	2.74	8.77	0.75	1.74	2.01	1.86	0.182
P35A	0.1	2.02	2.02	3.53	15.0	0.50	1.60	6.69	1.21	0
P35B	0.1	2.02	2.02	3.53	15.0	0.83	2.06	3.39	1.88	0
P35C	0.1	2.02	2.02	3.53	15.0	1.08	2.35	2.02	2.44	0.610
P40A	0.1	2.01	2.01	3.73	18.0	0.53	1.64	9.13	1.23	0
P40B	0.1	2.01	2.01	3.73	18.0	0.90	2.14	4.45	2.01	0
P40C	0.1	2.01	2.01	3.73	18.0	1.09	2.35	2.01	2.45	0.672
T12A	0.01	1.37	1.38	1.75	0.36	1.23	2.06	1.40	1.24	0.152
T13A	0.01	1.37	1.38	1.88	0.59	0.82	1.68	1.44	1.25	0.191
T15A	0.01	1.55	1.56	2.14	1.27	1.00	1.98	1.56	1.22	0.171
T18A	0.01	1.42	1.42	2.17	2.55	0.82	1.71	1.58	1.18	0.135
T20A	0.01	1.63	1.63	2.77	4.60	0.40	1.28	1.98	1.14	0.073
T22A	0.01	1.67	1.67	2.91	6.07	0.44	1.36	2.04	1.31	0.099
T25A	0.01	1.75	1.77	2.76	7.32	0.67	1.72	1.87	1.16	0.187
T30A	0.01	1.77	1.78	3.07	10.8	0.42	1.37	3.22	1.28	0
T30B	0.01	1.77	1.78	3.07	10.8	0.66	1.72	2.21	1.84	0.176
T35A	0.01	1.88	1.89	3.32	13.4	0.42	1.41	5.41	1.23	0
T35B	0.01	1.88	1.89	3.32	13.4	0.76	1.90	2.42	2.03	0.180
T35C	0.01	1.88	1.89	3.32	13.4	0.94	2.11	1.96	2.47	0.589
T40A	0.01	2.01	2.02	3.77	18.3	0.53	1.64	9.08	1.21	0
T40B	0.01	2.01	2.02	3.77	18.3	0.91	2.15	4.42	2.00	0
T40C	0.01	2.01	2.02	3.77	18.3	1.14	2.40	2.02	2.54	0.696
U12A	10 ⁻⁴	1.28	1.28	1.53	0.41	4.48	3.80	1.28	1.11	0.054
U13A	10 ⁻⁴	1.43	1.44	1.77	0.54	2.61	3.07	1.44	1.12	0.089
U15A	10 ⁻⁴	1.62	1.63	2.02	1.35	2.70	2.32	1.63	1.28	0.064
U18A	10 ⁻⁴	1.55	1.56	2.23	2.76	0.78	1.74	1.61	1.05	0.161
U20A	10 ⁻⁴	1.57	1.58	2.79	4.77	0.39	1.24	1.97	1.21	0.090
U22A	10 ⁻⁴	1.67	1.68	2.94	6.23	0.44	1.36	2.01	1.26	0.123
U25A	10 ⁻⁴	1.76	1.77	2.81	7.97	0.67	1.72	1.87	1.17	0.203
U30A	10 ⁻⁴	1.66	1.67	2.93	10.5	0.50	1.45	2.89	1.30	0
U30B	10 ⁻⁴	1.66	1.67	2.93	10.5	0.84	1.87	2.08	2.02	0.209
U35A	10 ⁻⁴	1.89	1.90	3.32	14.0	0.42	1.41	10.1	1.18	0
U35B	10 ⁻⁴	1.89	1.90	3.32	14.0	0.71	1.84	3.03	1.86	0
U35C	10 ⁻⁴	1.89	1.90	3.32	14.0	0.95	2.13	1.97	2.44	0.582
U40A	10 ⁻⁴	2.02	2.03	3.69	18.2	0.59	1.73	13.7	1.33	0
U40B	10 ⁻⁴	2.02	2.03	3.69	18.2	0.90	2.14	4.09	1.97	0
U40C	10 ⁻⁴	2.02	2.03	3.69	18.2	1.14	2.41	2.03	2.53	0.689
Z12A	0	1.35	1.35	1.56	0.38	2.69	3.03	1.35	1.28	0.081
Z13A	0	1.32	1.25	1.71	0.82	1.00	1.78	1.28	1.29	0.191
Z15A	0	1.46	1.46	2.03	1.86	0.93	1.85	1.53	1.27	0.160
Z18A	0	1.47	1.47	2.35	3.78	0.78	1.70	3.40	1.23	0
Z20A	0	1.63	1.63	2.87	5.19	0.39	1.27	4.12	1.15	0
Z22A	0	1.49	1.49	2.19	5.03	2.39	3.00	1.49	1.26	0.167
Z25A	0	1.68	1.68	2.89	7.26	0.47	1.41	6.36	1.22	0
Z25B	0	1.68	1.68	2.89	7.26	0.77	1.81	1.90	1.83	0.288
Z30A	0	1.54	1.54	2.37	8.48	1.02	1.99	8.17	1.18	0
Z30B	0	1.54	1.54	2.37	8.48	1.74	2.60	1.54	2.06	0.324
Z35A	0	1.73	1.71	3.11	13.8	0.43	1.36	12.8	1.26	0
Z35B	0	1.73	1.71	3.11	13.8	0.72	1.76	7.62	1.94	0
Z35C	0	1.73	1.71	3.11	13.8	0.93	2.00	1.85	2.49	0.577
Z40A	0	1.99	1.99	3.59	18.5	0.59	1.72	16.6	1.31	0
Z40B	0	1.99	1.99	3.59	18.5	0.90	2.12	12.2	1.92	0
Z40C	0	1.99	1.99	3.59	18.5	1.41	2.66	1.99	3.01	0.723

iron mass fraction remained above one-half out to $1.32 M_{\odot}$ (as a consequence of implosive burning just prior to core collapse). In this and all other cases the piston was placed at the Y_e discontinuity.

The piston was then moved rapidly *inward* for a brief period. This reflects the fact that in modern supernova models, the explosion is delayed for some time as the neutrino deposited energy builds up to a critical value and the accretion ram pressure declines. During this time, which realistically will vary from star to star, the inner mantle collapses appreciably. Here we adopted a constant value of 0.45 s for this interval. During this time the piston was moved inward at an accelerating rate so as to end up at 500 km in all stars. Initially the collapse speed is given by the value that characterized this region in the presupernova star (about -1000 km s^{-1}). Except for the condition that it end up at 500 km in 0.45 s, the remainder of the trajectory during the collapse phase is arbitrary, though it was adjusted to have a smooth, constant acceleration.

Upon reaching 500 km, the piston was abruptly moved outward with an initial velocity which was the principal parameter in the simulation $-v_0$ in Table 3. Also given in Table 3 is α , the multiplier on the effective gravitational potential. The outward motion of the piston was the trajectory of a projectile launched at speed v_0 in this potential (additionally defined by the current radius and the mass interior to the piston; Woosley & Weaver 1982)

$$\frac{dR}{dt} = [\alpha GM_{\text{pist}}(R^{-1} - R_{\text{min}}^{-1}) + v_0^2]^{1/2},$$

with $R_{\text{min}} = 500 \text{ km}$. The parameter α was chosen in such a way that, for the given v_0 and M_{pist} , the piston coasted to an asymptotic radius ($dR/dt = 0$) of 10^9 cm in all cases. Thus $\alpha = 0.40 v_0^2 / M_{\text{pist}}$ with v_0 and M_{pist} in the units of Table 3. The piston was then held at that maximum radius, 10^9 cm , permanently.

The velocity, v_0 , was adjusted in such a way as to give the desired final kinetic energy of the ejecta when sufficient time had passed that all the ejecta were moving at their final speed. Typically this was $1.2 \times 10^{51} \text{ ergs}$ for models lighter than $30 M_{\odot}$ though larger values were explored for the heavier models.

3. HYDRODYNAMICS AND “FALL BACK”

3.1. Propagation of the Shock

In general, an adiabatic shock passing through a medium having $\rho \propto r^{-n}$ with n less than 3 (i.e., a region of increasing ρr^3) must decelerate (Bethe 1990; Herant & Woosley 1994). One place where ρr^3 increases dramatically is at the interface between the helium core and the hydrogen envelope (Fig. 1) and it is this increase that is largely responsible for the formation of the “reverse shock” (Figs. 2 and 3) so important to mixing in SN 1987A and other supernovae (Chevalier & Klein 1978; Hachisu et al. 1990, 1992; and Fryxell, Arnett, & Müller 1991; Herant & Benz 1992; Herant & Woosley 1994). Because it occurs in a region behind and out of sonic communication with the outgoing shock, the deceleration propagates inward in Lagrangian coordinate as a shock wave.

However, Figure 1 also shows other important regions of increasing ρr^3 . One especially prominent region is the mantles of

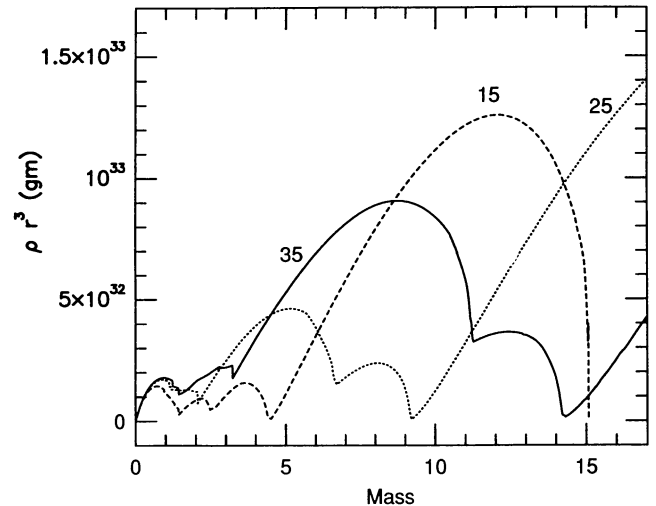


FIG. 1.—Distribution of density times radius cubed (ρr^3) in presupernova stars of 15, 25, and $35 M_{\odot}$ of solar metallicity. The helium core masses for these stars are 4.2 , 9.2 , and $14.2 M_{\odot}$, respectively.

more massive stars (e.g., between 3 and $8 M_{\odot}$ in the $35 M_{\odot}$ model). This region decreases in size and importance for lower mass supernovae. The outgoing shock slows here (Fig. 4), but because the sound speed is still high and the shock not so far from the core, deceleration of the outward moving material occurs smoothly—initially there is no reverse shock. Nevertheless this deceleration can lead to significant amounts of material falling back, under the influence of gravity, into the collapsed remnant. This has interesting implications.

3.2. Reimplosion of the Heavy Elements and the Final Remnant Mass

Figure 5 shows the binding energy of the mantles of our grid of presupernova (solar metallicity) stars and Figure 6 shows the location of the edge of the iron core (“ Y_e discontinuity”) and the base of the oxygen burning shell. A more finely spaced grid of presupernova models is given in Paper I (see also Timmes, Woosley, & Weaver 1995b), but here we show only those where explosion has been simulated. Both sets are characterized by a sharp increase in iron core mass for stars of main sequence mass near $19 M_{\odot}$. This is the boundary between stars that burn carbon and neon radiatively (high mass) or convectively (low mass) in the center of the star (Paper I).

In each case, the piston was situated at the Y_e discontinuity and given sufficient velocity that the final kinetic energy at infinity of all ejecta was at least $\sim 1.2 \times 10^{51} \text{ ergs}$ (§ 2.3; Table 3). *In all cases the entire hydrogen envelope was ejected with high velocity and (for all red supergiants) a normal Type II-*p* light curve was produced.* However, a variable amount of mass fell back onto the (stationary) piston well after the explosion had been launched (Fig. 7). For example, in what shall be our standard $25 M_{\odot}$ solar metallicity star (S25A; Table 3; § 4), the Y_e jump and piston were located at $1.78 M_{\odot}$, but $0.29 M_{\odot}$ of material reimplored. This included most, but not all of the $0.34 M_{\odot}$ of ^{56}Ni produced in the explosion ($0.13 M_{\odot}$ of ^{56}Ni was still ejected).

In a $30 M_{\odot}$ model with comparable kinetic energy (S30A;

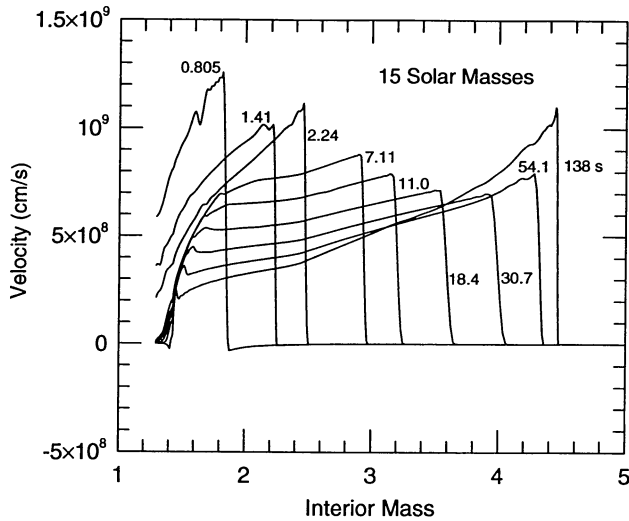


FIG. 2a

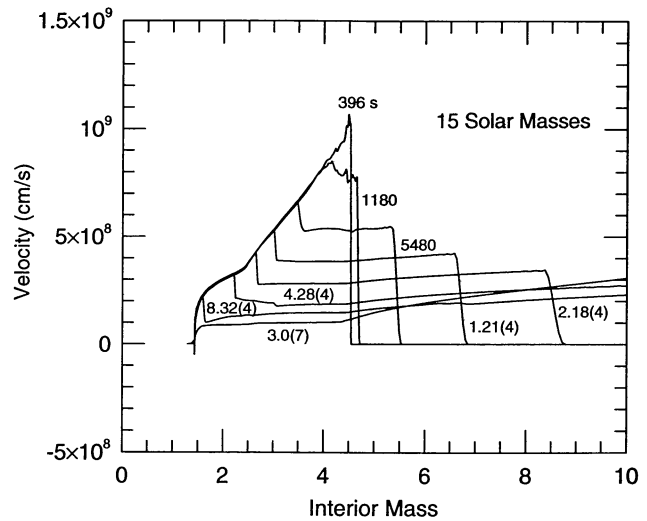


FIG. 2b

FIG. 2.—Propagation of the shock wave through a $15 M_{\odot}$ model (S15A; Table 3). (a) Propagation of the shock through the helium core which takes about a minute. The series of curves are labeled by the time, in seconds, at which each is edited. Note regions of shock speed up and slow down. Material behind the shock stays in sonic communication and no “reverse shock” is evident. (b) Subsequent propagation of the shock through the hydrogen envelope and the formation of an inwardly moving reverse shock which substantially shows material in the helium core and heavy element mantle. The shock erupts from the stellar surface (not shown) at 8.38×10^4 seconds.

Table 3) the piston was at $1.83 M_{\odot}$, but the final remnant mass was $4.24 M_{\odot}$. All of the ^{56}Ni fell back along with most of the freshly synthesized heavy elements. However, there was still a brilliant Type II-p display which lacked, of course, the radioactive tail.

The time history of shock propagation in Model S35B was given in detail in Figs. 3 and 4b. The final kinetic energy of the ejecta at infinity for this model, 1.9×10^{51} ergs, was, by choice, higher than the standard 1.2×10^{51} ergs used in the lighter stars. Even so, the final remnant mass was $3.86 M_{\odot}$, clearly a

black hole, but again a bright Type IIp supernova was produced.

It is possible, by turning up the explosion energy, to force the ejection of all material external to the piston. For a kinetic energy at infinity of 2.2×10^{51} ergs, the remnant mass in the $35 M_{\odot}$ model (S35C) decreases to $2.03 M_{\odot}$ and $0.57 M_{\odot}$ of ^{56}Ni is ejected, but this way of counting the energy (KE at infinity) can be misleading. The binding energy of the mantle of the $35 M_{\odot}$ presupernova star (beyond 10^9 cm in the presupernova model) is 1.6×10^{51} ergs. So the explosion mechanism would

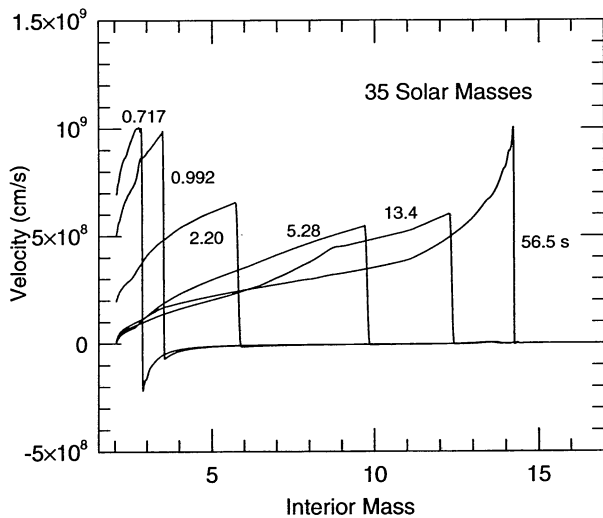


FIG. 3a

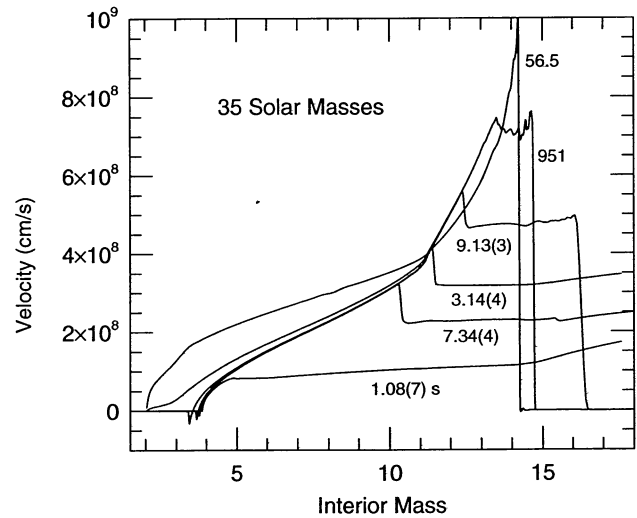


FIG. 3b

FIG. 3.—Same as Fig. 2 but for $35 M_{\odot}$ model S35B. The helium core mass here is $14.2 M_{\odot}$. Note the large amount of fall back that occurs prior to the development of any reverse shock. This $3.86 M_{\odot}$ remnant will certainly be a black hole. However, the hydrogen envelope and most of the heavy elements are still unbound with high velocity.

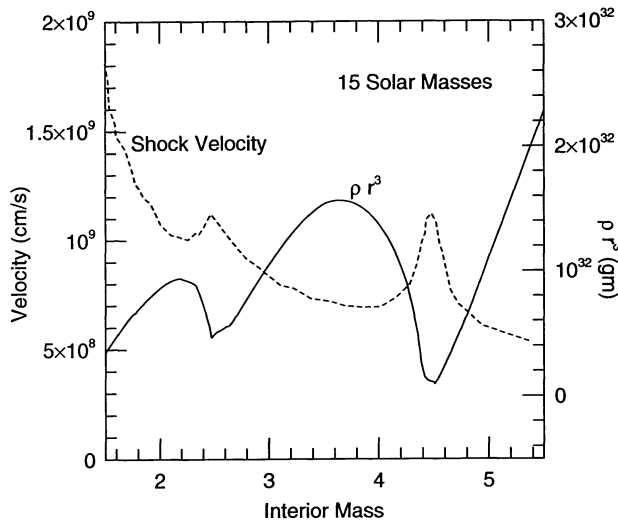


FIG. 4a

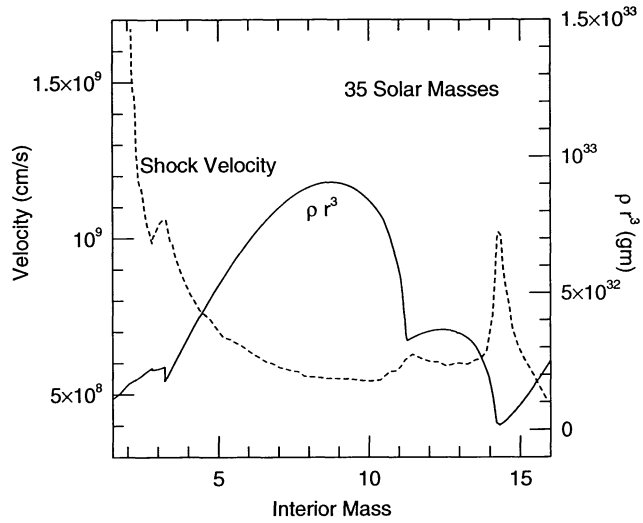


FIG. 4b

FIG. 4.—Material velocity just behind the shock front as a function of mass for the (a) $15 M_{\odot}$ model (S15A) and (b) $35 M_{\odot}$ model (S35B). Also shown is the product of density and radius cubed for the presupernova model (see also Fig. 1). Note the distinct anticorrelation.

actually have to provide 3.8×10^{51} ergs, very much more than the inferred explosion energy for SN 1987A. Further, since the fall back occurs many minutes after the shock has already been launched, the mechanism would have to deliver this much energy long before the large binding of its mantle was known.

Whether the explosion energy available from neutrino deposition increases substantially as one moves to stars of larger mass is an interesting question in need of study. Perhaps by providing more ram pressure during the infall stage the inner mantle sets up conditions that extract a larger fraction of the available neutrino energy. Maybe the larger cores provide larger neutrino luminosities.

If not, there will be a mass, somewhere around $30 M_{\odot}$, which distinguishes Type II supernovae that leave neutron stars from those that leave black holes. This would have many important implications for the number of black holes in our galaxy, for galactic chemical evolution, for the late time light curves of

Type II supernovae, and for the formation of accreting X-ray sources in binaries. We want to emphasize again that the bright optical display of supernovae that leave black holes is not affected, so long as a moderately energetic shock is launched (e.g., Figs. 3 and 4).

Others have suggested black hole formation in supernovae for reasons related to nucleosynthesis (Twarog & Wheeler 1982, 1987; Wheeler, Sneden, & Truran, 1989; Maeder (1992, 1993); a low critical mass for neutron stars (Brown 1988); absence of clear neutron star signatures in many supernova rem-

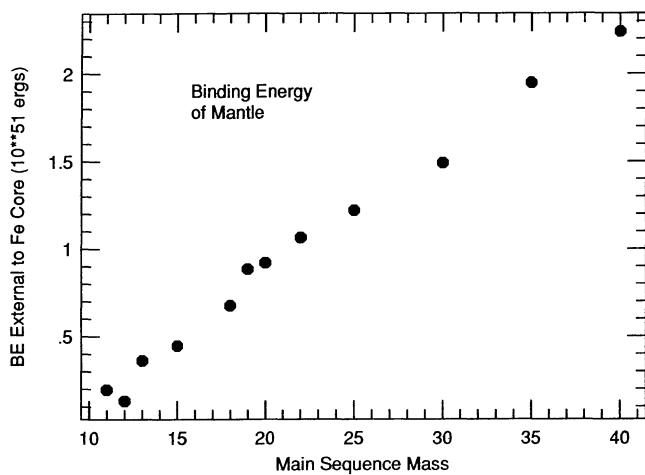


FIG. 5.—Net binding energy external to the piston mass point (Table 3) in stars of solar metallicity.

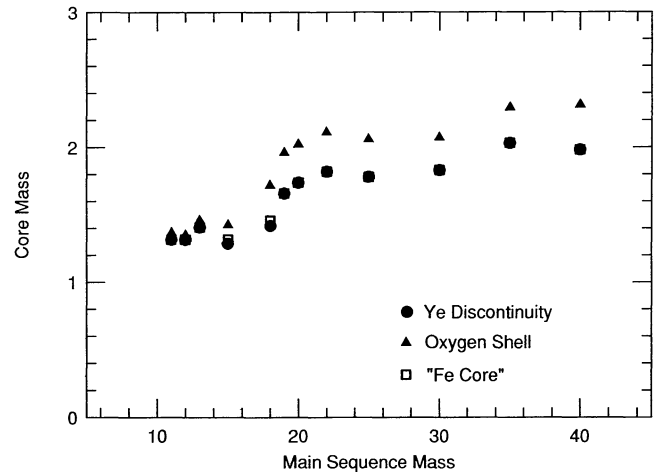


FIG. 6.—Location of several fiducial mass points in presupernova stars of initially solar metallicity. The “ Y_e discontinuity” is where electron capture has decreased the electron mole number substantially below 0.50 and where the piston is placed (Table 3). It is found at the outer boundary of the last convective silicon shell burning episode. If there has not been significant “implosive burning,” the Y_e discontinuity also corresponds to the iron core, where the mass fraction of iron group elements rises above one-half. The base of the oxygen shell is typically a place where there is a large jump in entropy (hence decline in ram pressure during the implosion) and may be a natural location for a mass cut to develop.

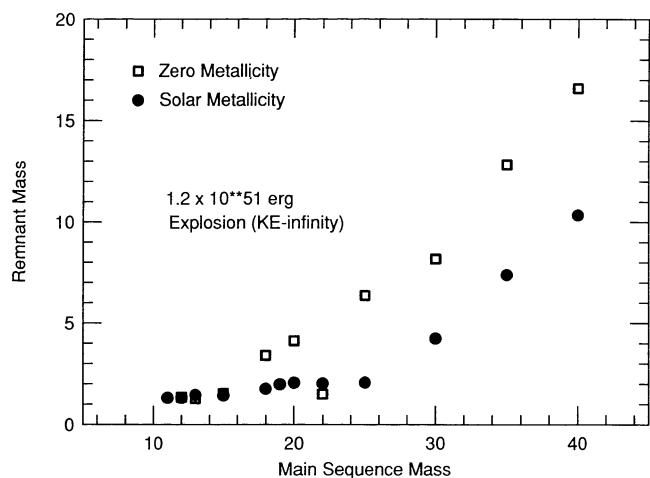


FIG. 7.—Final remnant mass for a series of supernova models that employed pistons at the edge of their iron core which communicated to their ejecta a final kinetic energy at infinity of approximately 1.2×10^{51} ergs. All were brilliant Type II-p optical events. The zero metallicity stars are more compact, more tightly bound configurations and consequently more difficult to explode (Table 3).

nants (Helfand & Becker 1984; Brown & Bethe 1994); and the light curve of SN 1987A (Brown, Bruenn, & Wheeler 1992). We have also previously suggested that some “successful” supernovae might leave black hole remnants (Wilson et al. 1986; Woosley & Weaver 1986; Woosley 1988; Bodenheimer & Woosley 1983). Still our conclusion here is novel. Without invoking a low critical mass, rotation, a “failure” of the basic supernova mechanism, or empirical restrictions based on nucleosynthesis or light curves, it seems quite possible that a massive black hole will frequently form in the explosion of a massive star for reasons that involve simple hydrodynamics. The nucleosynthetic implications of this conclusion will become obvious in the next section and have a considerable effect on Galactic chemical evolution (Paper III).

However, we should also point out that an important effect has been omitted from the present calculations that could greatly affect the possibility of black hole formation, namely mass loss. The kind of reimplosion we have calculated is most sensitive to the helium core structure and not so much to the reverse shock that forms later (though that too will increase the remnant mass). Stars above an uncertain limit, which is also around 30 to 40 M_{\odot} , may lose their entire envelope and then experience rapid mass dependent mass loss ending their lives with greatly reduced helium core masses (Woosley, Langer, & Weaver 1993, 1995). This provides a way for some massive stars to avoid the black hole fate, though the numbers are uncertain. However, the mass of stars that retain their envelopes will certainly be greater when the metallicity is lower. Thus, it would have been easier to make black holes in the past (and in galaxies with lower current metallicities).

For what it may be worth, remnant masses in those cases where large amounts of reimplosion does not occur, especially the abundant stars below 19 M_{\odot} , agree reasonably well with observational limits for neutron star masses (once the appropriate 15%–20% reduction for neutrino losses is applied). Kaspi, Taylor, & Ryba (1994) derive a gravitational mass for

PSR B1855+09 of $1.50 (+0.26, -0.14) M_{\odot}$ and mass limits for other (nonaccreting) neutron stars are similar, though typically smaller. The neutron star mass function resulting from this study will be discussed in detail in a separate paper (Timmes et al. 1995b).

4. NUCLEOSYNTHESIS IN 15 AND 25 M_{\odot} SUPERNOVAE

In § 5 we shall present the explosively ejected yields for a large grid of stars of variable mass and metallicity. However, it is useful to discuss in detail the yields of two exemplary events—Models S15A and S25A, the explosions of 15 and 25 M_{\odot} supernovae of initially solar metallicity. This may be a typical mass range for supernovae that contribute to the solar abundances (Weaver & Woosley 1980). Because many species are made as radioactive progenitors and it is interesting to see this information, the abundances plotted in the figures are evaluated at a relatively early time (2.5×10^4 s unless otherwise noted) when strong and electromagnetic reaction have ceased, but many nuclei have not yet decayed to their most stable form.

Our discussion will center on the 25 M_{\odot} model with results from S15A mostly given in the figures to illustrate the mass dependence. Figure 8 shows the temperature structure as the shock propagates through the 25 M_{\odot} model and Figure 9, the peak temperature as a function of mass. Using this latter figure and Figure 10, which shows the location of the important major constituents and shells, should help in keeping track of the various nucleosynthetic processes described in the following subsections.

4.1. Lithium, Beryllium, and Boron

While ${}^6\text{Li}$ is not made in appreciable abundance in any of our model supernovae, ${}^7\text{Li}$ is. Production occurs both as ${}^7\text{Li}$ itself and as radioactive ${}^7\text{Be}$. This production occurs chiefly in the helium shell (Fig. 11) and, to a lesser extent, in the inner-

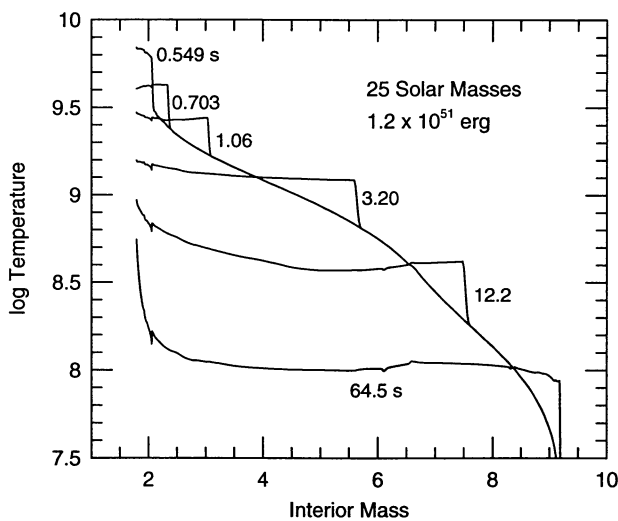


FIG. 8.—Temperature structure as the shock propagates through the mantle and helium core of a 25 M_{\odot} solar metallicity model. The kinetic energy of all ejecta at infinity is 1.2×10^{51} ergs. Curves are labeled by the time in seconds at which each is sampled. Note the presence, except near the collapsed core, of large nearly isothermal regions behind the shock.

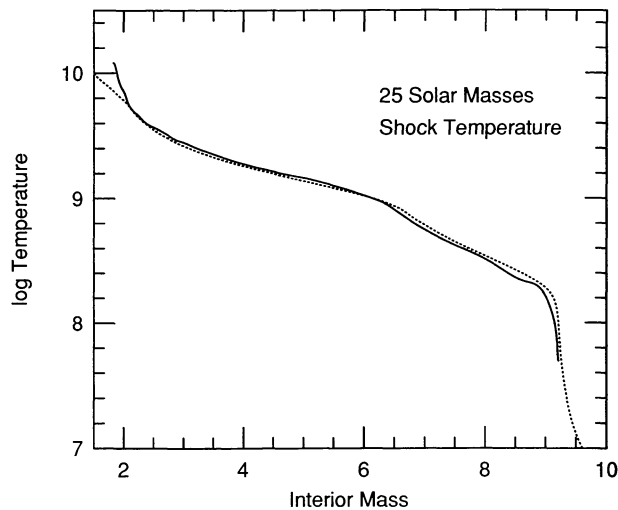


FIG. 9.—Shock temperature as a function of mass (*solid line*) for the same model shown in Fig. 8. The dashed line, which is a very good fit to the solid line except near the collapsed core, is given by $T = (3E_0/4\pi a R_{\text{PSN}}^3)^{1/4}$ where $E_0 = 1.2 \times 10^{51}$ ergs and R_{PSN} is the presupernova radius as a function of enclosed mass.

most ejecta where explosive silicon burning results in an alpha-rich freeze out. In both locations ${}^7\text{Li}$ synthesis is a consequence of neutrino irradiation (Woosley et al. 1990) and the reaction sequences ${}^4\text{He}(\nu_x, \nu'_x n){}^3\text{He}(\alpha, \gamma){}^7\text{Be}$, ${}^4\text{He}(\nu_x, \nu'_x p){}^3\text{H}(\alpha, \gamma){}^7\text{Li}$, and ${}^3\text{He}(n, p){}^3\text{H}(\alpha, \gamma){}^7\text{Li}$ where ν_x can be either a μ - or τ -neutrino or antineutrino. Most of this ${}^7\text{Li}$ and ${}^7\text{Be}$ is destroyed as the shock wave passes through the inner helium layer. Paper III will show that this process in massive supernovae is the source of a considerable fraction, though probably not all of the ${}^7\text{Li}$ found in meteorites in the solar system. Had the shock not destroyed so much, the full solar abundance could have been produced.

A small amount of ${}^{10}\text{B}$ and a much larger amount of ${}^{11}\text{B}$, are also made in our models (Fig. 12). The ${}^{11}\text{B}$ is due to neutrino interactions with carbon [${}^{12}\text{C}(\nu_x, \nu'_x n){}^{11}\text{C}$ and ${}^{12}\text{C}(\nu_x, \nu'_x p){}^{11}\text{B}$] in the carbon layer and, to a lesser extent, ${}^7\text{Li}(\alpha, \gamma){}^{11}\text{B}$ and ${}^7\text{Be}(\alpha, \gamma){}^{11}\text{C}$ in the helium layer. Dearborn et al. (1989) suggested that ${}^{11}\text{B}$ could be made in the envelope of a massive star by shock processing alone without neutrinos. This does not occur here (Table 4).

Compared to ${}^7\text{Li}$ and ${}^{11}\text{B}$, only small amounts of ${}^9\text{Be}$ are made here. Malaney (1992) suggested that ${}^9\text{Be}$ might be produced by ${}^7\text{Li}(t, n){}^9\text{Be}$ with tritons coming from ${}^3\text{He}(n, p){}^3\text{H}$ and ${}^4\text{He}(\nu_x, \nu'_x p){}^3\text{H}$ in the helium shell of low-metallicity stars. This reaction, as well as many others that destroy ${}^7\text{Li}$, ${}^3\text{H}$, and ${}^9\text{Be}$ have been included in the present study. The rate for ${}^7\text{Li}(t, n){}^9\text{Be}$ was taken from Malaney & Fowler (1989). We find no appreciable fraction of the solar abundance of ${}^9\text{Be}$ made in this fashion. The ejected abundance of ${}^9\text{Be}$, even in metal deficient stars (§ 5), is quite small compared with other isotopes like ${}^{11}\text{B}$.

Barring large unexpected changes in the neutrino cross sections, we presume that ${}^6\text{Li}$, ${}^9\text{Be}$, and ${}^{10}\text{B}$ are the products of cosmic-ray spallation (Olive et al. 1993; Prantzos, Casse, & Vangioni-Flam 1993; Reeves 1994; Paper III).

4.2. Carbon, Nitrogen, and Oxygen

The abundant nucleus ${}^{12}\text{C}$ is a product of helium burning. Its production is sensitive to the still uncertain rate for ${}^{12}\text{C}(\alpha, \gamma){}^{16}\text{O}$ (§ 2.2) and to details of convection at the end of helium burning, when a slight growth of the helium convective core can result in a dramatic decrease in carbon yield (Paper I). Compared to other nuclei produced by massive stars, the yield of this important isotope is too small to account for its solar abundance (Tables 5 and 6; Paper III) and lower mass stars must make up the difference. However, massive stars do contribute a non-negligible fraction and this might be important early in Galactic evolution.

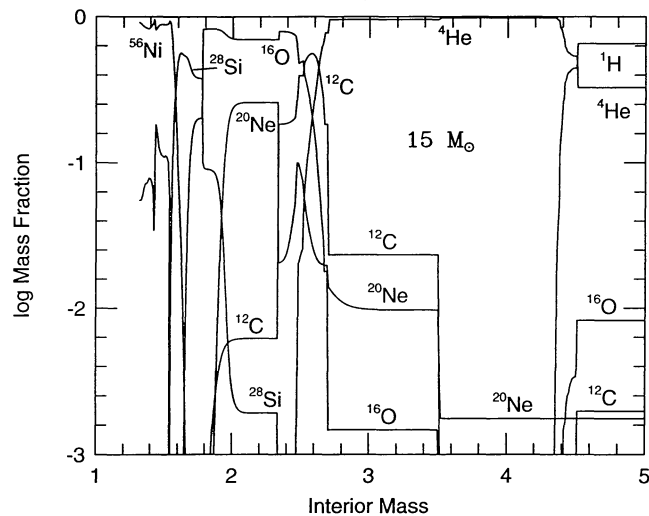


FIG. 10a

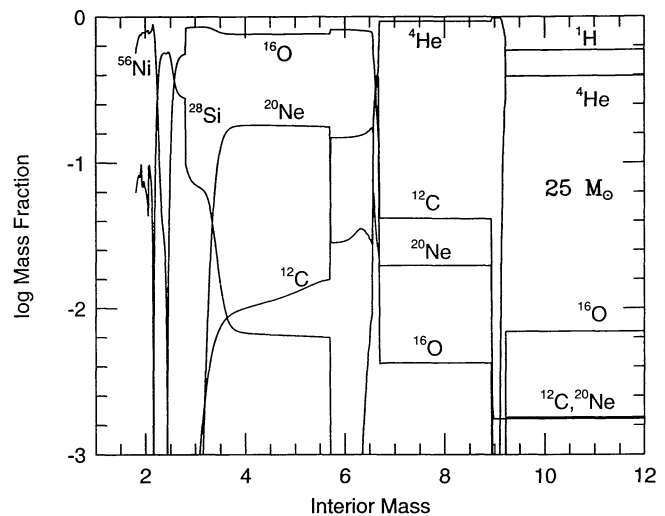


FIG. 10b

FIG. 10.—Final mass fractions of the major abundances — ${}^1\text{H}$, ${}^4\text{He}$, ${}^{12}\text{C}$, ${}^{16}\text{O}$, ${}^{20}\text{Ne}$, ${}^{28}\text{Si}$, and ${}^{56}\text{Ni}$ —(a) the inner $5 M_{\odot}$ of a $15 M_{\odot}$ solar metallicity supernova (model S15A); (b) the inner $12 M_{\odot}$ of the ejecta of a $25 M_{\odot}$ solar metallicity supernova (model S25A). Each had an explosion energy of 1.2×10^{51} ergs (Table 3).

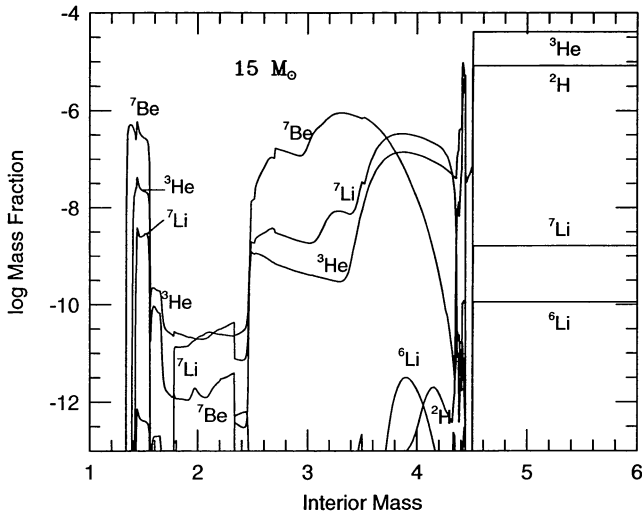


FIG. 11a

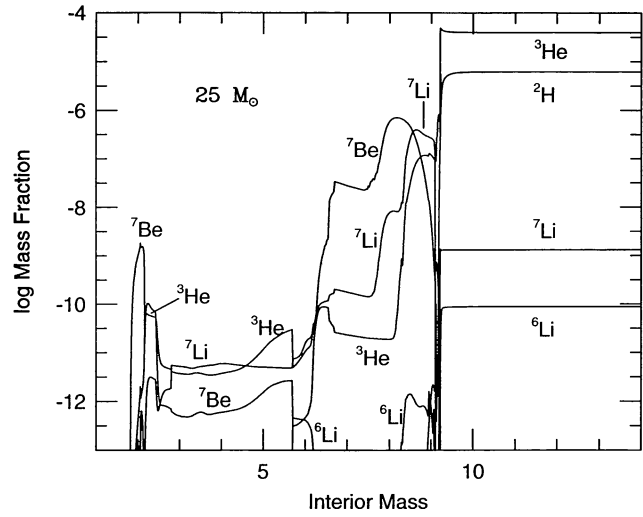


FIG. 11b

FIG. 11—Mass fractions of ^2H and the isotopes of He and Li and the ^7Li progenitor, ^7Be in the interior of models S15A (a) and S25A (b) at a time of 2.5×10^4 s. Note the large production of mass 7 in the helium layer by the neutrino process.

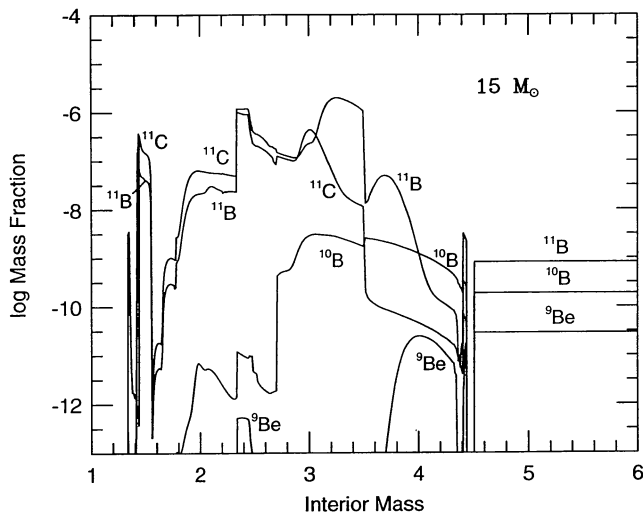


FIG. 12a

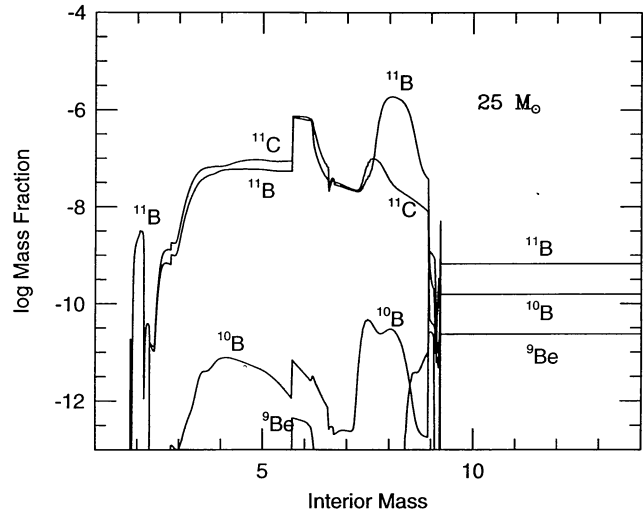


FIG. 12b

FIG. 12.—Mass fractions in of Be and B isotopes and the progenitor of ^{11}B , ^{11}C in the interiors of models S15A (a) and S25A (b) at a time 2.5×10^4 s after the explosion. Note the production of mass 11 from carbon by the neutrino process.

TABLE 4
25 M_{\odot} EXPLOSION WITH AND WITHOUT NEUTRINO IRRADIATION

Isotope	w/o ν	with ν $T_{\nu} = 8$	with ν $T_{\nu} = 6$	Isotope	w/o ν	with ν $T_{\nu} = 8$	with ν $T_{\nu} = 6$
$^7\text{Li}^*$	2.13E-08	7.31E-07	2.81E-07	^{40}K	3.13E-06	3.44E-06	3.31E-06
^{10}B	2.51E-09	2.75E-09	2.58E-09	^{41}K	2.74E-05	3.04E-05	2.96E-05
$^{11}\text{B}^*$	1.18E-08	2.35E-06	1.03E-06	^{43}Ca	6.36E-06	8.39E-06	7.92E-06
$^{15}\text{N}^*$	3.39E-05	2.33E-04	1.29E-04	^{45}Sc	4.20E-06	6.18E-06	5.00E-06
$^{19}\text{F}^*$	3.53E-05	1.48E-04	9.15E-05	^{47}Ti	9.98E-06	1.18E-05	1.11E-05
^{21}Ne	5.84E-04	6.41E-04	6.08E-04	^{50}V	2.21E-07	2.93E-07	2.94E-07
$^{22}\text{Na}^*$	1.59E-06	3.43E-06	2.57E-06	^{51}V	3.65E-05	6.51E-05	5.40E-05
^{26}Al	9.38E-05	1.29E-04	1.14E-04	^{53}Cr	3.65E-04	4.17E-04	3.96E-04
^{31}P	2.78E-03	3.18E-03	3.02E-03	^{54}Cr	3.39E-05	4.17E-05	4.18E-05
^{33}S	5.61E-04	6.60E-04	6.18E-04	^{55}Mn	1.37E-03	2.33E-03	1.86E-03
^{35}Cl	4.28E-04	7.01E-04	5.80E-04	^{57}Fe	1.30E-02	1.43E-02	1.42E-02
^{39}K	3.79E-04	5.39E-04	4.65E-04	^{59}Co	8.31E-04	1.54E-03	1.16E-03

TABLE 5A
 EJECTED MASSES AT 2.5×10^4 SECONDS; 11–25 M_{\odot} MODELS; $Z = Z_{\odot}$

	S11A	S12A	S13A	S15A	S18A	S19A	S20A	S22A	S25A
¹ H	5.59	5.96	6.32	6.98	7.89	8.08	8.24	8.79	9.40
⁴ He	3.73	4.11	4.51	5.24	6.28	6.46	6.72	7.51	8.64
² H	7.84E-05	8.27E-05	8.32E-05	8.84E-05	9.57E-05	9.91E-05	9.88E-05	1.02E-04	9.81E-05
³ He	3.53E-04	3.71E-04	3.94E-04	4.32E-04	4.88E-04	5.04E-04	5.26E-04	5.64E-04	6.29E-04
⁷ Li	2.18E-07	2.18E-07	1.98E-07	2.07E-07	2.73E-07	2.51E-07	2.51E-07	2.17E-07	2.40E-07
⁷ Be	3.35E-07	2.87E-07	6.17E-07	5.69E-07	4.43E-07	4.18E-07	4.18E-07	4.35E-07	5.04E-07
⁹ Be	2.88E-10	2.87E-10	2.97E-10	3.15E-10	3.35E-10	3.46E-10	3.45E-10	3.58E-10	3.84E-10
¹⁰ B	3.17E-09	2.63E-09	4.72E-09	4.96E-09	2.83E-09	2.57E-09	2.53E-09	2.58E-09	2.76E-09
¹¹ B	4.89E-07	4.62E-07	4.49E-07	9.48E-07	1.49E-06	1.85E-06	1.55E-06	1.49E-06	1.78E-06
¹¹ C	1.54E-07	1.67E-07	3.46E-07	3.06E-07	3.73E-07	7.79E-07	3.01E-07	4.65E-07	6.16E-07
¹² C	5.32E-02	8.05E-02	1.14E-01	1.61E-01	2.48E-01	2.84E-01	2.13E-01	2.41E-01	3.22E-01
¹³ C	9.61E-04	1.02E-03	1.14E-03	1.29E-03	1.35E-03	1.33E-03	1.33E-03	1.39E-03	1.45E-03
¹⁴ C	1.71E-05	3.97E-06	5.32E-06	8.15E-06	2.91E-05	1.31E-05	5.16E-06	4.30E-06	3.66E-06
¹⁴ N	3.67E-02	3.60E-02	4.68E-02	5.40E-02	5.68E-02	5.71E-02	5.98E-02	6.73E-02	7.93E-02
¹⁵ N	6.16E-05	9.76E-05	4.47E-05	1.49E-04	1.52E-04	1.24E-04	1.41E-04	1.70E-04	2.29E-04
¹⁶ O	1.36E-01	2.10E-01	2.72E-01	6.80E-01	1.13	1.43	1.94	2.38	3.25
¹⁷ O	5.19E-04	5.28E-04	5.33E-04	5.92E-04	8.24E-04	8.46E-04	8.51E-04	9.16E-04	1.01E-03
¹⁸ O	3.47E-03	8.36E-03	2.29E-03	4.38E-03	1.49E-02	1.60E-02	1.18E-02	3.87E-03	2.52E-03
¹⁹ F	1.29E-05	3.47E-05	8.88E-06	3.45E-05	9.21E-05	2.64E-05	2.83E-05	4.87E-05	1.33E-04
²⁰ Ne	3.12E-02	2.32E-02	4.46E-02	1.11E-01	2.77E-01	1.06E-01	1.05E-01	7.02E-02	3.94E-01
²¹ Ne	1.78E-04	1.57E-04	5.77E-04	4.49E-04	8.30E-04	5.94E-04	3.72E-04	5.21E-04	6.29E-04
²² Ne	2.47E-03	6.03E-03	3.50E-03	7.37E-03	1.64E-02	1.85E-02	2.28E-02	3.82E-02	4.76E-02
²² Na	2.14E-07	8.44E-08	1.45E-07	1.09E-06	3.76E-06	7.91E-07	2.96E-07	2.94E-07	3.43E-06
²³ Na	1.05E-03	8.71E-04	1.08E-03	3.42E-03	9.99E-03	2.71E-03	1.53E-03	1.93E-03	1.08E-02
²⁴ Mg	9.24E-03	8.21E-03	1.64E-02	2.67E-02	5.52E-02	2.51E-02	3.13E-02	4.16E-02	1.06E-01
²⁵ Mg	1.38E-03	1.23E-03	3.07E-03	6.66E-03	1.20E-02	9.38E-03	7.68E-03	8.01E-03	2.39E-02
²⁶ Mg	1.55E-03	1.69E-03	3.40E-03	6.50E-03	9.85E-03	1.14E-02	1.05E-02	1.28E-02	3.25E-02
²⁶ Al	1.68E-05	2.00E-05	2.84E-05	4.30E-05	8.14E-05	8.83E-05	3.47E-05	5.91E-05	1.27E-04
²⁷ Al	1.19E-03	1.13E-03	1.83E-03	4.62E-03	9.98E-03	3.77E-03	3.98E-03	8.40E-03	2.44E-02
²⁸ Si	2.17E-02	9.09E-02	5.85E-02	1.10E-01	1.37E-01	2.77E-01	2.88E-01	3.56E-01	3.15E-01
²⁹ Si	6.45E-04	1.09E-03	1.45E-03	2.48E-03	3.68E-03	4.29E-03	6.11E-03	1.23E-02	1.15E-02
³⁰ Si	6.97E-04	7.62E-04	1.97E-03	3.09E-03	5.41E-03	3.43E-03	5.82E-03	1.41E-02	1.26E-02
³¹ P	1.86E-04	8.91E-04	4.17E-04	7.82E-04	1.23E-03	2.02E-03	3.17E-03	4.96E-03	3.07E-03
³² S	9.71E-03	7.57E-02	2.60E-02	6.34E-02	5.46E-02	1.29E-01	1.52E-01	1.72E-01	1.41E-01
³³ S	6.72E-05	7.13E-04	1.39E-04	2.85E-04	3.40E-04	8.81E-04	1.26E-03	1.34E-03	6.52E-04
³⁴ S	6.29E-04	3.00E-03	1.52E-03	1.92E-03	3.68E-03	1.05E-02	2.22E-02	1.67E-02	7.13E-03
³⁵ S	6.97E-07	6.07E-06	5.41E-06	4.31E-06	5.17E-06	4.51E-05	2.84E-05	6.56E-05	1.65E-05
³⁶ S	1.95E-06	3.52E-06	7.66E-06	8.67E-06	1.26E-05	3.11E-05	2.49E-05	8.86E-05	4.18E-05
³⁵ Cl	4.90E-05	1.54E-03	1.01E-04	2.58E-04	2.73E-04	1.55E-03	2.09E-03	2.86E-03	6.84E-04
³⁶ Cl	2.50E-07	1.15E-05	7.84E-07	2.17E-06	2.57E-06	1.87E-05	2.75E-05	5.18E-05	6.28E-06
³⁷ Cl	1.32E-05	3.86E-05	2.32E-05	4.45E-05	7.63E-05	1.00E-04	1.06E-04	1.75E-04	1.88E-04
³⁶ Ar	1.69E-03	2.18E-02	4.46E-03	1.25E-02	8.71E-03	2.07E-02	2.62E-02	2.80E-02	2.25E-02
³⁷ Ar	2.22E-06	1.51E-04	6.23E-06	4.08E-05	1.60E-05	7.60E-05	1.22E-04	1.12E-04	6.54E-05
³⁸ Ar	2.81E-04	4.80E-03	6.00E-04	2.07E-03	1.34E-03	6.43E-03	1.03E-02	8.31E-03	4.90E-03
⁴⁰ Ar	7.75E-07	1.11E-06	3.39E-06	3.11E-06	4.44E-06	6.71E-06	4.72E-06	1.71E-05	1.38E-05
³⁹ K	5.05E-05	2.14E-03	7.70E-05	3.18E-04	1.47E-04	8.69E-04	9.37E-04	1.50E-03	5.04E-04
⁴⁰ K	1.74E-07	1.21E-05	2.45E-07	6.67E-07	1.05E-06	1.02E-05	9.48E-06	3.32E-05	3.45E-06
⁴¹ K	2.97E-06	4.52E-06	3.38E-06	4.37E-06	5.38E-06	6.03E-06	5.98E-06	1.02E-05	9.06E-06
⁴⁰ Ca	1.32E-03	1.44E-02	3.61E-03	1.10E-02	6.82E-03	1.35E-02	1.43E-02	1.73E-02	1.67E-02
⁴¹ Ca	1.92E-06	1.56E-04	2.77E-06	1.68E-05	5.21E-06	2.11E-05	2.87E-05	3.53E-05	2.01E-05
⁴² Ca	8.32E-06	3.74E-04	1.58E-05	9.00E-05	3.32E-05	1.93E-04	3.78E-04	2.61E-04	1.45E-04
⁴³ Ca	9.28E-07	1.03E-05	1.16E-06	1.81E-06	2.32E-06	9.44E-06	2.03E-05	2.50E-05	4.67E-06
⁴⁴ Ca	1.37E-05	1.98E-05	1.61E-05	1.97E-05	2.43E-05	2.94E-05	4.16E-05	5.33E-05	3.64E-05
⁴⁵ Ca	5.60E-08	6.02E-08	2.90E-07	5.69E-07	4.75E-07	8.40E-07	5.84E-07	1.37E-06	1.75E-06
⁴⁶ Ca	7.20E-08	5.80E-08	3.76E-07	3.33E-07	2.98E-07	4.84E-07	3.36E-07	1.16E-06	8.90E-07
⁴⁸ Ca	1.33E-06	1.43E-06	1.69E-06	1.80E-06	2.15E-06	2.19E-06	2.21E-06	2.43E-06	2.89E-06
⁴³ Sc	6.98E-07	1.79E-06	7.60E-07	1.31E-06	2.53E-07	8.43E-07	8.52E-07	1.20E-06	1.04E-06
⁴⁵ Sc	4.32E-07	3.36E-06	5.22E-07	7.87E-07	1.10E-06	3.25E-06	9.44E-06	1.20E-05	2.28E-06
⁴⁴ Ti	6.20E-05	8.26E-05	6.26E-05	5.68E-05	8.48E-06	1.92E-05	1.38E-05	6.15E-05	3.04E-05
⁴⁵ Ti	7.18E-07	1.69E-06	1.27E-06	1.71E-06	3.06E-07	6.43E-07	4.81E-07	1.23E-06	3.92E-07
⁴⁶ Ti	7.08E-06	1.05E-04	9.77E-06	4.86E-05	1.50E-05	5.35E-05	8.63E-05	6.97E-05	5.57E-05
⁴⁷ Ti	2.20E-06	9.62E-06	2.64E-06	3.62E-06	3.96E-06	6.63E-06	1.57E-05	1.45E-05	7.54E-06
⁴⁸ Ti	2.03E-05	2.43E-05	2.35E-05	2.72E-05	3.19E-05	3.37E-05	4.27E-05	4.31E-05	4.23E-05
⁴⁹ Ti	1.74E-06	2.09E-06	2.08E-06	2.93E-06	4.10E-06	4.13E-06	5.42E-06	6.49E-06	7.81E-06
⁵⁰ Ti	1.84E-06	2.00E-06	2.66E-06	4.41E-06	6.32E-06	6.23E-06	6.91E-06	1.02E-05	1.59E-05
⁴⁷ V	9.46E-07	1.40E-06	1.21E-06	1.44E-06	4.23E-07	8.09E-07	6.38E-07	1.24E-06	3.28E-07
⁴⁸ V	6.99E-07	1.43E-06	7.78E-07	1.00E-06	6.07E-07	1.24E-06	2.34E-06	7.91E-06	3.40E-05

TABLE 5B
 EJECTED MASSES AT 2.5×10^4 SECONDS; 30–40 M_{\odot} MODELS; $Z = Z_{\odot}$

KE $_{\infty}$	S30A 1.13	S30B 2.01	S35A 1.23	S35B 1.88	S35C 2.22	S40A 1.19	S40B 1.93	S40C 2.57
¹ H	10.5	10.5	11.5	11.5	11.5	11.1	11.1	11.1
⁴ He	10.4	10.4	11.9	11.9	12.0	13.0	13.0	13.0
² H	9.44E-05	9.45E-05	1.02E-04	1.02E-04	1.02E-04	8.87E-05	8.87E-05	8.87E-05
³ He	7.18E-04	7.18E-04	7.91E-04	7.91E-04	7.91E-04	7.74E-04	7.74E-04	7.74E-04
⁷ Li	2.74E-07	2.12E-07	1.94E-07	1.56E-07	1.45E-07	1.69E-07	1.34E-07	1.17E-07
⁷ Be	7.13E-07	6.25E-07	8.26E-07	7.34E-07	7.01E-07	8.19E-07	7.17E-07	6.62E-07
⁹ Be	3.79E-10	3.79E-10	4.40E-10	4.41E-10	4.41E-10	4.07E-10	4.07E-10	4.07E-10
¹⁰ B	2.90E-09	2.90E-09	3.18E-09	3.19E-09	3.19E-09	3.11E-09	3.11E-09	3.11E-09
¹¹ B	8.55E-07	7.41E-07	5.39E-07	5.89E-07	5.69E-07	3.79E-07	6.04E-07	5.99E-07
¹¹ C	3.14E-07	3.43E-07	3.73E-07	4.63E-07	4.65E-07	3.76E-07	5.76E-07	6.01E-07
¹² C	2.86E-01	2.90E-01	3.01E-01	3.20E-01	3.20E-01	3.13E-01	3.63E-01	3.68E-01
¹³ C	1.59E-03	1.59E-03	1.65E-03	1.65E-03	1.65E-03	1.62E-03	1.62E-03	1.62E-03
¹⁴ C	1.80E-06	1.88E-06	1.72E-06	1.81E-06	1.80E-06	2.05E-06	2.15E-06	2.12E-06
¹⁴ N	1.04E-01	1.04E-01	1.25E-01	1.25E-01	1.25E-01	1.41E-01	1.41E-01	1.41E-01
¹⁵ N	1.65E-04	2.15E-04	1.25E-04	2.70E-04	2.89E-04	9.06E-05	2.91E-04	3.40E-04
¹⁶ O	3.65	4.88	3.07	5.82	6.36	2.36	6.03	7.63
¹⁷ O	1.06E-03	1.06E-03	1.29E-03	1.29E-03	1.29E-03	1.23E-03	1.23E-03	1.23E-03
¹⁸ O	5.86E-04	5.74E-04	3.12E-04	3.09E-04	3.08E-04	2.31E-04	2.31E-04	2.30E-04
¹⁹ F	1.05E-04	1.07E-04	1.63E-04	2.26E-04	2.21E-04	1.68E-04	2.98E-04	2.92E-04
²⁰ Ne	3.81E-01	4.32E-01	5.15E-01	8.88E-01	8.81E-01	4.48E-01	1.24	1.29
²¹ Ne	3.01E-04	3.27E-04	5.48E-04	8.03E-04	8.00E-04	5.75E-04	1.26E-03	1.29E-03
²² Ne	5.41E-02	5.41E-02	5.77E-02	5.77E-02	5.77E-02	5.94E-02	5.94E-02	5.91E-02
²² Na	1.68E-06	1.94E-06	3.17E-06	5.81E-06	5.73E-06	3.60E-06	1.01E-05	1.02E-05
²³ Na	6.48E-03	6.89E-03	1.47E-02	2.16E-02	2.15E-02	1.61E-02	3.68E-02	3.67E-02
²⁴ Mg	2.12E-01	2.82E-01	1.23E-01	2.87E-01	3.03E-01	6.80E-02	2.30E-01	3.10E-01
²⁵ Mg	2.53E-02	2.88E-02	2.64E-02	4.45E-02	4.43E-02	2.21E-02	5.40E-02	5.71E-02
²⁶ Mg	3.24E-02	3.56E-02	3.85E-02	6.02E-02	5.99E-02	3.36E-02	7.95E-02	8.22E-02
²⁶ Al	1.83E-04	2.73E-04	1.33E-04	3.47E-04	3.45E-04	1.09E-04	2.51E-04	3.56E-04
²⁷ Al	3.94E-02	5.08E-02	2.97E-02	6.36E-02	6.53E-02	2.06E-02	6.46E-02	7.70E-02
²⁸ Si	9.77E-02	3.16E-01	4.16E-02	1.12E-01	4.29E-01	2.47E-02	5.46E-02	5.61E-01
²⁹ Si	2.39E-02	3.39E-02	1.04E-02	2.97E-02	3.24E-02	4.10E-03	1.65E-02	2.91E-02
³⁰ Si	1.98E-02	3.45E-02	6.79E-03	2.40E-02	3.24E-02	2.46E-03	8.96E-03	3.08E-02
³¹ P	4.77E-03	7.29E-03	1.99E-03	5.58E-03	6.71E-03	1.09E-03	2.96E-03	6.35E-03
³² S	1.38E-02	9.99E-02	1.08E-02	1.68E-02	1.69E-01	1.02E-02	1.15E-02	2.36E-01
³³ S	1.71E-04	5.62E-04	1.11E-04	2.64E-04	6.67E-04	9.85E-05	1.20E-04	8.26E-04
³⁴ S	1.73E-03	7.30E-03	7.29E-04	2.29E-03	8.77E-03	5.44E-04	7.72E-04	1.06E-02
³⁵ S	4.14E-05	5.79E-05	1.33E-05	4.17E-05	4.43E-05	6.51E-06	2.05E-05	3.48E-05
³⁶ S	6.52E-05	8.33E-05	4.58E-05	9.00E-05	9.21E-05	3.55E-05	8.91E-05	1.04E-04
³⁵ Cl	3.15E-04	7.10E-04	1.02E-04	3.60E-04	6.39E-04	7.69E-05	1.08E-04	7.50E-04
³⁶ Cl	6.21E-06	1.14E-05	1.56E-06	6.17E-06	8.98E-06	8.68E-07	1.94E-06	9.13E-06
³⁷ Cl	1.87E-04	2.08E-04	2.09E-04	3.16E-04	3.18E-04	1.91E-04	4.05E-04	4.21E-04
³⁶ Ar	1.72E-03	1.60E-02	1.87E-03	1.98E-03	2.86E-02	1.90E-03	1.93E-03	3.90E-02
³⁷ Ar	1.85E-06	3.13E-05	1.81E-06	3.30E-06	3.71E-05	1.85E-06	2.42E-06	5.48E-05
³⁸ Ar	5.94E-04	2.65E-03	5.96E-04	8.14E-04	3.30E-03	5.65E-04	8.46E-04	4.18E-03
⁴⁰ Ar	1.83E-05	2.14E-05	1.68E-05	3.08E-05	3.06E-05	1.31E-05	3.48E-05	3.76E-05
³⁹ K	1.28E-04	3.31E-04	1.20E-04	1.66E-04	3.96E-04	1.12E-04	1.60E-04	5.09E-04
⁴⁰ K	4.18E-06	5.08E-06	3.73E-06	6.22E-06	6.32E-06	3.22E-06	6.54E-06	7.43E-06
⁴¹ K	1.10E-05	1.18E-05	1.13E-05	1.50E-05	1.50E-05	1.06E-05	1.67E-05	1.73E-05
⁴⁰ Ca	1.31E-03	1.33E-02	1.46E-03	1.48E-03	2.41E-02	1.48E-03	1.52E-03	3.16E-02
⁴¹ Ca	3.42E-06	1.25E-05	3.60E-06	4.20E-06	1.46E-05	3.54E-06	4.28E-06	1.97E-05
⁴² Ca	1.66E-05	7.32E-05	1.70E-05	2.26E-05	8.94E-05	1.64E-05	2.45E-05	1.14E-04
⁴³ Ca	5.02E-06	7.34E-06	4.86E-06	7.26E-06	9.69E-06	4.39E-06	7.88E-06	9.87E-06
⁴⁴ Ca	4.26E-05	4.52E-05	4.50E-05	5.40E-05	5.43E-05	4.37E-05	5.77E-05	6.01E-05
⁴⁵ Ca	2.75E-06	3.24E-06	2.53E-06	4.93E-06	4.91E-06	1.97E-06	5.71E-06	6.14E-06
⁴⁶ Ca	1.80E-06	2.24E-06	1.13E-06	2.61E-06	2.60E-06	6.92E-07	2.21E-06	2.67E-06
⁴⁸ Ca	3.32E-06	3.37E-06	3.68E-06	3.94E-06	3.93E-06	3.71E-06	4.18E-06	4.20E-06
⁴⁵ Sc	1.32E-09	9.92E-07	5.66E-10	2.05E-09	1.31E-06	3.08E-10	1.30E-09	2.63E-06
⁴⁵ Sc	2.56E-06	5.12E-06	1.85E-06	3.17E-06	4.00E-06	1.51E-06	2.41E-06	3.45E-06
⁴⁴ Ti	4.92E-10	1.41E-04	1.00E-10	1.82E-09	1.98E-04	2.69E-11	1.47E-10	2.29E-04
⁴⁵ Ti	7.20E-10	7.30E-07	3.58E-10	1.54E-09	3.99E-07	2.13E-10	8.98E-10	7.27E-07
⁴⁶ Ti	7.13E-06	3.42E-05	7.40E-06	9.36E-06	3.92E-05	7.13E-06	9.25E-06	5.35E-05
⁴⁷ Ti	6.03E-06	1.10E-05	6.25E-06	7.82E-06	1.41E-05	6.08E-06	7.92E-06	1.47E-05
⁴⁸ Ti	4.79E-05	5.00E-05	5.24E-05	5.46E-05	5.69E-05	5.28E-05	5.58E-05	5.88E-05
⁴⁹ Ti	9.23E-06	1.02E-05	9.61E-06	1.31E-05	1.31E-05	9.25E-06	1.46E-05	1.54E-05
⁵⁰ Ti	1.96E-05	2.39E-05	1.76E-05	3.03E-05	3.11E-05	1.48E-05	3.19E-05	3.69E-05
⁴⁷ V	1.87E-10	3.52E-07	8.41E-11	6.06E-10	1.81E-07	4.42E-11	2.01E-10	1.26E-06
⁴⁸ V	1.18E-09	5.04E-05	4.49E-10	3.89E-09	1.09E-04	2.99E-10	1.02E-09	3.44E-05

TABLE 5B—Continued

KE _∞	S30A 1.13	S30B 2.01	S35A 1.23	S35B 1.88	S35C 2.22	S40A 1.19	S40B 1.93	S40C 2.57
⁴⁹ V	2.34E-07	9.86E-06	7.00E-08	4.55E-07	3.22E-05	2.95E-08	1.18E-07	2.38E-05
⁵⁰ V	3.29E-07	5.88E-07	1.22E-07	4.42E-07	5.69E-07	6.44E-08	1.95E-07	6.13E-07
⁵¹ V	1.00E-05	1.10E-05	1.06E-05	1.21E-05	1.30E-05	1.04E-05	1.23E-05	1.39E-05
⁴⁸ Cr	6.78E-12	3.54E-04	1.23E-12	1.69E-11	5.24E-04	3.66E-13	2.74E-12	7.08E-04
⁴⁹ Cr	3.26E-11	1.02E-05	1.64E-11	8.87E-11	5.70E-06	1.24E-11	1.60E-11	2.19E-05
⁵⁰ Cr	1.52E-05	1.50E-04	1.68E-05	1.69E-05	2.72E-04	1.70E-05	1.70E-05	3.96E-04
⁵¹ Cr	8.11E-08	1.50E-05	1.39E-07	2.96E-07	6.80E-05	1.96E-07	2.01E-07	4.91E-05
⁵² Cr	3.25E-04	3.69E-04	3.60E-04	3.65E-04	4.52E-04	3.66E-04	3.75E-04	4.51E-04
⁵³ Cr	3.95E-05	4.00E-05	4.38E-05	4.52E-05	4.53E-05	4.47E-05	4.68E-05	4.72E-05
⁵⁴ Cr	3.97E-05	4.56E-05	3.84E-05	5.90E-05	5.92E-05	3.54E-05	6.50E-05	7.07E-05
⁵¹ Mn	1.16E-10	2.81E-05	7.62E-11	1.96E-10	1.50E-05	5.25E-11	1.53E-10	5.47E-05
⁵² Mn	9.42E-10	2.47E-04	6.00E-10	2.05E-09	2.34E-03	4.12E-10	1.27E-09	5.29E-04
⁵³ Mn	7.03E-08	2.79E-04	2.48E-08	1.53E-07	6.58E-04	1.32E-08	3.49E-08	7.97E-04
⁵⁴ Mn	1.04E-07	4.94E-06	2.97E-08	3.20E-07	8.98E-06	1.15E-08	4.40E-08	1.16E-05
⁵⁵ Mn	3.03E-04	3.04E-04	3.29E-04	3.33E-04	3.33E-04	3.29E-04	3.34E-04	3.36E-04
⁵² Fe	1.62E-12	3.35E-03	3.13E-13	4.08E-12	4.10E-03	1.02E-13	6.18E-13	7.47E-03
⁵³ Fe	4.09E-10	6.08E-05	4.59E-10	4.42E-10	1.17E-05	4.27E-10	4.02E-10	3.82E-05
⁵⁴ Fe	1.49E-03	1.34E-02	1.65E-03	1.64E-03	2.60E-02	1.67E-03	1.67E-03	3.63E-02
⁵⁵ Fe	1.25E-05	3.02E-04	2.58E-05	2.75E-05	7.67E-04	3.76E-05	3.79E-05	4.44E-04
⁵⁶ Fe	2.50E-02	2.53E-02	2.77E-02	2.78E-02	2.82E-02	2.83E-02	2.84E-02	2.90E-02
⁵⁷ Fe	9.98E-04	1.03E-03	1.17E-03	1.26E-03	1.27E-03	1.27E-03	1.41E-03	1.43E-03
⁵⁸ Fe	9.92E-04	1.21E-03	9.16E-04	1.52E-03	1.56E-03	8.79E-04	1.69E-03	1.95E-03
⁵⁹ Fe	3.97E-05	4.82E-05	5.46E-05	1.01E-04	1.04E-04	9.62E-05	2.31E-04	2.62E-04
⁶⁰ Fe	1.88E-05	2.38E-05	2.51E-05	5.59E-05	5.63E-05	3.09E-05	8.32E-05	1.05E-04
⁵⁵ Co	3.36E-09	1.67E-03	2.85E-09	4.49E-09	2.57E-03	2.37E-09	4.37E-09	3.69E-03
⁵⁶ Co	1.20E-07	1.21E-02	9.94E-08	1.57E-07	1.87E-02	8.02E-08	1.54E-07	5.86E-03
⁵⁷ Co	8.48E-07	1.79E-03	2.53E-07	1.65E-06	2.49E-03	1.04E-07	4.27E-07	8.82E-04
⁵⁸ Co	5.32E-07	1.25E-05	2.13E-07	1.46E-06	2.35E-05	1.06E-07	5.00E-07	1.82E-05
⁵⁹ Co	3.31E-04	3.99E-04	3.46E-04	5.31E-04	5.55E-04	2.98E-04	5.74E-04	6.55E-04
⁶⁰ Co	8.64E-05	1.06E-04	6.69E-05	1.41E-04	1.40E-04	5.87E-05	1.69E-04	1.89E-04
⁶¹ Co	2.89E-05	4.46E-05	1.97E-05	6.92E-05	7.21E-05	6.25E-06	3.61E-05	7.11E-05
⁵⁶ Ni	2.93E-11	4.40E-01	6.41E-12	5.83E-11	5.68E-01	2.27E-12	1.73E-11	6.91E-01
⁵⁷ Ni	1.32E-09	1.36E-02	1.25E-09	1.40E-09	1.72E-02	1.09E-09	9.97E-10	2.11E-02
⁵⁸ Ni	1.02E-03	2.26E-02	1.13E-03	1.13E-03	3.79E-02	1.15E-03	1.15E-03	3.57E-02
⁵⁹ Ni	1.85E-05	1.12E-03	2.16E-05	2.25E-05	1.49E-03	2.14E-05	2.09E-05	1.56E-03
⁶⁰ Ni	6.97E-04	1.09E-02	7.53E-04	9.06E-04	1.30E-02	7.14E-04	9.73E-04	1.31E-02
⁶¹ Ni	2.48E-04	7.86E-04	2.24E-04	3.70E-04	9.79E-04	1.89E-04	4.23E-04	7.19E-04
⁶² Ni	7.77E-04	2.48E-03	5.28E-04	1.05E-03	3.24E-03	4.10E-04	9.26E-04	2.11E-03
⁶³ Ni	2.97E-04	3.45E-04	3.04E-04	5.67E-04	5.64E-04	2.38E-04	7.10E-04	7.49E-04
⁶⁴ Ni	1.18E-03	1.48E-03	9.51E-04	1.88E-03	1.91E-03	7.15E-04	1.92E-03	2.27E-03
⁶⁵ Ni	5.25E-06	7.15E-06	7.17E-06	1.57E-05	1.62E-05	6.33E-06	2.43E-05	2.96E-05
⁵⁹ Cu	3.67E-13	4.91E-10	4.94E-13	6.00E-13	1.34E-12	4.15E-13	4.97E-13	9.80E-13
⁶⁰ Cu	7.36E-09	1.31E-05	5.07E-09	1.07E-08	2.44E-07	2.96E-09	1.04E-08	1.68E-03
⁶¹ Cu	5.83E-08	1.73E-04	2.39E-08	7.54E-08	2.02E-04	1.23E-08	5.86E-08	6.02E-04
⁶² Cu	2.12E-08	3.83E-05	8.66E-09	2.80E-08	5.57E-05	4.57E-09	1.81E-08	7.38E-05
⁶³ Cu	5.70E-05	9.30E-05	6.25E-05	8.03E-05	1.22E-04	5.93E-05	8.67E-05	1.28E-04
⁶⁴ Cu	6.22E-06	9.85E-06	4.50E-06	1.18E-05	1.20E-05	3.02E-06	1.00E-05	1.50E-05
⁶⁵ Cu	2.01E-04	2.63E-04	2.16E-04	3.86E-04	4.10E-04	1.91E-04	4.39E-04	5.51E-04
⁶⁶ Cu	4.06E-07	1.16E-06	5.39E-07	1.92E-06	2.36E-06	5.93E-07	2.17E-06	3.91E-06
⁶⁰ Zn	6.22E-15	4.70E-08	2.29E-15	7.18E-15	1.19E-13	9.28E-16	4.43E-15	2.31E-09
⁶¹ Zn	4.38E-15	5.39E-11	9.38E-16	3.60E-15	5.02E-15	3.40E-16	1.72E-15	7.25E-14
⁶² Zn	2.29E-09	2.13E-03	1.83E-09	3.92E-09	3.09E-03	1.36E-09	3.77E-09	4.14E-03
⁶³ Zn	6.54E-09	6.19E-08	5.96E-09	1.19E-08	5.26E-08	4.38E-09	1.45E-08	7.48E-06
⁶⁴ Zn	5.58E-05	1.15E-04	6.66E-05	8.18E-05	1.44E-04	6.56E-05	1.03E-04	1.75E-04
⁶⁵ Zn	7.04E-06	1.10E-05	1.01E-05	1.72E-05	2.02E-05	1.03E-05	2.52E-05	3.01E-05
⁶⁶ Zn	3.26E-04	4.57E-04	3.51E-04	5.94E-04	6.92E-04	3.06E-04	7.45E-04	9.00E-04
⁶⁷ Zn	1.09E-04	1.27E-04	1.16E-04	2.03E-04	2.02E-04	9.81E-05	2.64E-04	2.75E-04
⁶⁸ Zn	9.98E-04	1.32E-03	7.60E-04	1.64E-03	1.71E-03	5.28E-04	1.53E-03	1.98E-03
⁶⁹ Zn	7.74E-06	1.14E-05	1.16E-05	2.87E-05	2.95E-05	8.10E-06	4.01E-05	4.85E-05
⁶⁵ Ga	7.08E-10	1.07E-09	5.33E-10	1.23E-09	1.37E-09	3.53E-10	1.38E-09	8.31E-08
⁶⁶ Ga	1.86E-08	4.64E-05	1.29E-08	3.13E-08	6.08E-05	8.05E-09	3.48E-08	3.66E-05
⁶⁷ Ga	2.52E-07	4.90E-07	9.89E-08	4.06E-07	5.73E-07	4.56E-08	2.65E-07	5.10E-07
⁶⁸ Ga	1.74E-07	3.01E-07	8.86E-08	3.39E-07	3.59E-07	4.78E-08	2.54E-07	3.84E-07
⁶⁹ Ga	6.48E-05	8.62E-05	7.75E-05	1.41E-04	1.48E-04	7.31E-05	1.76E-04	2.23E-04
⁷⁰ Ga	5.15E-06	9.99E-06	7.67E-06	2.60E-05	2.72E-05	3.99E-06	2.30E-05	3.53E-05
⁶⁴ Ge	8.13E-18	1.10E-14	3.86E-18	1.19E-17	1.62E-17	1.81E-18	7.85E-18	1.71E-17
⁶⁵ Ge	4.78E-21	3.45E-20	1.26E-21	7.54E-21	1.28E-20	4.17E-22	3.79E-21	9.88E-21
⁶⁶ Ge	5.11E-12	9.92E-06	1.30E-12	7.67E-12	1.23E-05	4.60E-13	4.74E-12	5.17E-05
⁶⁷ Ge	1.09E-11	2.27E-11	2.63E-12	1.53E-11	1.83E-11	8.76E-13	7.67E-12	4.79E-09
⁶⁸ Ge	7.99E-09	3.52E-08	5.66E-09	2.11E-08	9.33E-08	3.91E-09	1.83E-08	6.73E-08
⁶⁹ Ge	1.87E-07	4.39E-07	8.69E-08	3.55E-07	4.96E-07	5.10E-08	2.30E-07	5.61E-07
⁷⁰ Ge	1.44E-04	2.66E-04	1.13E-04	2.71E-04	3.36E-04	9.12E-05	2.33E-04	4.26E-04
⁷¹ Ge	8.14E-04	9.71E-04	7.25E-04	1.39E-03	1.38E-03	5.57E-04	1.61E-03	1.74E-03
Mass	25.9	28.2	27.8	31.3	33.2	27.7	32.5	36.0

TABLE 6A
 PRODUCTION FACTORS 11–25 M_{\odot} MODELS; $Z = Z_{\odot}$

	S11A	S12A	S13A	S15A	S18A	S19A	S20A	S22A	S25A
¹ H	.81	.79	.77	.72	.68	.67	.65	.62	.58
² H	.17	.16	.15	.13	.12	.12	.11	.11	.09
³ He	1.24	1.18	1.16	1.08	1.02	1.01	.99	.96	.93
⁴ He	1.39	1.39	1.41	1.39	1.40	1.37	1.35	1.36	1.36
⁶ Li	.17	.16	.15	.13	.12	.12	.11	.11	.09
⁷ Li	6.07	5.02	7.50	6.08	4.69	4.18	3.96	3.47	3.45
⁹ Be	.18	.16	.15	.14	.12	.12	.11	.11	.10
¹⁰ B	.31	.23	.38	.34	.16	.14	.13	.12	.11
¹¹ B	13.96	12.38	14.47	19.43	24.14	32.44	21.69	20.53	21.96
¹² C	1.80	2.47	3.25	3.89	5.01	5.46	3.89	3.95	4.60
¹³ C	2.70	2.60	2.69	2.60	2.27	2.13	2.02	1.90	1.72
¹⁴ N	3.41	3.03	3.65	3.58	3.15	3.02	3.00	3.03	3.11
¹⁵ N	1.45	2.09	.89	2.52	2.17	1.72	1.89	2.02	2.31
¹⁶ O	1.45	2.04	2.44	5.19	7.19	8.72	11.20	12.36	14.69
¹⁷ O	13.71	12.64	11.80	11.16	12.97	12.72	12.14	11.73	11.30
¹⁸ O	16.50	35.93	9.17	15.52	42.00	43.19	30.26	8.88	5.05
¹⁹ F	3.26	7.96	1.89	6.24	13.92	3.81	3.87	5.98	14.26
²⁰ Ne	1.98	1.33	2.37	5.01	10.47	3.84	3.59	2.16	10.56
²¹ Ne	4.43	3.53	12.03	7.97	12.32	8.41	4.99	6.28	6.61
²² Ne	1.95	4.31	2.31	4.15	7.71	8.29	9.71	14.59	15.86
²³ Na	3.22	2.43	2.78	7.50	18.31	4.74	2.54	2.88	14.03
²⁴ Mg	1.84	1.48	2.75	3.81	6.57	2.86	3.37	4.02	8.90
²⁵ Mg	2.09	1.69	3.91	7.21	10.87	8.10	6.29	5.89	15.31
²⁶ Mg	2.07	2.05	3.81	6.17	7.83	8.66	7.50	8.25	18.23
²⁷ Al	2.11	1.82	2.72	5.83	10.53	3.80	3.80	7.21	18.26
²⁸ Si	3.41	12.95	7.72	12.40	12.85	24.77	24.46	27.14	20.89
²⁹ Si	1.93	2.97	3.64	5.32	6.57	7.32	9.89	17.80	14.55
³⁰ Si	3.04	3.01	7.20	9.64	14.08	8.54	13.72	29.74	23.16
³¹ P	2.42	10.18	5.09	7.23	9.47	14.65	21.59	30.57	16.91
³² S	2.52	17.81	5.67	11.73	8.45	19.12	21.30	21.67	15.48
³³ S	2.15	20.63	3.77	6.52	6.50	16.11	21.81	20.94	8.85
³⁴ S	3.46	14.95	7.03	7.52	12.07	32.92	65.98	44.52	16.57
³⁶ S	2.14	3.71	7.05	6.81	8.23	19.56	15.02	47.50	19.38
³⁵ Cl	2.02	56.83	3.62	7.59	6.73	36.83	46.32	57.55	12.00
³⁷ Cl	1.85	20.68	2.97	7.32	6.61	12.03	14.79	16.71	12.88
³⁶ Ar	2.24	26.26	4.96	11.83	6.89	15.63	18.79	18.07	12.60
³⁸ Ar	1.88	29.02	3.37	9.87	5.34	24.41	36.99	26.88	13.81
⁴⁰ Ar	3.22	8.82	11.62	9.22	11.03	18.01	12.57	40.60	24.19
³⁹ K	1.51	57.49	1.98	6.79	2.69	14.95	15.10	21.63	6.45
⁴⁰ K	3.22	202.80	3.81	8.82	11.56	107.29	94.70	298.23	26.94
⁴¹ K	1.94	56.67	2.40	5.92	2.49	6.05	7.29	8.64	4.83
⁴⁰ Ca	2.26	22.40	5.19	13.42	6.97	13.17	13.21	14.38	12.06
⁴² Ca	2.05	82.95	3.38	15.76	4.90	26.95	49.88	31.04	15.07
⁴³ Ca	1.86	12.53	1.84	2.55	1.75	6.69	13.06	14.52	2.76
⁴⁴ Ca	5.45	6.74	4.76	3.94	1.41	2.00	2.17	4.02	2.03
⁴⁶ Ca	2.65	1.93	11.59	8.75	6.54	10.12	6.67	20.70	13.82
⁴⁸ Ca	.98	.96	1.05	.96	.95	.92	.89	.87	.90
⁴⁵ Sc	3.18	12.23	4.60	5.77	2.96	7.11	14.96	18.68	4.93
⁴⁶ Ti	3.26	44.00	3.78	15.97	4.14	14.05	21.65	16.06	10.89
⁴⁷ Ti	1.56	4.93	1.67	1.81	1.31	2.12	4.39	3.93	1.69
⁴⁸ Ti	6.76	7.10	7.17	6.64	3.51	5.07	4.97	7.18	4.89
⁴⁹ Ti	3.70	6.05	5.06	6.00	5.08	6.96	8.61	8.59	6.85
⁵⁰ Ti	1.15	1.13	1.39	1.96	2.35	2.21	2.33	3.10	4.19
⁵⁰ V	1.70	17.95	3.58	7.50	7.31	10.61	96.98	68.77	13.74
⁵¹ V	1.83	5.85	3.94	5.78	5.62	8.05	8.41	8.18	7.24
⁵⁰ Cr	2.57	13.66	5.91	12.11	8.44	13.02	12.29	12.66	12.22
⁵² Cr	2.78	3.99	6.11	8.12	7.65	11.17	10.99	12.12	10.18
⁵³ Cr	2.30	4.03	5.74	8.13	8.06	11.46	10.98	11.66	10.34
⁵⁴ Cr	1.26	1.49	1.71	2.47	3.03	3.06	2.79	3.30	4.14
⁵⁵ Mn	2.19	3.33	4.54	5.55	5.17	7.07	6.50	7.27	6.23
⁵⁴ Fe	2.20	3.88	5.22	7.80	7.53	10.79	9.84	10.64	9.96
⁵⁶ Fe	7.07	4.42	10.75	8.14	4.34	5.91	5.06	9.62	5.74
⁵⁷ Fe	18.55	10.28	19.36	12.22	5.00	6.30	5.08	11.80	6.46
⁵⁸ Fe	2.32	2.37	3.84	6.17	8.92	7.10	5.95	8.52	10.86

TABLE 6A—Continued

	S11A	S12A	S13A	S15A	S18A	S19A	S20A	S22A	S25A
⁵⁹ Co	12.81	8.60	13.76	9.59	6.53	6.24	5.30	10.23	7.61
⁵⁸ Ni	33.46	12.17	18.51	9.13	3.94	4.48	3.64	8.78	4.63
⁶⁰ Ni	14.45	9.28	17.76	11.48	3.51	5.44	4.38	11.73	5.29
⁶¹ Ni	29.33	16.90	36.57	21.47	11.17	13.26	9.74	25.28	16.88
⁶² Ni	87.40	36.99	54.18	28.53	10.40	14.16	17.36	35.34	17.16
⁶⁴ Ni	3.23	3.26	5.58	15.59	19.97	20.42	21.92	34.38	53.85
⁶³ Cu	5.47	4.38	5.58	12.64	17.29	14.27	10.25	10.67	26.24
⁶⁵ Cu	5.06	2.89	12.53	14.36	17.70	18.72	25.26	29.81	40.06
⁶⁴ Zn	2.90	2.16	3.03	2.53	1.76	2.37	2.55	3.38	3.34
⁶⁶ Zn	10.11	5.73	7.71	8.14	8.91	12.68	25.96	24.45	25.51
⁶⁷ Zn	2.01	2.07	2.30	8.16	12.28	14.34	11.69	14.28	44.92
⁶⁸ Zn	2.22	2.27	3.42	11.89	15.67	18.57	35.95	48.58	74.35
⁷⁰ Zn	1.67	.14	4.74	10.81	12.11	29.24	8.42	15.69	42.49
⁶⁹ Ga	6.82	3.16	19.42	24.24	31.77	47.18	62.16	74.80	109.40
⁷¹ Ga	11.04	14.47	20.88	110.58	141.15	174.80	169.03	223.36	810.84
⁷⁰ Ge	3.52	4.71	6.79	25.58	32.47	51.19	219.69	246.45	141.67

¹³C is a product of the partial CN cycle in the deep envelope dredged up when the star becomes a red supergiant (Fig. 13). Its abundance is also too low to be considered a dominant product of massive stellar evolution, though its ratio to ¹²C and ¹⁴N is approximately solar for a wide range of masses (Table 6).

The abundant isotope of nitrogen, ¹⁴N, is also produced by the CNO cycle (in the deep envelope from the partial CN cycle), but again not enough to account for its solar abundance. Intermediate and low mass stars need to contribute. However, the production of ¹⁴N in massive stars (and for that matter of ^{12,13}C) is not negligible, accounting typically for about $\frac{1}{4}$ of their solar abundance (Table 4). It should also be noted that owing to the metallicity dependence of these secondary isotopes, solar like ratios of nitrogen to oxygen, say, could be produced in massive stars if the stars were super metal rich (by a factor of 4 or more).

¹⁵N here is chiefly a product of neutrino nucleosynthesis (Table 4), the dominant reactions being ¹⁶O($\nu_x, \nu'_x p$)¹⁵N and ¹⁶O($\nu_x, \nu'_x n$)¹⁵O. It does not seem that adequate synthesis occurs here to explain the full solar abundance (Paper III) and most of ¹⁵N must therefore come from another source, presumably classical novae. Again though, the abundance relative to the ^{12,13}C and ¹⁴N made in massive stars alone, is approximately solar (Table 6).

In massive stars of decreasing metallicity one would expect to produce similar amounts of ¹⁵N and ¹²C, since both are primary, but decreasing amounts of ¹³C and ¹⁴N. This expectation should be treated with caution, however, because in some massive stars it is possible that the convective helium shell penetrates into the hydrogen layer with the consequent production of large amounts of (primary) ¹⁴N and ¹³C. This has been observed to occur in our unpublished calculations (in 1992) of several very low-metallicity stars of 30 M_\odot and greater and also in one finely zoned 10 M_\odot model of solar metallicity. In the latter case a full convective link up between the helium convective shell and the fully convective hydrogen envelope occurred. However, both these occurrences are sensitive to uncertain details of convective overshoot and did not occur in any of the stars studied in this paper (our study here is restricted to $M \geq 11 M_\odot$).

The isotopes of oxygen are made in three different locations in the star and putting together the final correct isotopic pattern for oxygen poses both a challenge and an interesting constraint on the models. The isotope ¹⁶O is produced by both helium burning and neon burning and is the most abundant heavy element made in massive stars. Its synthesis is, to first order, independent of metallicity as well as the parameterization of the explosion (Tables 7 and 8). The less abundant isotopes, ¹⁷O and ¹⁸O are made, respectively, by the CNO tri-cycle during hydrogen shell burning and by alpha-capture on ¹⁴N during helium shell burning (Fig. 13). Their ejected abundances will therefore be linearly dependent upon the initial metallicity of the star.

4.3. Fluorine, Neon, and Sodium

Table 4 shows that most of the ¹⁹F produced in our models is a result of the neutrino process (Woosley & Haxton 1988), i.e., spallation of ²⁰Ne by μ and τ -neutrinos, ²⁰Ne($\nu_x, \nu'_x p$)¹⁹F and ²⁰Ne($\nu_x, \nu'_x n$)¹⁹Ne. This occurs in the regions of the star where neon is abundant, especially close to the collapsed core (Fig. 14). Part of the ¹⁹F so produced is destroyed in the shock (Woosley et al. 1990), but the remainder is adequate to produce the solar abundance relative to other species that must be made in massive stars (Paper III). Table 4 also shows that a small, but significant abundance of ¹⁹F is produced even without neutrinos. This occurs as a consequence of pre-explosive burning in the helium shell and the reaction sequence ¹⁴N(α, γ)¹⁸F followed by ¹⁸F($e^+ \nu$)¹⁸O(p, α)¹⁵N, ¹⁸F(n, p)¹⁸O(p, α)¹⁵N, or ¹⁸F(n, α)¹⁵N followed by ¹⁵N(α, γ)¹⁹F (see also Meynet & Arnould 1993). Protons come from ¹⁴N(n, p)¹⁴C. Our present study suggests that the neutrino contribution is about 4 times larger in a 25 M_\odot star (which should be typical).

The isotopes of neon, ²⁰Ne, ²¹Ne, and ²²Ne are made in the neon and helium layers (Fig. 14). ²⁰Ne is the principal product of carbon burning and remains abundant until partly consumed by neon burning. ²¹Ne is coproduced with ²⁰Ne though it has a significant, but lesser abundance in the helium shell. In the neon shell, ²¹Ne is a product of carbon burning where protons and (chiefly) neutrons capture on ²⁰Ne (e.g., Arnett & Thielemann 1985). In the helium shell production of ²¹Ne is due to neutron capture on ²⁰Ne, which is much more abundant

TABLE 6B
 PRODUCTION FACTORS 30–40 M_{\odot} MODELS; $Z = Z_{\odot}$

KE $_{\infty}$	S30A	S30B	S35A	S35B	S35C	S40A	S40B	S40C
	1.13	2.01	1.23	1.88	2.22	1.19	1.93	2.57
¹ H	.57	.53	.58	.52	.49	.57	.48	.44
² H	.08	.07	.08	.07	.06	.07	.06	.05
³ He	.95	.87	.97	.86	.81	.95	.81	.73
⁴ He	1.46	1.35	1.56	1.38	1.31	1.71	1.45	1.31
⁶ Li	.08	.07	.08	.07	.07	.07	.06	.06
⁷ Li	4.07	3.17	3.92	3.04	2.73	3.82	2.80	2.31
⁹ Be	.09	.08	.10	.08	.08	.09	.08	.07
¹⁰ B	.10	.10	.11	.10	.09	.11	.09	.08
¹¹ B	9.54	8.11	6.93	7.10	6.59	5.77	7.67	7.04
¹² C	3.64	3.39	3.58	3.37	3.18	3.74	3.68	3.37
¹³ C	1.68	1.54	1.63	1.45	1.37	1.61	1.37	1.23
¹⁴ N	3.63	3.34	4.05	3.59	3.40	4.61	3.92	3.54
¹⁵ N	1.46	1.76	1.03	1.99	2.01	.75	2.06	2.17
¹⁶ O	14.67	18.03	11.50	19.37	19.98	8.91	19.31	22.08
¹⁷ O	10.48	9.62	11.91	10.57	9.99	11.39	9.69	8.75
¹⁸ O	1.04	.94	.52	.46	.43	.39	.33	.30
¹⁹ F	10.03	9.40	14.48	17.77	16.45	15.00	22.61	20.01
²⁰ Ne	9.07	9.45	11.43	17.50	16.42	9.99	23.60	22.17
²¹ Ne	2.81	2.81	4.78	6.21	5.85	5.04	9.38	8.67
²² Ne	16.02	14.71	15.94	14.15	13.36	16.50	14.03	12.61
²³ Na	7.49	7.31	15.87	20.62	19.38	17.43	33.89	30.54
²⁴ Mg	15.90	19.39	8.56	17.77	17.78	4.78	13.73	16.71
²⁵ Mg	14.44	15.09	14.04	21.00	19.73	11.79	24.52	23.42
²⁶ Mg	16.19	16.40	17.91	24.91	23.41	15.73	31.58	29.54
²⁷ Al	26.15	30.98	18.37	34.97	33.95	12.81	34.23	36.82
²⁸ Si	5.77	17.16	2.29	5.48	19.81	1.37	2.57	23.85
²⁹ Si	26.87	35.03	10.91	27.65	28.52	4.32	14.80	23.55
³⁰ Si	32.48	51.95	10.37	32.53	41.52	3.77	11.71	36.39
³¹ P	23.26	32.51	9.16	22.80	25.74	4.96	11.77	22.35
³² S	1.35	8.95	.99	1.36	12.90	.93	.90	16.56
³³ S	2.09	6.26	1.26	2.67	6.34	1.12	1.18	7.20
³⁴ S	3.58	13.86	1.41	3.92	14.17	1.05	1.27	15.71
³⁶ S	26.88	31.54	17.59	30.65	29.67	13.67	29.20	30.79
³⁵ Cl	5.43	10.75	1.64	5.06	8.14	1.19	1.56	8.61
³⁷ Cl	8.53	9.94	8.89	11.94	12.53	8.14	14.66	15.46
³⁶ Ar	.86	7.34	.87	.82	11.16	.89	.77	13.99
³⁸ Ar	1.49	6.10	1.39	1.69	6.47	1.33	1.69	7.54
⁴⁰ Ar	28.67	30.77	24.48	39.75	37.34	19.28	43.19	42.12
³⁹ K	1.56	3.53	1.38	1.75	3.65	1.29	1.69	4.34
⁴⁰ K	29.11	32.45	24.18	35.78	34.36	20.99	36.23	37.22
⁴¹ K	2.12	3.27	2.05	2.35	3.41	1.95	2.48	3.93
⁴⁰ Ca	.85	7.90	.88	.79	12.11	.90	.78	14.67
⁴² Ca	1.62	6.29	1.52	1.85	6.55	1.43	1.90	7.65
⁴³ Ca	2.16	3.29	1.95	2.58	3.70	1.77	2.70	3.87
⁴⁴ Ca	1.15	4.62	1.14	1.21	5.33	1.11	1.24	5.63
⁴⁶ Ca	24.88	28.40	14.48	29.83	28.05	8.95	24.31	26.57
⁴⁸ Ca	.93	.86	.96	.91	.86	.97	.93	.84
⁴⁵ Sc	5.26	8.28	4.04	6.65	7.21	3.23	6.41	7.36
⁴⁶ Ti	1.37	5.60	1.26	1.49	5.43	1.21	1.39	6.80
⁴⁷ Ti	1.25	2.10	1.13	1.33	2.19	1.07	1.24	2.23
⁴⁸ Ti	.86	7.50	.88	.81	9.68	.89	.80	10.36
⁴⁹ Ti	2.24	6.56	2.13	2.65	9.42	2.05	2.77	10.38
⁵⁰ Ti	4.59	5.15	3.85	5.88	5.70	3.26	5.96	6.23
⁵⁰ V	13.71	22.50	4.74	15.23	18.55	2.51	6.46	18.37
⁵¹ V	1.03	5.09	1.02	1.05	7.68	1.02	1.02	8.68
⁵⁰ Cr	.79	7.18	.81	.73	11.04	.83	.70	14.79
⁵² Cr	.84	9.46	.87	.78	13.99	.89	.77	15.79
⁵³ Cr	.89	7.85	.92	.84	12.56	.94	.84	14.27
⁵⁴ Cr	3.53	4.11	3.17	4.35	4.72	2.94	4.59	5.24
⁵⁵ Mn	.91	6.07	.96	.87	8.34	1.00	.86	9.34
⁵⁴ Fe	.80	6.67	.83	.74	10.98	.85	.72	14.14
⁵⁶ Fe	.82	14.46	.85	.76	15.85	.87	.75	17.23
⁵⁷ Fe	1.35	20.33	1.47	1.41	22.15	1.61	1.52	22.75
⁵⁸ Fe	10.36	11.67	8.91	13.10	12.90	8.59	14.09	14.75
⁵⁹ Co	4.47	16.51	4.52	6.22	19.29	4.48	7.56	20.46
⁵⁸ Ni	.80	16.19	.82	.73	23.15	.84	.71	20.05

TABLE 6B—Continued

KE_{∞}	S30A	S30B	S35A	S35B	S35C	S40A	S40B	S40C
	1.13	2.01	1.23	1.88	2.22	1.19	1.93	2.57
^{60}Ni	1.58	20.07	1.55	1.80	20.34	1.48	1.92	21.30
^{61}Ni	12.42	41.40	10.18	16.31	43.99	8.23	16.42	44.97
^{62}Ni	10.80	59.29	6.84	12.03	69.42	5.34	10.26	63.20
^{64}Ni	62.65	72.35	47.12	82.67	79.31	35.64	81.15	86.84
^{63}Cu	23.75	26.99	22.89	35.91	35.93	18.71	42.57	42.68
^{65}Cu	31.14	37.66	31.66	50.51	50.82	28.34	56.73	64.05
^{64}Zn	2.31	4.33	2.51	2.86	4.61	2.46	3.37	5.15
^{66}Zn	21.41	31.02	21.52	32.36	39.38	18.87	39.05	46.89
^{67}Zn	48.12	51.36	47.63	74.13	69.75	40.47	92.70	87.14
^{68}Zn	94.90	115.15	67.37	128.81	127.01	47.01	115.85	135.71
^{70}Zn	14.84	26.43	20.59	62.02	61.29	10.78	52.82	73.23
^{69}Ga	70.77	87.66	80.93	136.96	135.80	74.17	167.92	190.40
^{71}Ga	1193.63	1308.63	990.57	1687.31	1581.88	765.50	1877.02	1833.20
^{70}Ge	128.50	217.85	94.15	200.02	234.77	76.27	165.47	273.54

than ^{21}Ne . Note that the synthesis of neon isotopes is not significantly affected by the explosion, nor are other isotopes up to at least silicon (Weaver & Woosley 1993). Because significant weak interactions during carbon burning (Arnett & Truran 1969; Arnett 1974) begin to change the neutron excess, the synthesis of ^{21}Ne declines with decreasing metallicity, but in a less than linear way. ^{22}Ne on the other hand is made in the helium shell by α -capture on ^{14}N and ^{18}O . Its production is thus directly proportional to the initial metallicity.

Both ^{23}Na and the longer lived radioactivity, ^{22}Na , are produced mainly by carbon burning. ^{23}Na is a primary product, but its final abundance is sensitive to the neutron excess. It thus scales in a less than linear way with metallicity (similar to ^{21}Ne). Some ^{23}Na , about 10% of the sodium in S25A, is produced in the hydrogen envelope as consequence of the neon-sodium cycle. Indeed the abundance of ^{23}Na in the convective envelope is a little over twice solar (Table 2) and this may have interesting consequences for the (Type IIp) supernova spectrum. Some ^{23}Na is also made by neutron capture on ^{22}Ne in

helium burning. ^{22}Na is made by proton capture on ^{21}Ne in the carbon shell. Interestingly, its ejected abundance is effectively doubled by neutrino irradiation (Table 4). This is because ^{22}Na is produced by proton capture on ^{21}Ne using protons spalled from abundant elements such as ^{16}O and ^{20}Ne by the neutrinos.

4.4. Magnesium and Aluminum (Including ^{26}Al)

Magnesium and aluminum are mostly the products of hydrostatic carbon and neon burning (e.g., Arnett & Thielemann 1985; Thielemann & Arnett 1985) and have their largest abundances in those shells (Fig. 15). ^{25}Mg and ^{26}Mg also have appreciable abundances in the outer carbon layer (5.7 to 6.4 M_{\odot} of Model S25A) as a result of the reactions $^{22}\text{Ne}(\alpha, n)^{25}\text{Mg}$ and $^{25}\text{Mg}(n, \gamma)^{26}\text{Mg}$ during helium burning. Within the region of unburned carbon their abundance should scale linearly with the initial metallicity [since their production scales with ^{14}N at the beginning of helium burning and ^{25}Mg is the main sink for

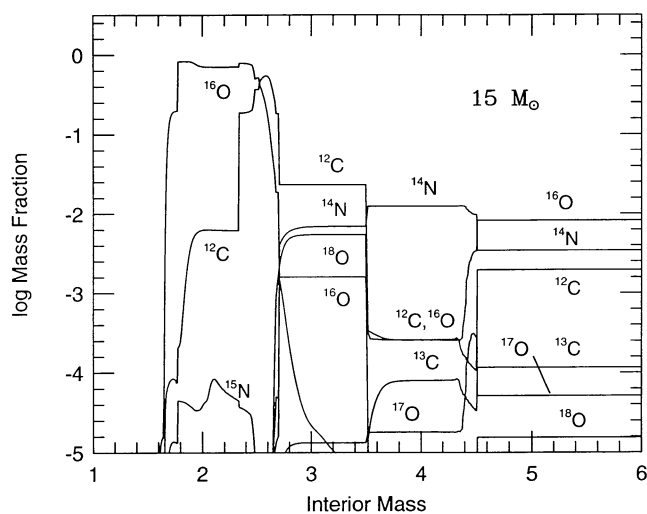


FIG. 13a

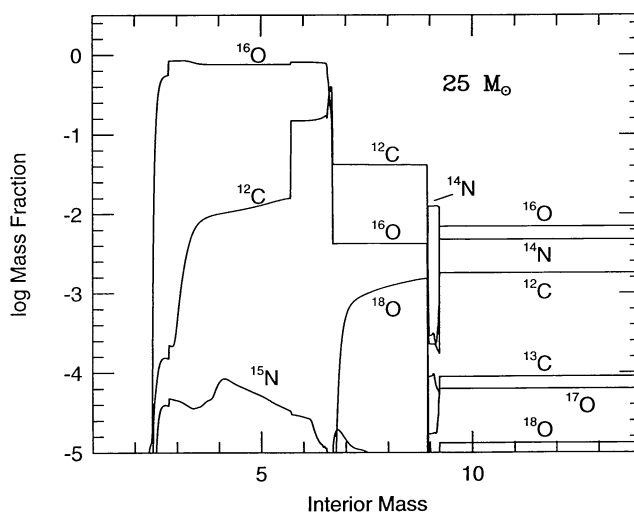


FIG. 13b

FIG. 13.—Mass fractions in 15 M_{\odot} (a) and 25 M_{\odot} (b) explosions of the isotopes of C, N, and O. The abundances, shown here only for the base of the hydrogen envelope, persist to the surface of the stars.

TABLE 7
NUCLEOSYNTHESIS—PRESUPERNOVA AND POST-EXPLOSION IN S25A

Isotope	PreSN	Post SN	Isotope	PreSN	PostSN
¹ H	9.40(0)	9.40(0)	⁴¹ K	3.26(-5)	2.93(-5)
² H	9.81(-5)	9.81(-5)	⁴⁰ Ca	5.76(-3)	1.67(-2)
³ He	6.29(-4)	6.29(-4)	⁴² Ca	2.93(-4)	1.46(-4)
⁴ He	8.63(0)	8.64(0)	⁴³ Ca	4.59(-6)	5.71(-6)
⁶ Li	1.41(-9)	1.41(-9)	⁴⁴ Ca	3.91(-5)	6.68(-5)
⁷ Li	2.12(-8)	7.44(-7)	⁴⁶ Ca	8.30(-7)	8.90(-7)
⁹ Be	3.78(-10)	3.84(-10)	⁴⁸ Ca	2.95(-6)	2.89(-6)
¹⁰ B	2.51(-9)	2.76(-9)	⁴⁵ Sc	3.93(-6)	4.42(-6)
¹¹ B	1.08(-8)	2.40(-6)	⁴⁶ Ti	4.63(-5)	5.61(-5)
¹² C	3.25(-1)	3.21(-1)	⁴⁷ Ti	6.45(-6)	8.13(-6)
¹³ C	1.45(-3)	1.45(-3)	⁴⁸ Ti	4.20(-5)	2.42(-4)
¹⁴ N	7.93(-2)	7.93(-2)	⁴⁹ Ti	8.41(-6)	2.58(-5)
¹⁵ N	3.31(-5)	2.33(-4)	⁵⁰ Ti	1.60(-5)	1.59(-5)
¹⁶ O	3.45(0)	3.25(0)	⁵⁰ V	8.10(-8)	2.93(-7)
¹⁷ O	1.01(-3)	1.01(-3)	⁵¹ V	1.03(-5)	6.29(-5)
¹⁸ O	2.72(-3)	2.52(-3)	⁵⁰ Cr	3.22(-5)	2.09(-4)
¹⁹ F	3.59(-5)	1.33(-4)	⁵² Cr	2.86(-4)	3.49(-3)
²⁰ Ne	4.86(-1)	3.94(-1)	⁵³ Cr	3.54(-5)	4.09(-4)
²¹ Ne	5.27(-4)	6.29(-4)	⁵⁴ Cr	3.49(-5)	4.16(-5)
²² Ne	4.81(-2)	4.76(-2)	⁵⁵ Mn	2.78(-4)	1.91(-3)
²³ Na	1.40(-2)	1.08(-2)	⁵⁴ Fe	1.33(-3)	1.64(-2)
²⁴ Mg	1.04(-1)	1.06(-1)	⁵⁶ Fe	2.18(-2)	1.55(-1)
²⁵ Mg	2.77(-2)	2.39(-2)	⁵⁷ Fe	8.74(-4)	4.25(-3)
²⁶ Mg	3.82(-2)	3.26(-2)	⁵⁸ Fe	8.86(-4)	9.26(-4)
²⁷ Al	2.59(-2)	2.44(-2)	⁵⁹ Co	4.21(-4)	5.90(-4)
²⁸ Si	2.37(-1)	3.15(-1)	⁵⁸ Ni	9.04(-4)	5.28(-3)
²⁹ Si	8.50(-3)	1.15(-2)	⁶⁰ Ni	1.50(-3)	2.39(-3)
³⁰ Si	5.16(-3)	1.26(-2)	⁶¹ Ni	2.51(-4)	3.35(-4)
³¹ P	2.13(-3)	3.18(-3)	⁶² Ni	5.95(-4)	1.10(-3)
³² S	9.82(-2)	1.41(-1)	⁶⁴ Ni	9.22(-4)	9.03(-4)
³³ S	6.54(-4)	6.57(-4)	⁶³ Cu	4.01(-4)	3.48(-4)
³⁴ S	1.14(-2)	7.13(-3)	⁶⁵ Cu	2.19(-4)	2.45(-4)
³⁶ S	4.20(-5)	4.19(-5)	⁶⁴ Zn	7.13(-5)	7.65(-5)
³⁵ Cl	4.82(-4)	7.00(-4)	⁶⁶ Zn	3.46(-4)	3.46(-4)
³⁷ Cl	3.01(-4)	2.54(-4)	⁶⁷ Zn	1.08(-4)	9.08(-5)
³⁶ Ar	1.32(-2)	2.25(-2)	⁶⁸ Zn	6.50(-4)	6.96(-4)
³⁸ Ar	1.09(-2)	4.90(-3)	⁷⁰ Zn	8.56(-6)	1.31(-5)
⁴⁰ Ar	1.59(-5)	1.41(-5)	⁶⁹ Ga	8.98(-5)	1.00(-4)
³⁹ K	5.37(-4)	5.16(-4)	⁷¹ Ga	5.80(-4)	4.92(-4)
⁴⁰ K	3.41(-6)	3.44(-6)	⁷⁰ Ge	8.90(-5)	1.41(-4)

TABLE 8
SENSITIVITY^a TO MASS CUT (25 M_{\odot} EJECTA^b)

Isotope	Piston (M_{\odot})	Piston Production	Eject (M_{\odot})	Eject Production
⁴ He	8.657(0)	1.35	8.637(0)	1.36
³³ S	6.63(-4)	8.81	6.57(-4)	8.85
³⁵ Cl	7.02(-4)	11.9	7.01(-4)	12.0
³⁹ K	5.38(-4)	6.63	5.16(-4)	6.45
⁴¹ K	3.04(-5)	4.95	2.93(-5)	4.83
⁴⁰ Ca	1.68(-2)	12.0	1.67(-2)	12.1
⁴² Ca	1.48(-4)	15.1	1.46(-4)	15.1
⁴³ Ca	8.29(-6)	3.96	5.71(-6)	2.76
⁴⁴ Ca	2.04(-4)	6.12	6.68(-5)	2.03
⁴⁵ Sc	6.28(-6)	6.91	4.42(-6)	4.93
⁴⁶ Ti	5.80(-5)	11.1	5.61(-5)	10.9
⁴⁷ Ti	1.17(-5)	2.41	8.13(-6)	1.69
⁴⁸ Ti	4.91(-4)	9.79	2.43(-4)	4.89
⁴⁹ Ti	3.12(-5)	8.17	2.58(-5)	6.85
⁵¹ V	6.52(-5)	7.41	6.29(-5)	7.24
⁵² Cr	3.82(-3)	11.0	3.49(-3)	10.2
⁵³ Cr	4.18(-4)	10.4	4.09(-4)	10.3
⁵⁵ Mn	2.34(-3)	7.54	1.91(-3)	6.23
⁵⁶ Fe	3.73(-1)	13.7	1.55(-1)	5.74
⁵⁷ Fe	1.44(-2)	21.5	4.25(-3)	6.46
⁵⁸ Fe	9.46(-4)	11.0	9.26(-4)	10.9
⁵⁹ Co	1.54(-3)	19.6	5.90(-4)	7.61
⁵⁸ Ni	3.25(-2)	28.1	5.28(-3)	4.63
⁶⁰ Ni	9.05(-3)	19.8	2.39(-3)	5.29
⁶¹ Ni	9.33(-4)	46.5	3.35(-4)	16.9
⁶² Ni	6.20(-3)	95.7	1.10(-3)	17.2
⁶³ Cu	3.87(-4)	28.8	3.48(-4)	26.2
⁶⁵ Cu	2.48(-4)	40.1	2.45(-4)	40.1
⁶⁴ Zn	1.16(-4)	5.00	7.65(-5)	3.34
⁶⁶ Zn	4.64(-4)	33.8	3.46(-4)	25.5
⁶⁷ Zn	9.12(-5)	44.5	9.08(-5)	44.9

^a Only those ejecta whose production factor changes by more than 0.1% are given.

^b Piston was at 1.78 M_{\odot} ; ejecta were external to 2.07 M_{\odot} .

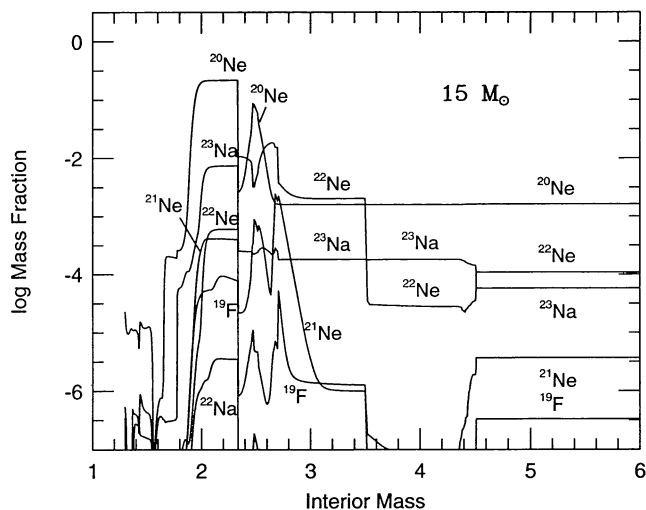


FIG. 14a

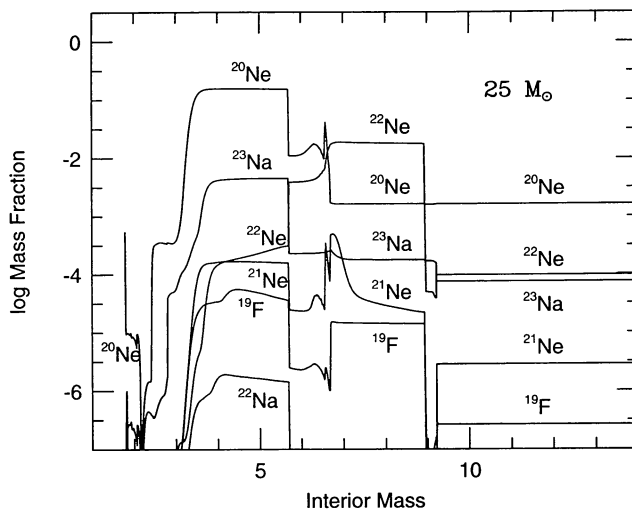


FIG. 14b

FIG. 14.—Mass fractions in the interiors of the $15 M_{\odot}$ (a) and $25 M_{\odot}$ (b) explosion of the isotopes of F, Ne, and Na

the neutrons from the (α, n) reaction]. In the neon shell (3.1 to $5.7 M_{\odot}$ for S25A) weak interactions have changed the neutron excess and the abundance of $^{25,26}\text{Mg}$ and ^{27}Al are not so sensitive to the initial metallicity.

The long-lived radioactivity, ^{26}Al , is synthesized, in Model S25A, mostly in the neon shell ($1.0 \times 10^{-4} M_{\odot}$), but an appreciable quantity is also made in the hydrogen shell and dredged up by the red giant envelope ($2.5 \times 10^{-5} M_{\odot}$ exterior to $8.9 M_{\odot}$). In Model S15A, ^{26}Al also exists in the outer part of the helium core (3.5 to $4.5 M_{\odot}$) where it is an unburned residual of hydrogen burning. In all cases the ^{26}Al is produced by $^{25}\text{Mg}(p, \gamma)^{26}\text{Al}$. The synthesis of ^{26}Al in the neon shell is sensitive to the treatment of convection during the last hour of the star's life as the fragile isotope is made in the superheated neon shell (see also § 4.9) and mixed out to cooler regions where its decay is inhibited. The synthesis of ^{26}Al is also augmented in the neon shell by neutrino irradiation ($\sim 40\%$ in S25A) owing to extra

proton capture on ^{25}Mg with the protons liberated by the neutrino flux interacting with ^{16}O and ^{20}Ne .

4.5. The Intermediate Mass Elements—Silicon Through Scandium

The production of intermediate mass elements, mostly by oxygen burning, is sensitive to a variety of factors, among them the rate for $^{12}\text{C}(\alpha, \gamma)^{16}\text{O}$ and the treatment of semiconvection (Weaver & Woosley 1993; Thielemann & Arnett 1985); the treatment of convection and convective overshoot mixing during the last stages of shell oxygen burning (Bazan & Arnett 1994; Arnett 1994); the density structure near the iron core (i.e., the stellar mass); the initial location of the mass cut; and finally the amount of mass that falls back in the explosion (Table 8; § 3.2). These species are produced by a combination of hydrostatic oxygen shell burning and explosive oxygen

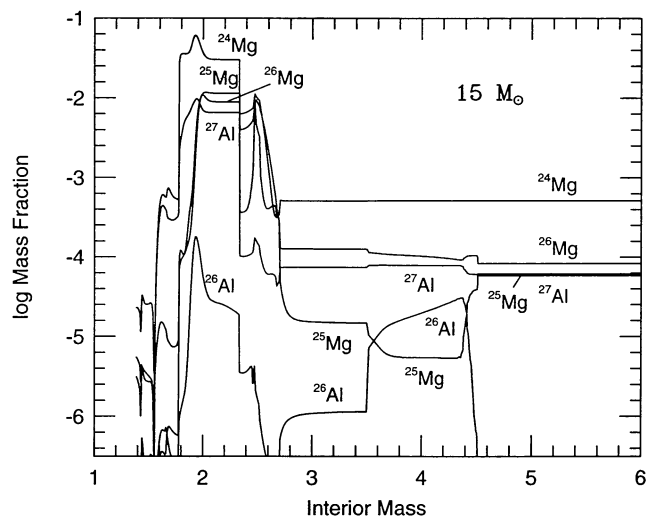


FIG. 15a

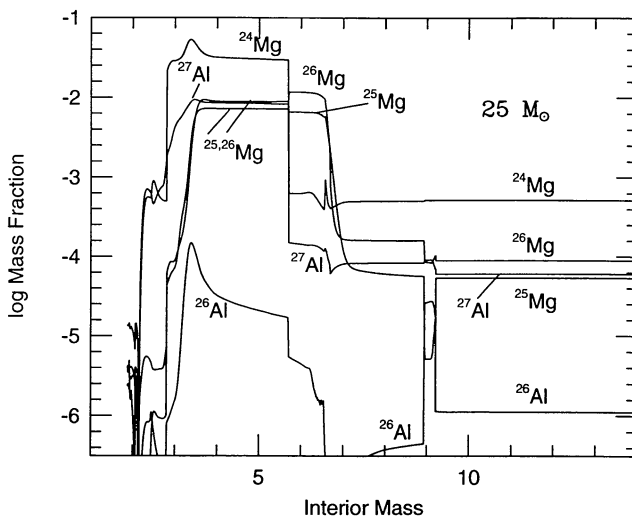


FIG. 15b

FIG. 15.—Mass fractions in the interiors of the $15 M_{\odot}$ (a) and $25 M_{\odot}$ (b) explosions of the isotopes of Mg and Al

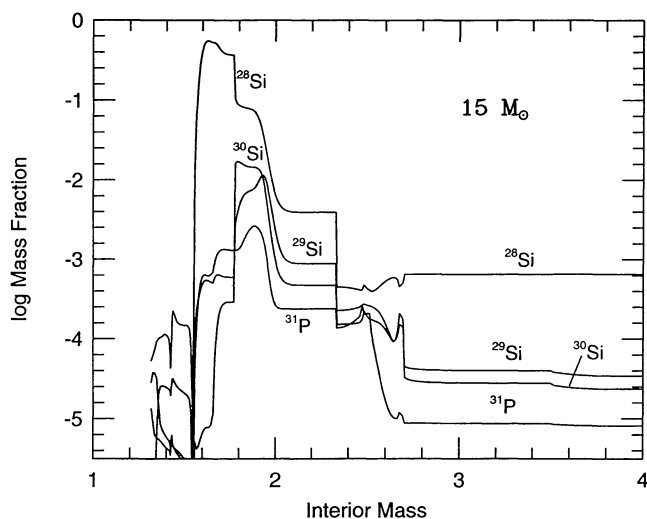


FIG. 16a

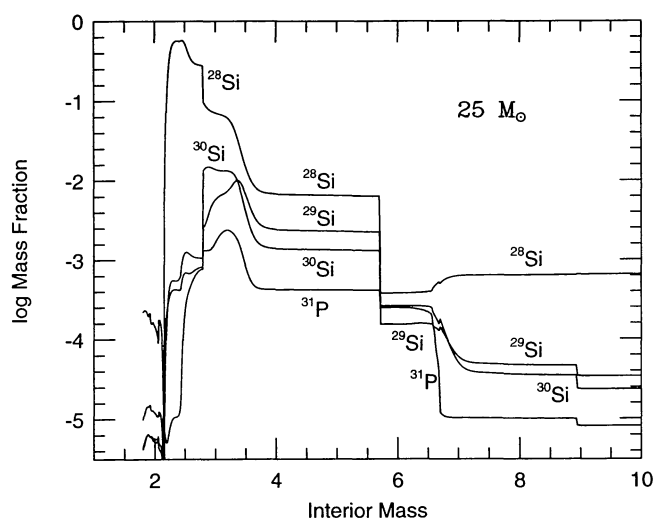


FIG. 16b

FIG. 16.—Mass fractions in the interiors of the $15 M_{\odot}$ (a) and $25 M_{\odot}$ (b) explosions of the isotopes of Si and P

burning in proportions that vary from star to star (Weaver & Woosley 1993). There can be appreciable “implosive” burning as the temperature at the base of the oxygen shell rises in some models, notably S25A, during the last minutes of the star’s life (§ 4.6). There is also substantial tradeoff between the silicon and sulfur, for example, that get burned into iron group isotopes, and the same species created, farther out, by explosive oxygen burning (Table 7). In the pre-supernova Model S25A, for example, the mass of ^{28}Si in the star exterior to the iron core is $0.359 M_{\odot}$ and the base of the silicon shell, i.e., the edge of the iron core, is at $1.78 M_{\odot}$. In the exploded version, the total ^{28}Si mass is 0.315 , not much different; but the location where the sum of silicon and sulfur mass fractions first exceeds 0.5 is now at $2.22 M_{\odot}$. Interior to this, most of the mass is ^{56}Ni . In fact, most of what was the silicon shell in the pre-explosive star (in Model S25A) is first burned to ^{56}Ni and then falls back to be-

come part of the compact remnant. In some stars of other masses and in other $25 M_{\odot}$ stars using different rates for $^{12}\text{C}(\alpha, \gamma)^{16}\text{O}$, the fraction of silicon that is made in the pre-explosive star and survives ejection is much greater (Weaver & Woosley 1993). So the fraction of each intermediate mass isotope that comes from explosive and hydrostatic burning is difficult to unravel. In fact, this fraction is sensitive to all the factors mentioned at the beginning of this paragraph.

The neutron-rich isotopes of silicon, $^{29,30}\text{Si}$, and ^{31}P are produced in both the oxygen burning and neon burning shells and their ejection is less sensitive to the explosion mechanism (Fig. 16; Table 7). Other rare neutron-rich isotopes, ^{36}S , ^{40}Ar , ^{40}K , and $^{43,46}\text{Ca}$, are also made in the neon and carbon shells (Figs. 16–20) and are also insensitive to the explosion mechanism, but are sensitive to the initial metallicity.

Other intermediate-mass isotopes directly attributable to ox-

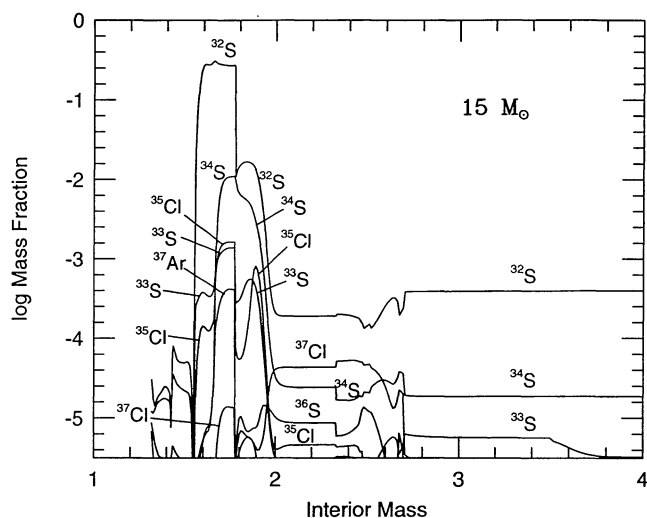


FIG. 17a

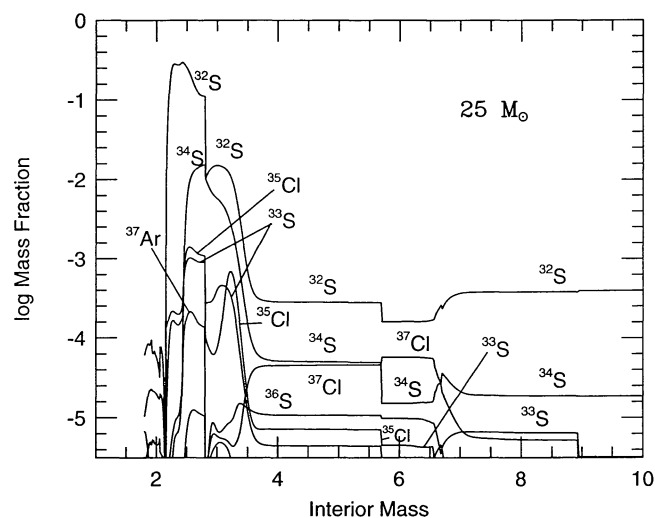


FIG. 17b

FIG. 17.—Mass fractions in the interiors of the $15 M_{\odot}$ (a) and $25 M_{\odot}$ (b) explosion of the isotopes of Cl and S and their progenitors

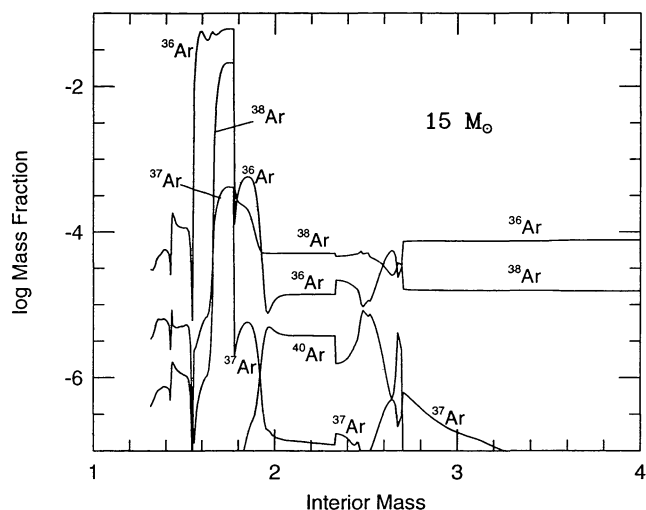


FIG. 18a

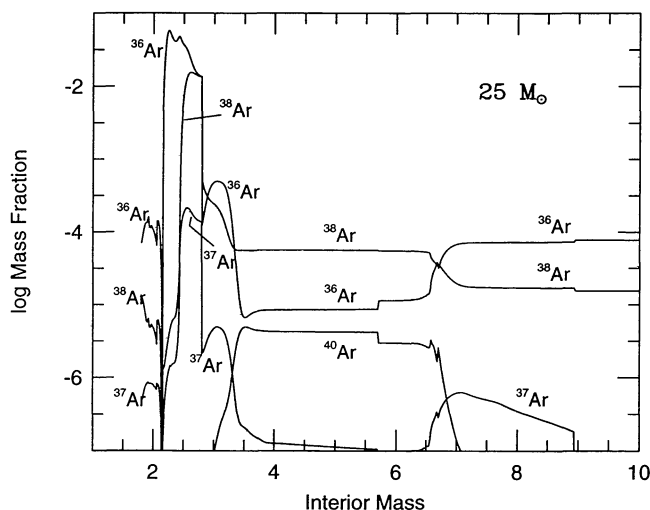


FIG. 18b

FIG. 18.—Mass fractions in the interiors of the $15 M_{\odot}$ (a) and $25 M_{\odot}$ (b) explosions of the isotopes of Ar

xygen burning are $^{32,33,34}\text{S}$, $^{35,37}\text{Cl}$, $^{36,38}\text{Ar}$, $^{39,41}\text{K}$, and $^{40,42}\text{Ca}$. Beginning with chlorine, the contribution to the solar abundances from progenitors that are unstable in the laboratory to electron capture and positron decay becomes appreciable (see, e.g., Woosley, Arnett, & Clayton 1973), first in isolated cases, but increasingly so as one goes higher in mass. The reason for this is simple. High temperature is required to surmount the Coulomb barrier, but at high temperature and moderate density, weak interactions are not sufficiently efficient in the given time to change the pre-existing neutron-proton (near) equality. At the same time the valley of beta stability differs from the line $Z = N$ above calcium.

Thus ^{37}Cl is made both as ^{37}Ar in oxygen burning and as itself in neon burning (Fig. 17). Similarly, ^{41}K is made as ^{41}Ca in oxygen burning (Fig. 19), but also as itself in neon burning. Scandium, ^{45}Sc , is made both as the radioactive progenitor ^{45}Ti

in explosive oxygen and silicon burning, and as itself during neon burning (Fig. 21).

The nucleus ^{44}Ca is a special case. It is made almost entirely as radioactive ^{44}Ti in the α -rich freezeout that characterizes material just outside the mass cut. As such, its production is most sensitive to details of the explosion mechanism—especially the location of the mass cut (Figs. 20 and 29, Tables 7 and 8, § 4.7) and the entropy (high entropy favors an alpha-rich freezeout and ^{44}Ti production). ^{44}Ti will only be ejected by those Type II supernovae that also eject large quantities of ^{56}Ni and other iron group species. ^{44}Ti is also produced in some models for Type Ia supernovae in which helium detonation plays an important role (Woosley, Taam, & Weaver 1986; Woosley & Weaver 1994).

Finally we note that ^{48}Ca is not produced in quantities appropriate to its solar abundance in any of our models. The req-

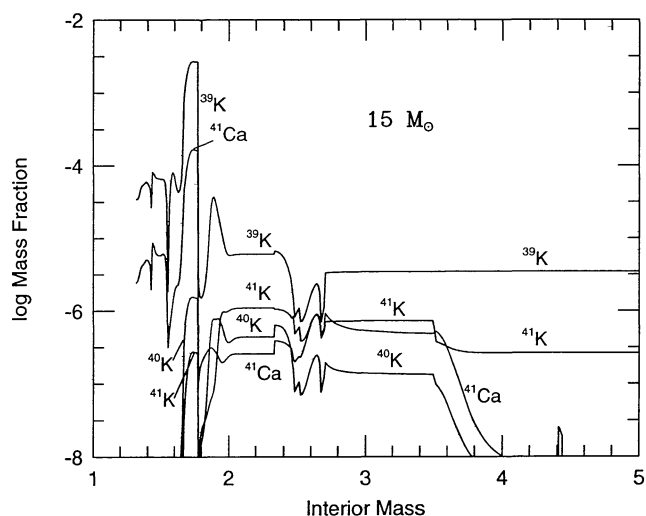


FIG. 19a

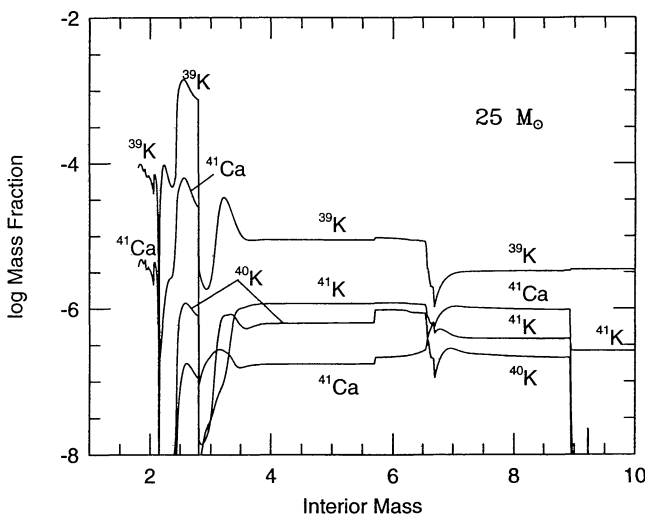


FIG. 19b

FIG. 19.—Mass fractions in the interiors of the $15 M_{\odot}$ (a) and $25 M_{\odot}$ (b) explosions of the isotopes of K (and their progenitors)

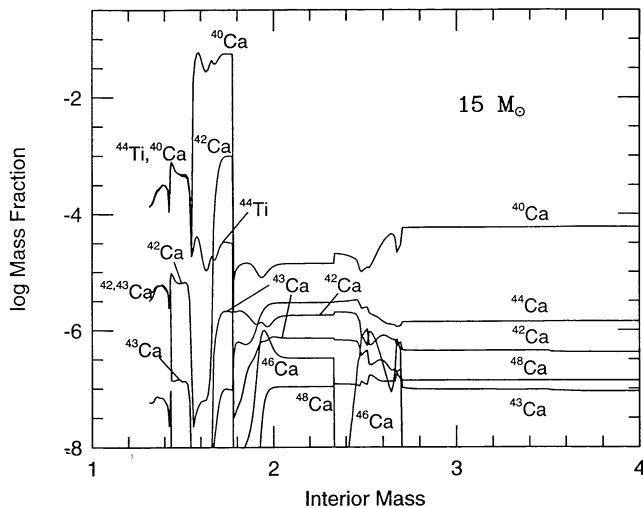


FIG. 20a

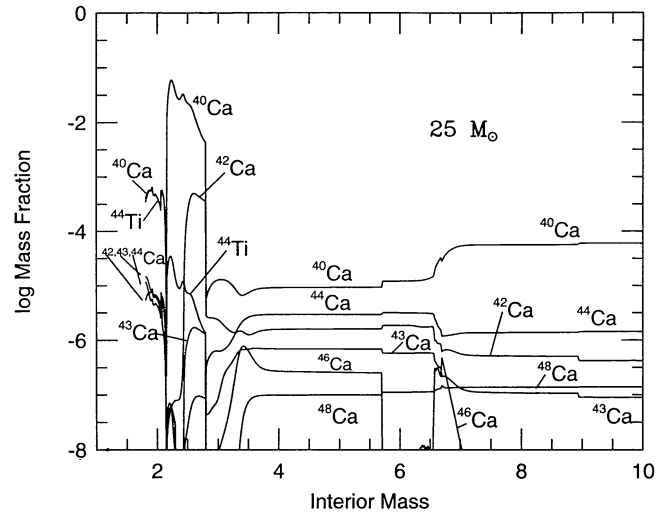


FIG. 20b

FIG. 20.—Mass fractions in the interiors of the $15 M_{\odot}$ (a) and $25 M_{\odot}$ (b) explosions of the isotopes of Ca

uisite conditions, $Y_e \sim 0.42$ and a low entropy freezeout from nuclear statistical equilibrium (Hartmann, Woosley, & El Eid 1985), do not exist here. One expects a small amount of mass to be ejected with small Y_e from the proto-neutron star, but this material has very high entropy (e.g., Woosley et al. 1994) and will be alpha-rich. It will not make ^{48}Ca . We believe that ^{48}Ca , along with several other neutron-rich isotopes of the iron group— ^{50}Ti , ^{54}Cr , ^{66}Zn , and part of ^{58}Fe —are made in Type Ia supernova of a special variety, namely those that ignite a carbon deflagration very near the Chandrasekhar mass (Woosley & Eastman 1995; Woosley et al. 1995).

4.6. The Lower Iron Group—Titanium Through Iron

As we move upwards in mass, the nucleosynthesis becomes increasingly sensitive to the changes that occur during the explosion (Table 7) and consequently, uncertain. It also becomes less sensitive to the initial metallicity of the star as electron capture during the advanced burning stages erodes memory of the neutron excess generated from $^{14}\text{N}(\alpha, \gamma)^{18}\text{F}(e^+ \nu)^{18}\text{O}$ during helium burning. Each even mass element has a number of isotopes which may come from different processes. It may be helpful to keep in mind in what follows that, for Model S25A, peak temperatures between 3 and 4 billion K occur in the explosion between 2.35 and $2.75 M_{\odot}$ (Fig. 9). We call this explosive oxygen burning. Peak temperatures above this, and therefore masses interior to this, are referred to as explosive silicon burning ($4 \lesssim T_9 \lesssim 5$), or nuclear statistical equilibrium (if $T_9 \gtrsim 5$).

Titanium is a good example. ^{46}Ti is produced mostly by explosive oxygen burning (Fig. 21; Woosley et al. 1973). The small amount of ^{47}Ti made here is produced by explosive oxygen burning, but also by explosive silicon burning. Interior to $2.5 M_{\odot}$ ^{47}Ti is made as ^{47}V which has mostly decayed ($\tau_{1/2} = 32.6$ m) by the time Figure 21 was edited (note that the time of the edit, 2.5×10^4 s unless otherwise noted, is not always the time of the last nuclear update since the reaction network ceased to be evolved once the temperature fell below 10^7 K, a

zone dependent occurrence. This may cause some inconvenience when tracing short-lived radioactive progenitors, for which we apologize). Exterior to $2.5 M_{\odot}$, ^{47}Ti is made as itself. ^{48}Ti and ^{49}Ti are made as radioactive ^{48}Cr and ^{49}Cr produced by explosive silicon burning (Fig. 22), and to a lesser extent, explosive oxygen burning. In Figure 22, ^{49}Cr has already decayed ($\tau_{1/2} = 42.3$ m) to ^{49}V . ^{50}Ti is not made in appreciable quantities in these calculations.

All six titanium isotopes may also have an appreciable component from Type Ia supernovae (Woosley & Weaver 1994; Woosley & Eastman 1995; Woosley et al. 1995). This is particularly important for ^{47}Ti and ^{50}Ti which are underproduced here.

^{50}V is made, as itself, both by explosive oxygen burning and by neon burning (Fig. 23). Interior to $2.8 M_{\odot}$, ^{51}V in Model S25A is made as both ^{51}Cr and ^{51}Mn by explosive oxygen and silicon burning. Outside of $2.8 M_{\odot}$, a lesser amount of ^{51}V is made as itself.

^{50}Cr is made, as itself, by explosive oxygen and silicon burning (Fig. 23) while the abundant isotopes of chromium, ^{52}Cr , and ^{53}Cr are made chiefly as $^{52,53}\text{Fe}$ during explosive silicon burning (Fig. 24). ^{54}Cr is underproduced here. What little is made comes from the neon and carbon shells where it was made at an earlier time, by the helium burning *s*-process. Most of ^{54}Cr probably comes from Type Ia supernovae (Woosley & Eastman 1995; Woosley et al. 1995).

The single isotope of manganese, ^{55}Mn , is made mostly in explosive silicon burning and nuclear statistical equilibrium as ^{55}Co (Fig. 25).

Iron is another element whose isotopes reflect the operation of several different nucleosynthetic processes and sites (it is interesting the modern situation is quite contrary to early arguments regarding the synthesis of iron in nuclear statistical equilibrium, e.g., Hoyle 1946; Fowler & Hoyle 1964). ^{54}Fe is made by explosive oxygen and silicon burning (Fig. 25), but only at a sufficiently low entropy that all α -particles reassemble during the expansion. Otherwise ^{58}Ni would be made instead (§ 4.7; Woosley et al. 1973). ^{56}Fe and ^{57}Fe are produced as radioactive

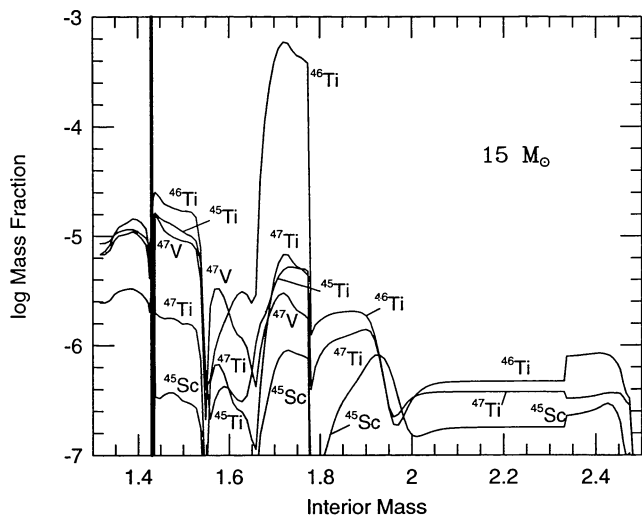


FIG. 21a

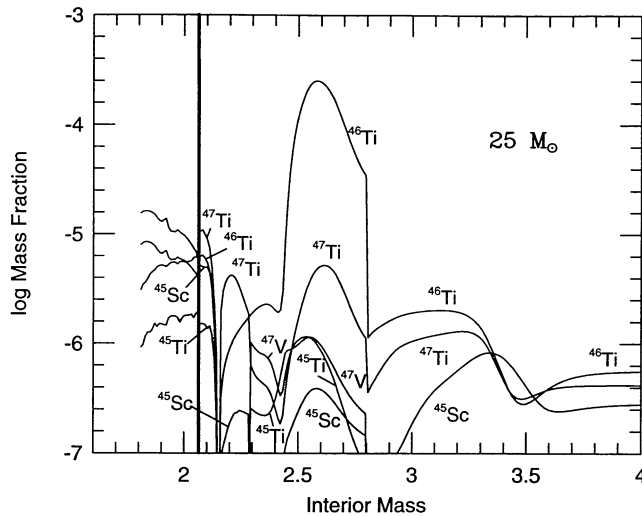


FIG. 21b

FIG. 21.—Mass fractions in the interiors of the $15 M_{\odot}$ (a) and $25 M_{\odot}$ (b) explosions of ^{45}Sc and $^{46,47}\text{Ti}$ (and their progenitors). The dark vertical bar denotes the final mass cut (Table 3).

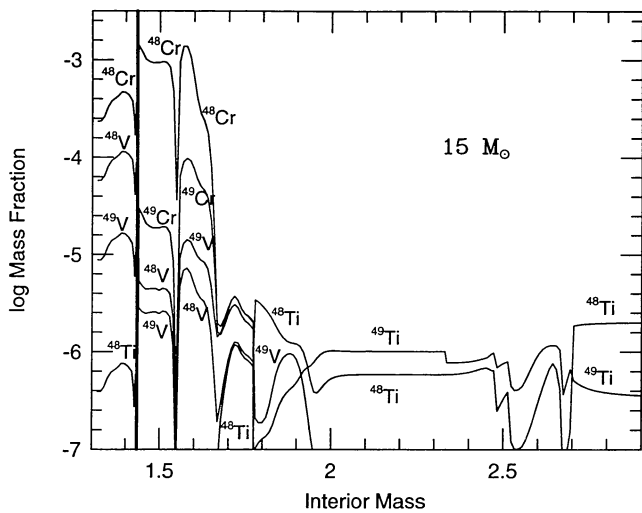


FIG. 22a

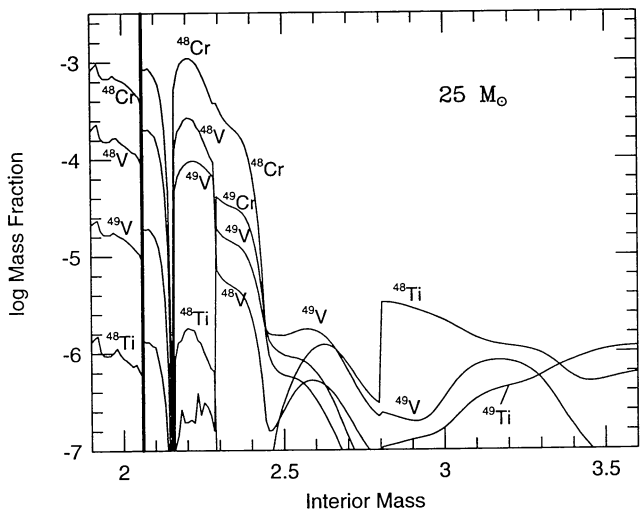


FIG. 22b

FIG. 22.—Mass fractions in the interiors of the $15 M_{\odot}$ (a) and $25 M_{\odot}$ (b) explosion of the $^{48,49}\text{Ti}$ (and their progenitors). The dark vertical bar denotes the final mass cut (Table 3).

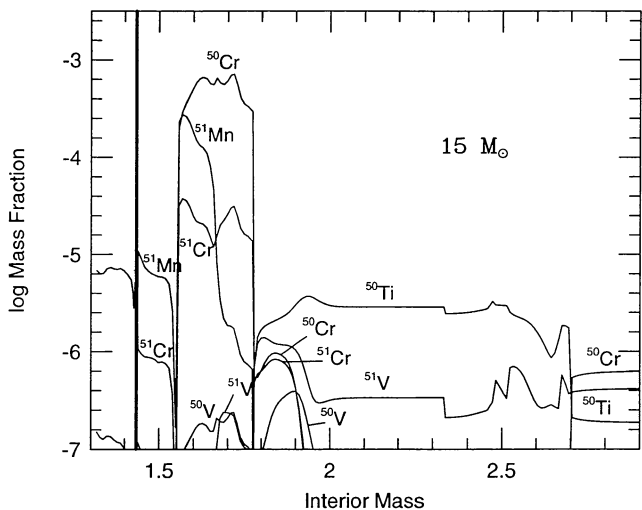


FIG. 23a

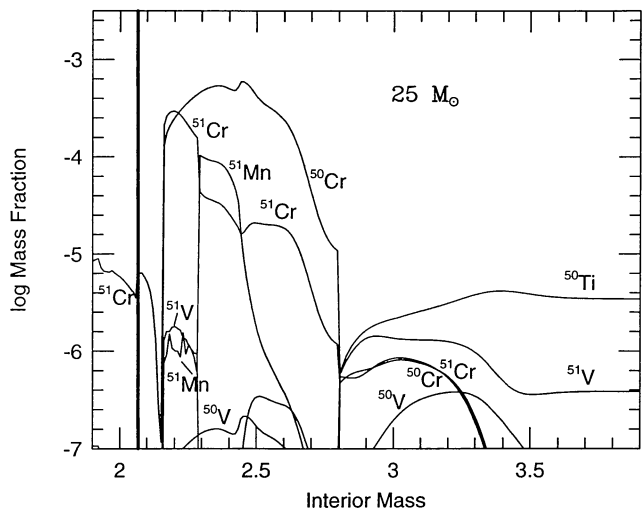


FIG. 23b

FIG. 23.—Mass fractions in the interiors of the $15 M_{\odot}$ (a) and $25 M_{\odot}$ (b) explosions of ^{50}Ti , $^{50,51}\text{V}$, and ^{50}Cr (and their progenitors). The dark vertical bar denotes the final mass cut (Table 3).

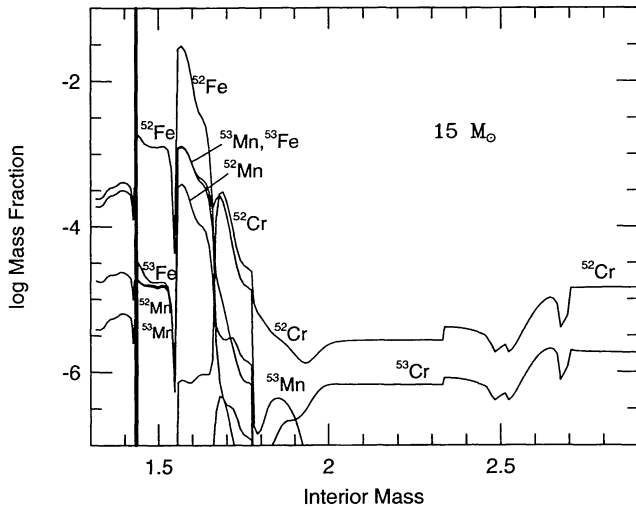


FIG. 24a

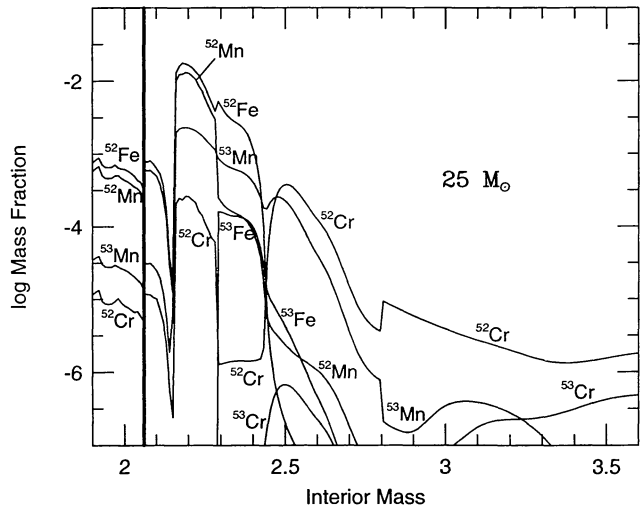


FIG. 24b

FIG. 24.—Mass fractions in the interiors of the $15 M_{\odot}$ (a) and $25 M_{\odot}$ (b) explosions of $^{52,53}\text{Cr}$ (and their progenitors). The dark vertical bar denotes the final mass cut (Table 3).

^{56}Ni and ^{57}Ni (Figs. 25 and 28, § 4.7). These isotopes require high temperatures ($T_9 \gtrsim 4$) for their synthesis and are made when either oxygen or silicon-rich layers with a low neutron excess (typically $Y_e \gtrsim 0.498$) are heated to this temperature (Table 7). The production of these species is thus very sensitive to fall back (Table 8; § 3.2) and the location of the piston. They are produced whether the material ejected is alpha-rich or not (though the synthesis of ^{57}Ni is favored if the alpha-fraction is large; § 4.7). ^{58}Fe is a product of the s -process operating during helium core and shell burning (Table 9; Fig. 26).

The long-lived ($\tau_{1/2} = 1.5 \times 10^6$ yr) radioactive nucleus ^{60}Fe is of interest to gamma-ray astronomy (Clayton 1971; Timmes et al. 1995c). The nucleus is produced in massive stars in two locations—the neon shell, mostly prior to explosion, and the

base of the helium shell (Fig. 27). In the neon shell ^{60}Fe is synthesized in the presupernova star as small quantities of ^{22}Ne and $^{25,26}\text{Mg}$ are mixed into a superheated neon burning region ($T_9 \approx 1.8$) along with iron seed that has already seen an s -process during helium burning. The light isotopes provide neutrons which capture sufficiently rapidly on ^{58}Fe to bridge the intermediate radioactivity at ^{59}Fe . At the base of the helium shell, ^{60}Fe is made by a mild r -process during explosive helium burning (§ 4.10). A substantial abundance of ^{60}Co ($\tau_{1/2} = 5.27$ yr) is also produced (Fig. 27 and Table 5). This may also be of interest to the gamma-ray astronomers and to the power budgets of young supernova remnants. Synthesis here is chiefly in the superheated neon convective shell by the same neutron flux that makes ^{60}Fe .

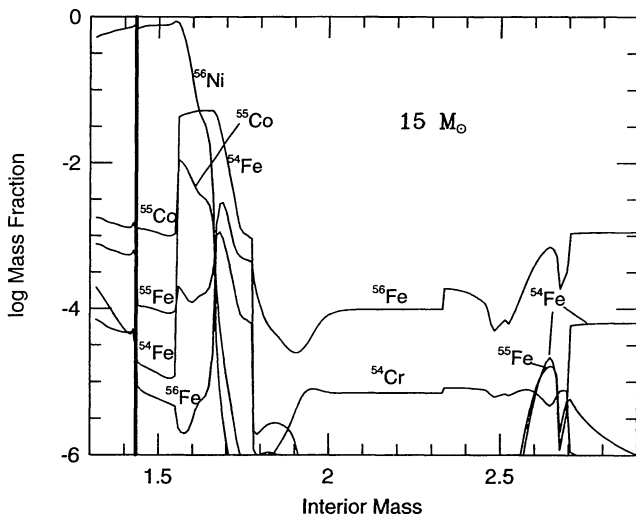


FIG. 25a

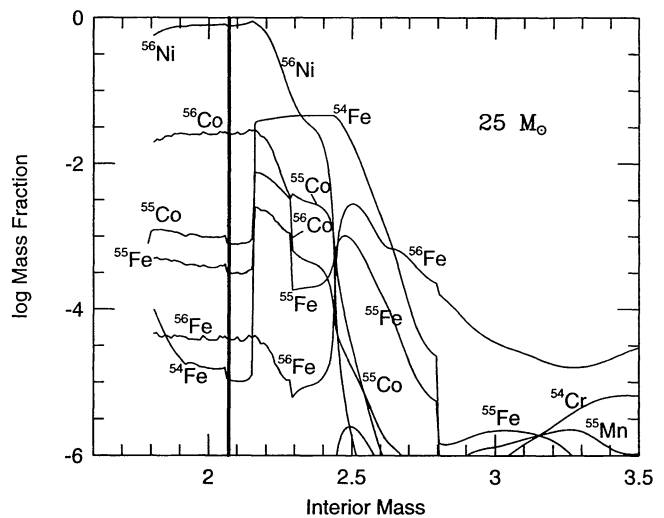


FIG. 25b

FIG. 25.—Mass fractions in the interiors of the $15 M_{\text{ex}}$ (a) and $25 M_{\odot}$ (b) explosions of ^{54}Cr , $^{54,56}\text{Fe}$, ^{55}Mn and their progenitors

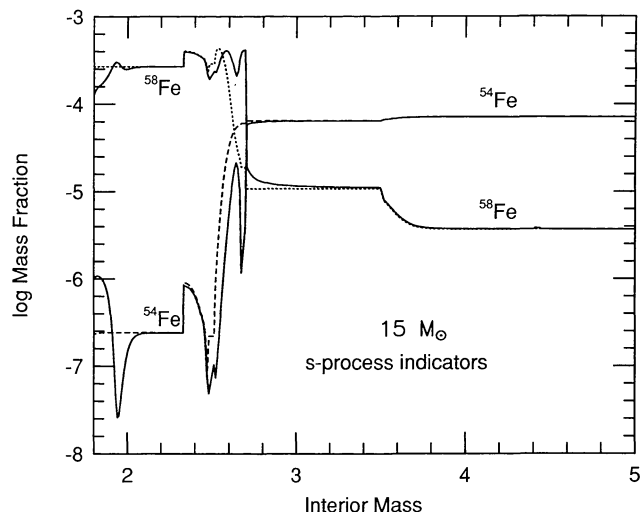


FIG. 26a

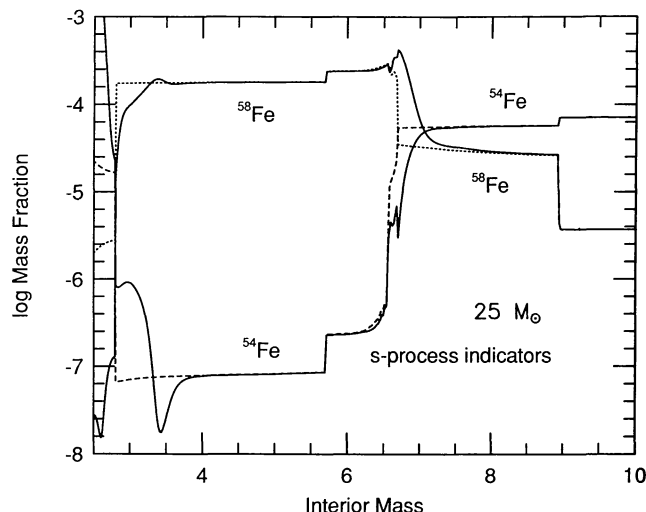


FIG. 26b

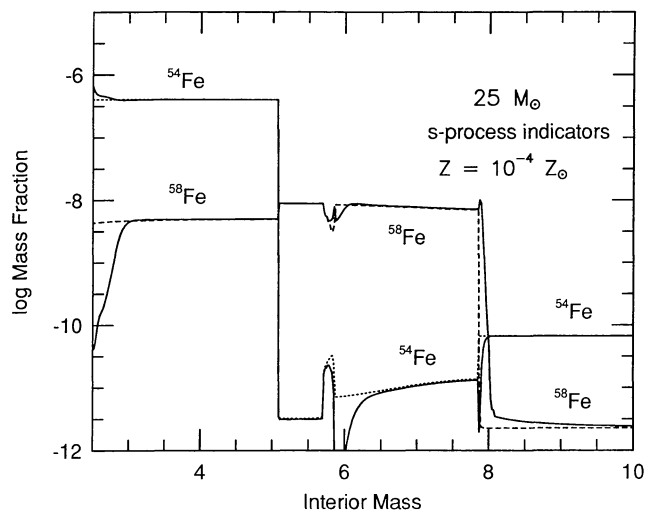


FIG. 26c

FIG. 26.—Mass fractions of ^{54}Fe and ^{58}Fe in the interiors of $15 M_{\odot}$ (a) and $25 M_{\odot}$ (b) explosions and presupernova stars. These two nuclei are *s*-process indicators. Where ^{54}Fe has its solar value, -4.15 in (a) and (b), no *s*-process has occurred. Where ^{58}Fe is large, there has been extensive *s*-processing. The abundance of ^{54}Fe can, in some circumstances, be used to obtain the integrated neutron exposure (§ 4.8). The dashed and dotted lines show the abundances of these two isotopes in the persupernova star; solid lines are post-explosion values. In (a) and (b) there is a substantial depletion of ^{54}Fe and enhancement of ^{58}Fe in the explosion of both models at the base of the helium shell (2.54 and 6.56 in S15A and S25A, respectively; § 4.10). This is due to explosive helium burning. Fig. 26c shows similar abundances for the explosion of a very low-metallicity $25 M_{\odot}$ star, Model U25A.

4.7. The Upper Iron Group—Nickel, Copper, and Zinc

Generally speaking, the isotopes in the mass range 57 to 66 originate from two processes—neutron capture on iron group nuclei during helium burning and later burning stages (Table 9) and the alpha-rich freezeout from material heated to in excess of 5×10^9 K in the deepest layers ejected. Many isotopes have contributions from both, making their evolution sensitive in a complicated way to the hydrodynamics of the explosion

(Tables 3 and 7), especially the amount of mass that falls back (Table 8), and, in the case of species made by neutron capture, the initial metallicity of the star.

The species ^{44}Ca (^{44}Ti), ^{57}Fe , and ^{58}Ni are unambiguously products of the alpha-rich freezeout (Tables 7 and 8; Figs. 28 and 29). ^{60}Ni is also made in appreciable quantities in the alpha-rich freezeout as ^{60}Zn (which has already partly decayed in Fig. 29), but has a non-negligible contribution from neutron capture (Table 9; Fig. 30). Which is the larger fraction depends sensitively upon fall back (Table 8). In Model S25 at 100 s after the explosion and external to $2.07 M_{\odot}$, the masses of ^{60}Zn , ^{60}Cu , and ^{60}Ni in S25A were $9.1 \times 10^{-4} M_{\odot}$, $5.4 \times 10^{-4} M_{\odot}$, and $8.7 \times 10^{-4} M_{\odot}$, respectively. The stable ^{60}Ni is chiefly in the oxygen-neon layer, a residual of helium burning.

The other neutron-rich isotopes of nickel, $^{61,62,64}\text{Ni}$, as well as ^{59}Co , are produced, in Model S25A, mainly by neutron capture, especially during helium burning (Table 9; Fig. 30), though there is an important contribution from the alpha-rich freezeout in each case (Figs. 28 and 29). For example, at age 100 s, there are $7.9 \times 10^{-5} M_{\odot}$ of ^{61}Zn and ^{61}Cu external to the mass cut and $2.1 \times 10^{-4} M_{\odot}$ of ^{61}Ni . The former comes from the alpha-rich freezeout, the latter from neutron capture farther out. Similarly there are $3.6 \times 10^{-4} M_{\odot}$ of ^{62}Zn and $6.6 \times 10^{-4} M_{\odot}$ of ^{62}Ni . There are $1.5 \times 10^{-4} M_{\odot}$ of ^{59}Cu and ^{59}Ni and $3.3 \times 10^{-4} M_{\odot}$ of ^{59}Co . In each case the stable isotope, or at least that portion not present in the original star, has been produced by neutron capture and the proton-rich progenitors have been produced by the alpha-rich freezeout. A small shift of the mass cut can dramatically affect the production of any of these species, even changing qualitatively the process responsible for their synthesis.

The isotope ^{64}Ni is produced chiefly by the *s*-process during helium core and shell burning (Table 9; Figs. 31 and 32) and ejected in the oxygen-neon shell.

^{63}Cu is produced as three different isotopes in three separate locations. Stable ^{63}Cu is made by the *s*-process in the helium shell. However, much of the ^{63}Cu abundance that existed in the star following helium burning is destroyed during later burning stages (Table 9). The largest contributor to ^{63}Cu in the $25 M_{\odot}$

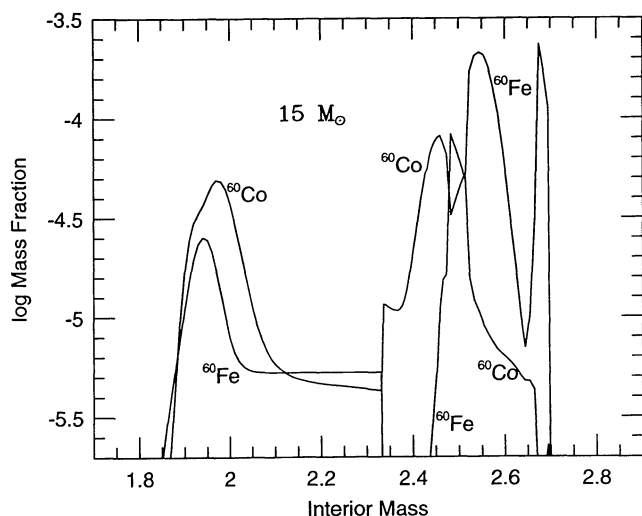


FIG. 27a

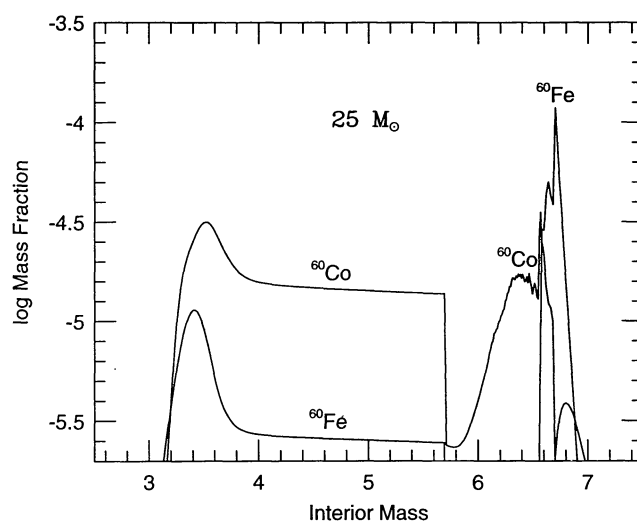


FIG. 27b

FIG. 27.—Mass fractions in interiors of the $15 M_{\odot}$ (a) and $25 M_{\odot}$ (b) explosions of ^{60}Fe and its daughter, ^{60}Co . Both are interesting candidates for γ -ray astronomy.

star is, in fact, ^{63}Ni ($\tau_{1/2} = 100$ yr), which is made by neutron capture on ^{62}Ni during helium and carbon shell burning and ejected in the neon-oxygen layer. Some ^{63}Zn is produced explosively in the deepest layers (Fig. 31) of the explosion though, in the present calculation, most of this falls back into the core. At 100 s after the explosion (much less than the half-life of any of these isotopes) and external to the mass cut at $2.07 M_{\odot}$, there are $2.3 \times 10^{-6} M_{\odot}$ of ^{63}Zn ; $6.6 \times 10^{-5} M_{\odot}$ of ^{63}Cu ; and $2.8 \times 10^{-4} M_{\odot}$ of ^{63}Ni in the $25 M_{\odot}$ supernova. Almost all this ^{63}Ni is in the oxygen-neon shell.

^{65}Cu is made chiefly as itself by neutron capture during he-

lium burning and to a much lesser extent as ^{65}Zn in the alpha-rich freezeout. At 100 s, the abundances external to $2.07 M_{\odot}$ of ^{65}Zn and ^{65}Cu are $9.5 \times 10^{-6} M_{\odot}$ and $2.1 \times 10^{-4} M_{\odot}$, respectively. Contributions from ^{65}Ge and ^{65}Ga are near $2 \times 10^{-7} M_{\odot}$. The material that falls back into the remnant contains negligible mass 65 ($2.9 \times 10^{-6} M_{\odot}$). There is also a small contribution from ^{65}Ni (Fig. 31).

^{64}Zn is also produced by neutron capture during helium burning (Table 9; Fig. 32). To a lesser extent, ^{64}Zn is made as unstable ^{64}Ge in an α -rich freezeout in the innermost zones (Fig. 31). In this particular explosion, however, most of the

TABLE 9
ABUNDANCES^a OF SELECT ISOTOPES IN $25 M_{\odot}$ AT VARIOUS EVOLUTIONARY POINTS

Isotope	ZAMS	Carbon Ignition	Carbon Depletion	Oxygen Depletion	Pre-SN	Post-Exp. ^b (2.5×10^4 s)
^{56}Fe	2.70(-2)	2.19(-2)	2.18(-2)	2.17(-2)	2.18(-2)	2.19(-2)
^{57}Fe	6.58(-4)	7.69(-4)	8.65(-4)	8.77(-4)	8.70(-4)	9.05(-4)
^{58}Fe	8.52(-5)	1.18(-3)	1.21(-3)	1.04(-3)	8.86(-4)	9.22(-4)
^{59}Fe		5.08(-11)	8.85(-7)	2.00(-6)	4.82(-5)	8.52(-5)
^{60}Fe		5.10(-8)	5.92(-8)	2.67(-6)	8.00(-6)	2.10(-5)
^{59}Co	7.74(-5)	4.94(-4)	4.95(-4)	4.83(-4)	3.55(-4)	3.31(-4)
^{60}Co		2.72(-9)	3.73(-6)	7.16(-6)	5.07(-5)	5.36(-5)
^{58}Ni	1.14(-3)	9.07(-4)	8.93(-4)	8.89(-4)	9.04(-4)	5.28(-3)
^{59}Ni		6.11(-6)	1.29(-5)	1.42(-5)	1.80(-5)	1.74(-4)
^{60}Ni	4.52(-4)	9.99(-4)	9.96(-4)	8.87(-4)	1.44(-3)	2.31(-3)
^{61}Ni	1.98(-5)	2.59(-4)	2.63(-4)	2.93(-4)	2.41(-4)	2.82(-4)
^{62}Ni	6.40(-5)	6.75(-4)	6.76(-4)	5.95(-4)	5.95(-4)	8.29(-4)
^{63}Ni		5.61(-8)	8.35(-6)	3.56(-4)	3.29(-4)	2.79(-4)
^{64}Ni	1.68(-5)	9.99(-4)	1.00(-3)	1.01(-3)	9.20(-4)	8.98(-4)
^{63}Cu	1.33(-5)	2.58(-4)	2.51(-4)	9.46(-4)	7.25(-5)	6.94(-5)
^{65}Cu	6.10(-6)	3.30(-4)	3.31(-4)	2.97(-4)	1.96(-4)	2.14(-4)
^{64}Zn	2.29(-5)	1.59(-4)	1.60(-4)	9.28(-5)	6.78(-5)	6.98(-5)
^{66}Zn	1.36(-5)	4.40(-4)	4.42(-4)	4.38(-4)	3.41(-4)	3.35(-4)
^{67}Zn	2.02(-6)	9.43(-5)	9.53(-5)	1.34(-4)	1.08(-4)	9.06(-5)
^{68}Zn	9.36(-6)	5.79(-4)	5.83(-4)	6.65(-4)	6.50(-4)	6.96(-4)
^{69}Ga	9.14(-7)	7.07(-5)	7.15(-5)	1.02(-4)	6.63(-5)	7.31(-5)
^{70}Ge	9.96(-7)	1.03(-4)	1.04(-4)	1.23(-4)	8.90(-5)	1.41(-4)
^{71}Ge		4.06(-4)	4.11(-4)	6.56(-4)	5.80(-4)	4.92(-4)

^a In solar masses external to $2.07 M_{\odot}$.

^b Does not include radioactive progenitors that have not decayed at 25×10^4 s.

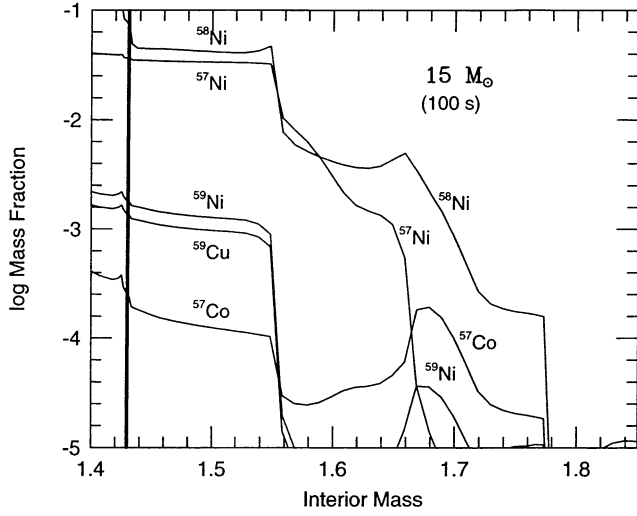


FIG. 28a

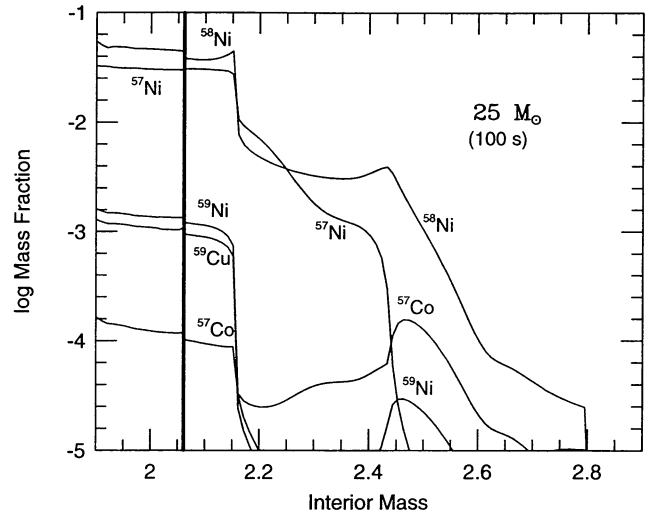


FIG. 28b

FIG. 28.—Mass fractions in the interiors of the $15 M_{\odot}$ (a) and $25 M_{\odot}$ (b) explosions of the progenitors of ^{57}Fe and ^{59}Co . Note that unlike previous figures, this and subsequent ones are evaluated at 100 s to emphasize some short lived radioactivities. The dark vertical bar denotes the final mass cut (Table 3).

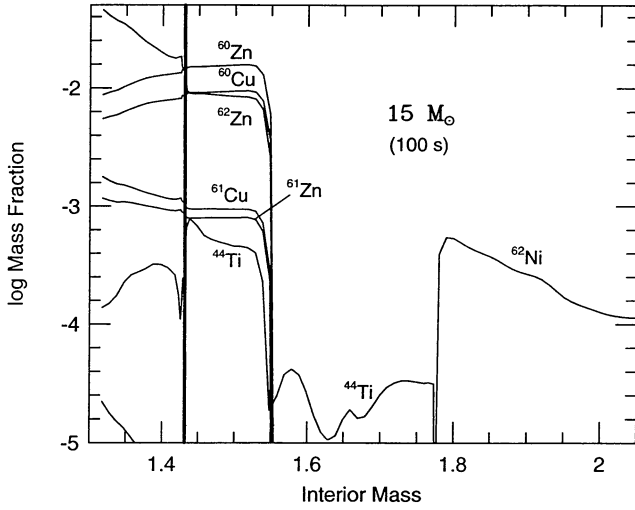


FIG. 29a

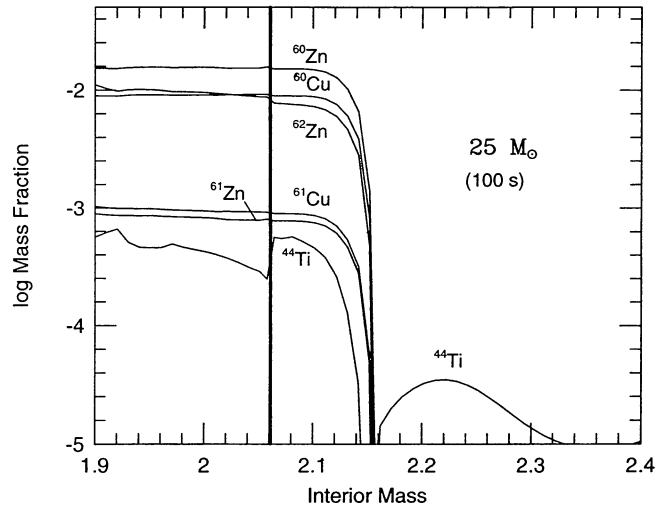


FIG. 29b

FIG. 29.—Mass fractions in interiors of the $15 M_{\odot}$ (a) and $25 M_{\odot}$ (b) explosions of several products of the α -rich freeze out. ^{44}Ti will decay to ^{44}Ca . The others make $^{60,61,62}\text{Ni}$. The dark vertical bar denotes the final mass cut (Table 3).

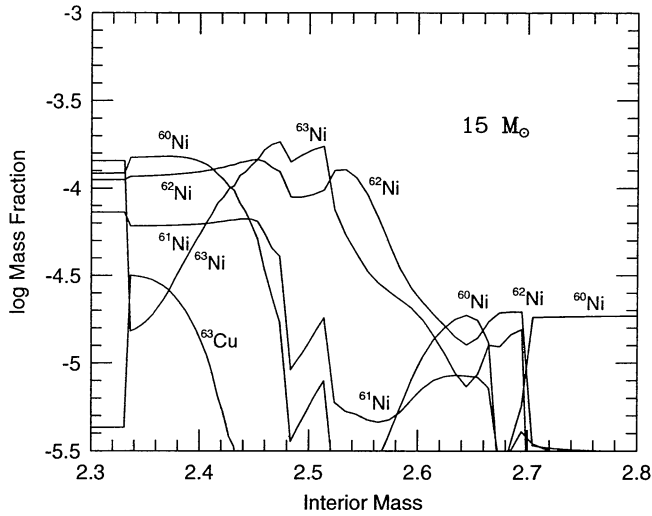


FIG. 30a

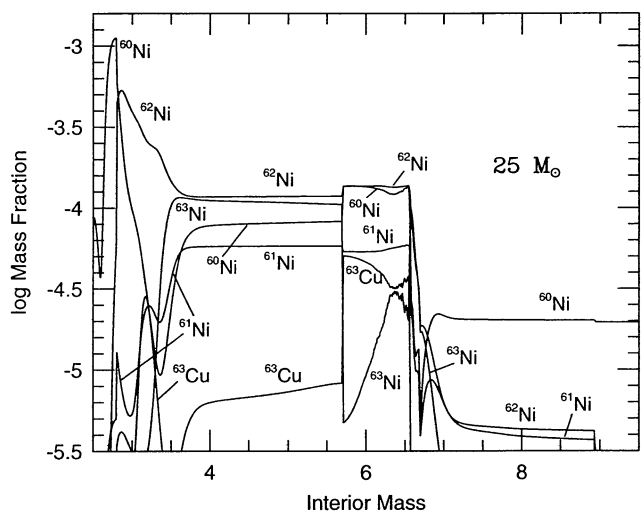


FIG. 30b

FIG. 30.—Mass fractions in the interiors of the $15 M_{\odot}$ (a) and $25 M_{\odot}$ (b) explosions of the progenitors of $^{60,61,62}\text{Ni}$ and ^{63}Cu . Here the plots emphasize those species having substantial production by neutron capture farther out in the star.

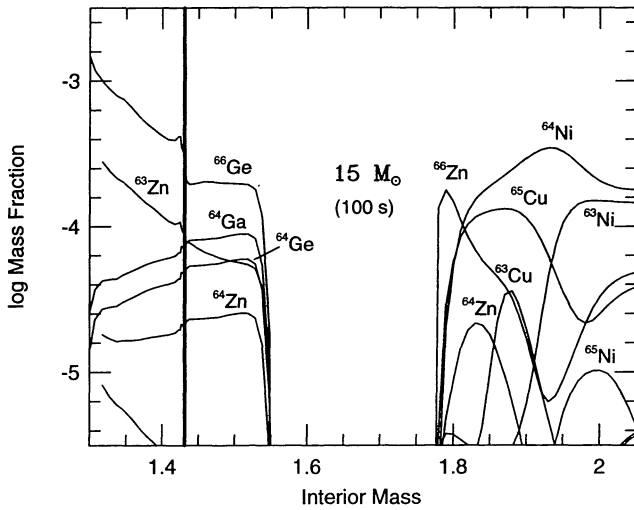


FIG. 31a

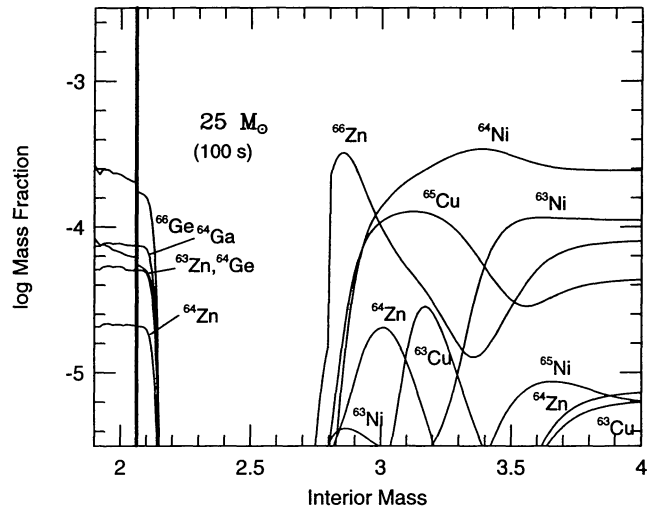


FIG. 31b

FIG. 31.—Mass fractions in interiors of the $15 M_{\odot}$ (a) and $25 M_{\odot}$ (b) explosions of ^{64}Ni , $^{63,65}\text{Cu}$, and ^{64}Zn and their progenitors. The dark bar at 1.43 and $2.07 M_{\odot}$ is the mass cut.

^{64}Ge so produced fell back onto the remnant. At 100 s, external to the ultimate mass cut at $2.07 M_{\odot}$, there was $2.0 \times 10^{-6} M_{\odot}$ of ^{64}Ge ; $3.0 \times 10^{-6} M_{\odot}$ of ^{64}Ga (mostly from ^{64}Ge decay); and $6.3 \times 10^{-5} M_{\odot}$ of ^{64}Zn . External to the *piston* there was $4.0 \times 10^{-5} M_{\odot}$ of ^{64}Ge and ^{64}Ga combined. Clearly the synthesis of this species is sensitive uncertain details concerning the simulation of the explosion. Substantial ^{64}Zn production is also found in the neutrino driven wind that accompanies the *r*-process. In particular an extreme alpha-rich freezeout with $Y_e \approx 0.49$ seems to make ^{64}Zn in great abundance (Woosley & Hoffman 1992, their Table 5; Hoffman et al. 1995). This is probably the source of ^{64}Zn in nature, but the yield from this process was not calculated here and is not included in the tables.

^{66}Zn is the last isotope whose synthesis we deem to have been accurately determined by our network (Table 1). It is again produced by the *s*-process during helium core burning (Table 9; Fig. 31 and 32). A small amount is also made as ^{66}Ge . It may be that ^{66}Zn is a product of the low entropy freezeout of neutron-rich material ejected from some varieties of Type Ia supernovae (Woosley & Eastman 1995).

4.8. The *s*-process

While we have not explicitly followed the synthesis of very heavy nuclei by neutron capture, we do keep careful track of the *s*-process for isotopes lighter than $A = 66$. This includes all of the sources, and most of the major sinks of neutrons. The

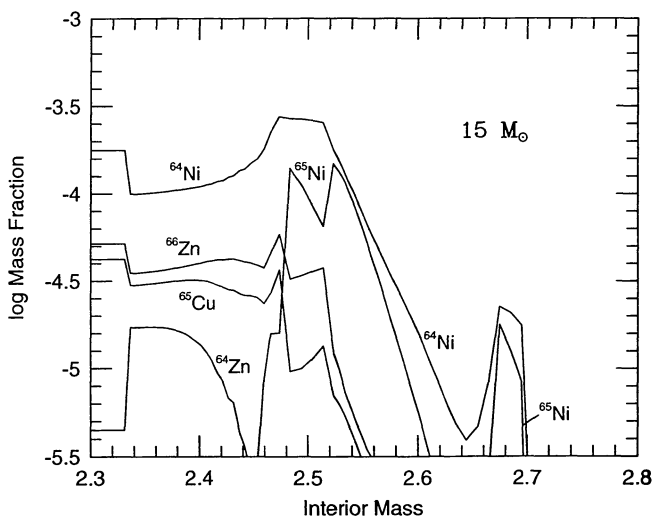


FIG. 32a

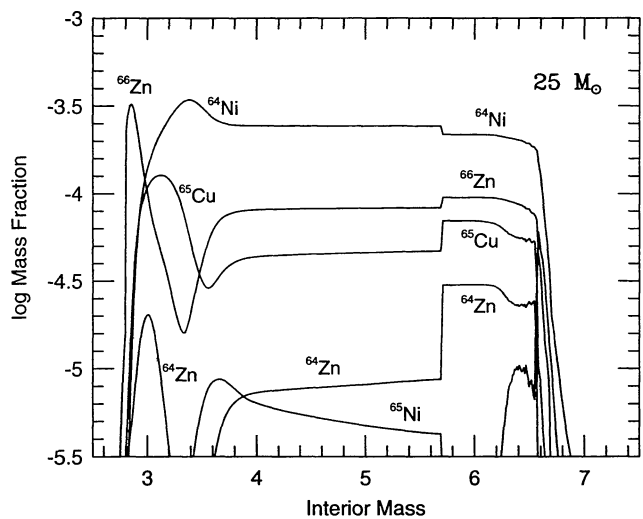


FIG. 32b

FIG. 32.—Mass fractions in interiors of the $15 M_{\odot}$ (a) and $25 M_{\odot}$ (b) explosions of the progenitors of ^{64}Ni , and ^{65}Cu , and ^{66}Zn . Here the plots emphasize those species having substantial production by neutron capture farther out in the star.

calculations have automatic neutron monitors in the form of the abundances of ^{54}Fe and ^{58}Fe , for example, which integrate over the exposure history seen by material in various stellar zones. This is true so long as neutron capture remains the dominant source of ^{58}Fe and no other source contributes to the synthesis or destruction of ^{54}Fe . In practice, this means the monitors are good until oxygen burning, or in the $25 M_{\odot}$ star, exterior to $2.9 M_{\odot}$ (Fig. 26*b*). Since at the temperatures appropriate to oxygen shell burning ($T_9 \gtrsim 2.0$), *s*-process seed are destroyed by photodisintegration (Arnould 1976; Woosley & Howard 1978). The actual ^{54}Fe abundance thus tells us the neutron exposure everywhere that *s*-process can possibly survive.

In Model S25A, for example, the ^{54}Fe abundance is given by

$$X(^{54}\text{Fe}) = X_0(^{54}\text{Fe}) \exp(-\phi_n),$$

where $X_0(^{54}\text{Fe}) = 7.1 \times 10^{-5}$ is the solar (Anders & Grevesse, 1989; Table 2) abundance of ^{54}Fe and

$$\phi_n = \int_0^{\infty} \lambda_{n\gamma}(^{54}\text{Fe}) \rho X_n dt.$$

The neutron capture rate, $\lambda_{n\gamma}(^{54}\text{Fe}) = N_A \langle \sigma v \rangle$, is not sensitive to temperature, and is $4.2 \times 10^6 \text{ cm}^3 \text{ g}^{-1} \text{ s}^{-1}$ between 3×10^8 and 10^9 K. Thus the exposure strength

$$\tau_n = \int_0^{\infty} \rho X_n dt$$

is

$$\tau_n = -2.4 \times 10^{-7} [9.55 + \ln X(^{54}\text{Fe})] \text{ g s cm}^{-3},$$

where $\ln X(^{54}\text{Fe})$ is just the value given for ^{54}Fe in Figures 26*a* and 26*b* times 2.302.

Figures 26*a* and 26*b* then show that most of the *s*-process in massive stars takes place during helium burning. For reference, the ^{54}Fe mass fraction at the center of the $25 M_{\odot}$ solar metallicity star at helium depletion ($T_c = 5 \times 10^8$ K) is 2.29×10^{-7} (i.e., -6.64 in Fig. 26*b*), corresponding to a neutron exposure $\tau_n = 1.3 \times 10^{-6} \text{ g s cm}^{-3}$. This value persists for Model S25A at Lagrangian coordinate $6 M_{\odot}$. Further out there has been a weak *s*-process where only a little helium has burned. Interior to $5.5 M_{\odot}$, however, there has been a non-negligible additional *s*-process during carbon and neon burning. Interior to $3.68 M_{\odot}$, the *s*-process is destroyed during the explosion (§ 4.9). Interior to $2.80 M_{\odot}$, all or part of the *s*-process seed has been destroyed by convective oxygen burning even before the explosion.

Fig. 26*c* shows how different things can be in another star, or in this case, the same mass star with another metallicity. This figure shows the distribution of ^{54}Fe and ^{58}Fe in the pre- and post-explosion Model U25A, a star of initially $10^{-4} Z_{\odot}$. Because the initial abundances of the low metal stars come from a Galactic chemical evolution calculation (Paper III), the abundance of heavy nuclei like iron is not simply 10^{-4} times their solar value. Solar ^{54}Fe times 10^{-4} , for example, would be -8.15 on this plot. The actual initial value in U25A value is

-10.18 , 100 times smaller. (One reason for this is the predominance of the α -rich freeze out in those regions where nse is achieved in the explosion; ^{58}Ni uses the neutrons in many Type II supernovae that might otherwise have been in ^{54}Fe . Another reason is the low production of iron, in general, compared to oxygen, in the very massive Z-series stars [Table 17*b* below]. We do not regard this value as very accurate for ^{54}Fe .) In the above equation for τ_n , one would then replace 9.55 by 23.44. One might think that the larger ratio of CNO (which *is*, by sum, $\sim 10^{-4}$ of solar) to iron, about four times the solar value, might mean that these stars would produce a more extensive *s*-process. There *is* more ^{22}Ne per iron during helium burning, but in fact, they do not. On the one hand, this particular star has a convective oxygen burning shell that extends to $5.03 M_{\odot}$. In this shell, one expects most of the *s*-process to be destroyed, or at least to have a substantially altered composition (§ 4.9; the mass fraction of ^{28}Si in this shell is 0.076). Exterior to $8.02 M_{\odot}$, the hydrogen envelope retains the original abundances of heavy nuclei. That is, the helium core is substantially smaller in Model U25A than in S25A. In between, one sees evidence for a weak *s*-process in which the ^{54}Fe abundance has declined by about 5 to 10 (rather than the 10^3 seen in S25A; Fig. 26*b*). The *s*-process is weak here because very little helium and ^{22}Ne have burned ($5.8\text{--}7.8 M_{\odot}$), but also because of the competition of light poisons such as ^{12}C [$10 \mu\text{barn}$ cross section, but ^{13}C is reprocessed by (α, n)], ^{16}O , and ^{20}Ne (0.12 mbarn); (see also Baraffe, El Eid, & Prantzos 1992). Both are many orders of magnitude more abundant than iron in the helium burning regions of low metallicity stars. And of course, once a little ^{22}Ne burns, the $^{22}\text{Ne}(\alpha, n)^{25}\text{Mg}$ neutron source itself is well known to be self-limiting owing to the neutron poisons (especially ^{25}Mg) which it produces.

We conclude that the *s*-process yields of massive stars can, in general, only be derived by following the heavy element abundances all the way to iron core collapse in a self-consistent calculation. Such calculations have yet to be done, though the ^{54}Fe abundance external to the oxygen burning shell in all our models could be used as the basis for one.

Table 9 also shows the time history of the *s*-process production of many isotopes above ^{56}Fe .

4.9. The *p*-process

The *p*- or γ -process is expected to occur in those zones of the supernova that experience shock induced temperatures in the range $2\text{--}3.2 \times 10^9$ K during their explosive ejection (Woosley & Howard 1978; Prantzos et al. 1990; Rayet, Prantzos, & Arnould 1990; Rayet et al. 1995) and which retain their *s*-process seed in those regions (§§ 4 and 8). We have not calculated the yield of *p*-process isotopes in the present models, but feel that it is important to do a careful treatment of the last stages of convective neon and oxygen shell burning before proceeding to do so. During the last hour of the star's life, the oxygen and neon shells become superheated owing to the contraction of the silicon-iron core. In the solar metallicity $25 M_{\odot}$ model, for example, the temperature at the base of the oxygen burning shell rises in the last few minutes of the stars life to 3.0×10^9 K. Under these conditions oxygen begins to burn explosively, i.e., in nearly a hydrodynamic time. Further the entropy barri-

ers separating the convective carbon, neon, and oxygen shells are small, at least in Model S25. It is quite probable that all these convective shells become linked at the end (Arnett 1994; Bazan & Arnett 1994), at least for Model S25A. The complex coupling of multidimensional hydrodynamics and nuclear reactions, especially among the heavy nuclei, is a formidable problem, but we speculate that a considerable part of the p -process may be made by photodisintegration of s -process seed *before* the shock is ever born (see also Arnould 1976) and in a larger fraction of the star than just that part experiencing shock temperatures between 2 and 3 billion K. A preliminary exploration of the p -process in this environment is underway (Howard & Woosley 1995).

The mass that experiences 2 to 3.2 billion degrees in Model S25A, a nucleosynthetically typical supernova, is $1.0 M_{\odot}$, the region between 2.65 and $3.68 M_{\odot}$ (Fig. 9). This inner boundary is dangerously inside of the $2.80 M_{\odot}$ extent of the oxygen burning shell in the presupernova star emphasizing again the need for a self consistent calculation of pre-explosive and explosive processing of the heavy elements. Based, however, upon a prior helium burning s -process which enhances the seed distribution (Fig. 26*b*), the typical p -process production factor in this region should be around 200 (Woosley & Howard 1978). This $1 M_{\odot}$ is about 4% of the total ejecta ($23 M_{\odot}$), so the production factor for the supernova is around 10, comparable to other major productions in this star (Table 6). The comparable mass for Model S15A is $0.33 M_{\odot}$, which would give a total production factor near 5.

4.10. The r -process

Also not explicitly calculated here is the yield of neutron-rich isotopes heavier than zinc. These have traditionally (Burbidge et al. 1957) been attributed to rapid neutron capture in an explosive environment, i.e., the r -process. It is our belief that such isotopes are produced in a wind driven from the nascent neutron star during the first 20 seconds of its life and thus constitute the bottom-most layers to be ejected by all supernovae that leave neutron star remnants. Details of this nucleosynthesis have been presented for a $20 M_{\odot}$ model by Woosley et al. (1994), but it has not been studied here.

A limited amount of neutron capture also occurs in the helium shells of some of these stars as the shock wave passes (Fig. 26). In Model S25A, the peak temperature experienced at the base of the helium shell [$6.56 M_{\odot}$; $X(^4\text{He}) = 0.21$] was 8.4×10^8 K. Prior to shock passage this zone contained 0.96% ^{22}Ne , 0.43% ^{25}Mg , and 0.73% ^{26}Mg by mass. After the explosion these were changed to 0.76%, 0.56%, and 0.83%, respectively indicating the burning of some ^{22}Ne . This caused an order-of-magnitude increase in ^{60}Fe , for example, (to 3×10^{-5} by mass) and the significant production of some other moderately neutron-rich isotopes. The process, which could scarcely be termed an r -process, was also quite limited in extent. At $6.84 M_{\odot}$, $0.3 M_{\odot}$ farther out, the temperature only rose to 6.8×10^8 K, the ^{22}Ne abundance did not change discernibly, and ^{60}Fe rose only to 5×10^{-6} . A somewhat stronger exposure occurred at the base of the helium shell in S15A [$2.54 M_{\odot}$, $X(^4\text{He}) = 0.12$]. There the ^{22}Ne mass fraction declined from 1.61% to 1.22% in a shock that had peak temperature 1.0×10^9 K (owing to the smaller radius of the helium shell). The ^{60}Fe

abundance rose almost two orders of magnitude to 2.0×10^{-4} . The peak temperature declined however to 7×10^8 K, effectively shutting off the exposure, at $2.71 M_{\odot}$.

5. YIELDS AS A FUNCTION OF MASS AND METALLICITY

Tables 5, 6, and 10–17 give the final nucleosynthesis for our grid of supernovae of varying mass and metallicity. For each supernova, the yields are given both in terms of absolute mass (in solar masses) and their *production factors*, i.e., the ratio of each isotope's mass fraction in the total ejecta divided by its corresponding mass fraction in the Sun (Anders & Grevesse 1989; Table 2). Except where otherwise noted, these yields are evaluated at 2.5×10^4 seconds. As noted previously, this does not mean that the last update of the nuclear network took place at this time. The nuclear network ceased to be evolved once the temperature fell below 10^7 K, a zone-dependent occurrence. Both strong and weak interactions were shut off at this point. Production factors, which express total yield of a given stable isotope are unaffected by this edit procedure, but the masses of radioactive isotopes with half lives less than or on the order of 2.5×10^4 s may have decayed to a greater extent at the edit time than indicated by the tables. Those interested in Galactic chemical evolution should simply add the masses of all progenitors. This should also be equal to the production factor times the Anders and Grevesse mass fraction (Table 2) times the total ejected mass (given at the end of each mass yield table). However, the latter procedure will result in a loss of precision, especially for the more metal-deficient stars. In cases where the production factor was less than 0.01, it is not edited in the tables.

Two further notes of explanation are in order here. First recall that the model naming followed a convention of using a number that is close to but not exactly the stellar mass on the main sequence. Thus S25A is *not* (as one might logically assume) a star of $25 M_{\odot}$, but one of 5.0×10^{34} g (or $25.14 M_{\odot}$). Also for one star, the S40 progenitor, instabilities in the Cepheid variable strip required the removal of $2 M_{\odot}$ of envelope from the presupernova star. Yields in the helium core will not be affected by this operation, but the total masses in Tables 2 and 5B do not sum to $40.22 M_{\odot}$.

6. DISCUSSION AND CONCLUSIONS

Nucleosynthesis in massive stars is sensitive to the explosion mechanism, but in a way that might not have been anticipated. Only a few isotopes are directly and significantly affected by the explosion energy and the location of the piston (Table 7 plus the r -process) so long as that mass cut is near the neutron star. However, depending upon the exact explosion energy, large amounts of heavy elements can fall back (§ 3; Tables 3 and 8), especially in the more massive stars. This is very important for determining the nature of the compact remnant, but it is also of critical importance for the nucleosynthesis.

The reimplosion that occurs as the shock passes through regions of increasing ρr^3 in the mantle should result in larger amounts of matter falling back in more massive stars and stars of initially zero metallicity. Depending upon the actual energy in the initial shock, this may lead to a critical mass above which black hole remnants of varying size are produced in Type IIp

TABLE 10A
 EJECTED MASSES AT 2.5×10^4 SECONDS; $11-25 M_{\odot}$ MODELS; $Z = 0.1 Z_{\odot}$

	P12A	P13A	P15A	P18A	P20A	P22A	P25A	P12A	P13A	P15A	P18A	P20A	P22A	P25A
¹ H	6.26	6.67	7.42	8.36	8.95	9.44	10.3	³⁹ K	1.73E-05	5.49E-05	3.44E-05	4.88E-05	6.07E-04	1.25E-03
⁴ He	3.91	4.30	5.04	6.18	6.70	7.42	8.60	⁴⁰ K	2.09E-08	4.45E-08	5.99E-08	1.13E-07	1.56E-06	3.24E-06
² H	1.07E-04	1.11E-04	1.13E-04	1.26E-04	1.31E-04	1.31E-04	1.42E-04	⁴¹ K	1.85E-07	1.93E-07	2.36E-07	3.14E-07	4.73E-07	6.34E-07
³ He	4.62E-04	4.89E-04	5.44E-04	6.12E-04	6.58E-04	7.13E-04	7.78E-04	⁴⁰ Ca	2.84E-03	5.23E-03	5.90E-03	7.84E-03	1.87E-02	2.78E-02
⁷ Li	2.61E-07	2.45E-07	2.28E-07	2.56E-07	2.06E-07	1.95E-07	2.11E-07	⁴¹ Ca	1.43E-06	3.51E-06	2.40E-06	2.74E-06	2.85E-05	3.64E-05
⁷ Be	2.19E-07	2.76E-07	2.34E-07	1.50E-07	1.48E-07	2.30E-07	3.37E-07	⁴² Ca	1.99E-06	5.82E-06	3.60E-06	4.81E-06	1.07E-04	1.77E-04
⁹ Be	8.99E-12	6.69E-12	5.43E-12	4.94E-12	3.22E-12	2.57E-12	1.97E-12	⁴³ Ca	3.34E-08	6.89E-08	7.09E-08	1.22E-07	1.50E-06	2.69E-06
¹⁰ B	4.48E-11	8.34E-11	5.44E-11	1.89E-10	1.05E-10	4.94E-07	5.24E-07	⁴⁴ Ca	4.45E-07	5.24E-07	6.63E-07	9.01E-07	1.18E-06	2.21E-06
¹¹ B	4.60E-07	3.80E-07	4.04E-07	1.16E-06	1.01E-06	2.51E-06	3.80E-06	⁴⁵ Ca	1.01E-08	1.87E-08	2.81E-08	3.10E-08	2.99E-08	2.31E-06
¹¹ C	2.38E-07	2.44E-07	2.09E-07	2.72E-07	4.25E-07	3.71E-07	3.23E-07	⁴⁶ Ca	8.80E-09	1.11E-08	1.50E-08	1.54E-08	9.95E-09	4.53E-09
¹² C	8.93E-02	1.09E-01	1.42E-01	2.25E-01	2.46E-01	2.32E-01	2.67E-01	⁴⁷ Ca	3.12E-09	2.56E-09	3.10E-09	3.43E-09	1.43E-09	2.54E-10
¹³ C	4.65E-05	5.26E-05	6.22E-05	7.79E-05	8.65E-05	9.23E-05	1.08E-04	⁴⁸ Ca	2.75E-09	1.59E-09	1.74E-09	2.63E-09	1.45E-09	1.30E-09
¹⁴ C	8.22E-07	2.46E-06	1.08E-05	5.01E-06	1.76E-06	1.06E-06	7.89E-07	⁴⁹ Sc	5.14E-07	8.18E-07	5.25E-07	3.03E-07	4.87E-07	1.00E-06
¹⁴ N	2.90E-03	4.03E-03	4.85E-03	5.67E-03	6.30E-03	6.94E-03	8.36E-03	⁴⁸ Sc	6.81E-08	7.59E-08	1.02E-07	1.16E-07	6.36E-07	2.27E-06
¹⁵ N	1.39E-05	2.08E-05	5.29E-05	6.36E-05	3.00E-03	3.66E-03	4.28E-03	⁴⁴ Ti	6.30E-05	5.53E-05	5.49E-05	3.02E-05	1.03E-04	1.58E-06
¹⁶ O	1.45E-01	2.80E-01	5.58E-01	9.94E-01	7.73E-05	1.07E-04	1.31E-04	⁴⁵ Ti	1.62E-06	1.79E-06	2.73E-06	1.62E-06	7.91E-07	6.60E-07
¹⁷ O	3.70E-05	3.85E-05	4.18E-05	4.20E-05	3.65E-05	3.90E-05	3.60E-05	⁴⁶ Ti	2.85E-06	5.16E-06	2.67E-06	2.34E-06	5.56E-06	2.58E-05
¹⁸ O	1.84E-04	3.44E-04	4.11E-04	8.25E-04	4.09E-04	1.02E-04	3.54E-05	⁴⁷ Ti	1.68E-07	2.37E-07	2.02E-07	1.93E-07	8.74E-07	2.16E-06
¹⁹ F	2.39E-05	1.00E-05	1.92E-05	4.72E-05	1.62E-05	6.80E-06	7.42E-06	⁴⁸ Ti	1.49E-06	1.62E-06	1.85E-06	2.18E-06	2.46E-06	3.37E-06
²⁰ Ne	1.21E-02	4.22E-02	7.46E-02	2.06E-01	9.61E-02	3.59E-02	4.44E-02	⁴⁹ Ti	8.16E-08	9.49E-08	1.26E-07	1.84E-07	2.42E-07	3.03E-07
²¹ Ne	6.44E-05	7.26E-05	1.55E-04	1.49E-04	1.03E-04	6.87E-05	3.99E-05	⁵⁰ Ti	3.28E-08	6.57E-08	1.09E-07	2.08E-07	2.63E-07	3.25E-07
²² Ne	1.36E-03	3.48E-04	5.51E-04	1.84E-03	3.00E-03	3.66E-03	4.28E-03	⁴⁷ V	8.54E-07	1.27E-06	1.08E-06	6.74E-07	5.13E-07	5.13E-07
²² Na	1.10E-07	4.11E-07	6.21E-07	2.02E-06	7.93E-07	2.34E-07	5.17E-07	⁴⁸ V	7.81E-07	7.91E-07	7.92E-07	8.53E-07	3.61E-06	2.54E-05
²³ Na	1.14E-04	4.09E-04	6.38E-04	1.92E-03	5.93E-04	2.12E-04	3.35E-04	⁴⁹ V	5.97E-07	1.13E-06	7.29E-07	9.86E-07	1.73E-06	4.60E-06
²⁴ Mg	5.47E-03	1.69E-02	2.17E-02	7.79E-02	5.15E-02	1.73E-02	3.05E-02	⁵⁰ V	9.71E-10	1.90E-08	3.97E-09	1.01E-08	2.28E-08	3.30E-08
²⁵ Mg	2.12E-04	4.17E-04	6.01E-04	1.27E-03	1.15E-03	7.12E-04	7.92E-04	⁵¹ V	8.01E-08	9.43E-08	1.08E-07	1.38E-07	1.72E-07	2.08E-07
²⁶ Mg	1.69E-04	3.16E-04	5.19E-04	1.18E-03	1.23E-03	9.99E-04	1.21E-03	⁴⁸ Cr	1.55E-04	1.60E-04	1.66E-04	1.50E-04	2.28E-04	3.01E-04
²⁷ Al	8.53E-06	1.65E-05	1.87E-05	6.51E-05	4.77E-05	1.03E-05	1.74E-05	⁴⁹ Cr	3.96E-06	8.34E-06	5.19E-06	6.00E-06	9.62E-06	7.46E-06
²⁸ Si	3.02E-02	8.70E-04	1.09E-03	4.04E-03	2.84E-03	1.75E-03	3.03E-03	⁵⁰ Cr	3.16E-06	6.64E-05	8.40E-06	1.77E-05	2.81E-05	3.05E-05
²⁹ Si	1.56E-04	3.34E-04	4.16E-04	1.08E-03	1.18E-03	1.66E-03	2.24E-03	⁵¹ Cr	7.35E-07	2.70E-06	1.45E-06	2.55E-06	6.16E-06	7.07E-06
³⁰ Si	9.52E-05	3.98E-04	4.36E-04	1.39E-03	1.18E-03	1.05E-03	1.83E-03	⁵² Cr	1.09E-05	1.65E-05	1.36E-05	1.65E-05	1.98E-05	2.36E-05
³¹ P	6.54E-05	1.67E-04	1.79E-04	4.42E-04	7.04E-04	1.35E-03	2.14E-03	⁵⁴ Cr	6.01E-07	6.67E-07	7.52E-07	9.25E-07	1.08E-06	1.23E-06
³² S	1.36E-02	3.15E-02	3.40E-02	4.80E-02	1.29E-01	1.84E-01	2.17E-01	⁵¹ Mn	4.60E-06	1.71E-05	9.87E-06	6.55E-07	7.72E-07	6.55E-07
³³ S	4.67E-05	9.60E-05	1.04E-04	1.83E-04	5.46E-04	1.08E-03	1.66E-03	⁵² Mn	1.35E-05	1.83E-05	2.12E-05	1.55E-05	2.40E-05	1.90E-05
³⁴ S	1.07E-04	1.97E-04	2.44E-04	5.36E-04	1.17E-03	3.81E-03	4.68E-03	⁵³ Mn	2.57E-05	7.15E-05	4.35E-05	6.72E-05	1.04E-04	1.34E-04
³⁵ S	2.06E-07	3.56E-07	4.01E-07	6.64E-07	1.34E-06	3.49E-06	4.66E-06	⁵⁴ Mn	1.02E-07	2.36E-06	8.05E-07	8.05E-07	1.18E-06	9.94E-07
³⁶ S	2.10E-07	2.56E-07	3.45E-07	5.57E-07	8.20E-07	1.02E-06	1.27E-06	⁵⁵ Mn	2.33E-06	2.57E-06	2.90E-06	3.45E-06	3.87E-06	4.35E-06
³⁶ Cl	1.90E-05	5.10E-05	4.23E-05	8.43E-05	3.93E-04	1.07E-03	1.90E-03	⁵⁷ Fe	9.44E-04	1.36E-03	1.51E-03	2.02E-03	3.35E-03	3.06E-03
³⁶ Cl	1.53E-07	4.31E-07	4.19E-07	7.10E-07	3.40E-06	7.78E-06	1.16E-05	⁵⁹ Fe	2.32E-05	7.80E-05	4.73E-05	6.20E-05	8.97E-05	4.98E-05
³⁷ Cl	1.80E-06	3.00E-06	4.26E-06	7.31E-06	1.27E-05	2.20E-05	3.07E-05	⁵⁴ Fe	3.55E-04	5.63E-03	1.00E-03	1.88E-03	2.46E-03	2.30E-03
³⁶ Ar	2.88E-03	6.08E-03	6.63E-03	8.93E-03	3.99E-02	3.99E-02	5.07E-02	⁵⁹ Fe	2.29E-05	6.74E-05	3.10E-05	2.83E-05	4.42E-05	7.72E-05
³⁷ Ar	2.67E-06	7.82E-06	5.68E-06	8.36E-06	6.58E-05	1.55E-04	2.65E-04	⁵⁶ Fe	6.97E-04	8.03E-04	8.56E-04	1.01E-03	1.17E-03	1.33E-03
³⁸ Ar	3.94E-05	1.41E-04	1.04E-04	1.80E-04	1.07E-03	2.31E-03	3.22E-03	⁵⁷ Fe	2.32E-05	2.62E-05	3.00E-05	4.00E-05	4.65E-05	5.37E-05
⁴⁰ Ar	1.16E-07	1.45E-07	2.03E-07	2.96E-07	3.58E-07	3.48E-07	3.92E-07	⁵⁸ Fe	4.75E-06	1.09E-06	1.32E-06	2.63E-06	2.07E-06	2.26E-06
								⁵⁹ Fe	1.67E-06	4.16E-06	4.60E-06	5.70E-06	4.22E-06	2.05E-06
								⁶⁰ Fe	1.89E-06	2.93E-06	3.05E-06	3.51E-06	1.83E-06	3.91E-07

TABLE 10A—Continued

Table with 14 columns: P12A, P13A, P15A, P18A, P20A, P22A, P25A. Rows list various chemical elements from 55Co to 71Ge and a Mass row.

TABLE 10B

EJECTED MASSES AT 2.5 x 10^4 SECONDS; 30-40 M_sun MODELS; Z = 0.1 Z_sun

Table with 14 columns: KE_infinity, P30A, P30B, P35A, P35B, P35C, P40A, P40B, P40C. Rows list various chemical elements from 1H to 40Ar.

TABLE 11A
PRODUCTION FACTORS 11–25 M_{\odot} MODELS; $Z = 0.1 Z_{\odot}$

	P12A	P13A	P15A	P18A	P20A	P22A	P25A		P12A	P13A	P15A	P18A	P20A	P22A	P25A
¹ H	.83	.80	.77	.72	.70	.67	.63	⁴⁰ Ca	4.44	7.42	7.25	7.98	17.19	19.02	15.65
² H	.21	.20	.17	.16	.15	.14	.13	⁴² Ca	.45	1.19	.64	.71	5.39	12.78	18.26
³ He	1.48	1.42	1.37	1.27	1.24	1.22	1.15	⁴³ Ca	.57	.84	.49	.29	.67	1.20	1.78
⁴ He	1.33	1.33	1.35	1.37	1.34	1.35	1.35	⁴⁴ Ca	4.17	3.33	2.87	1.33	.99	.92	3.21
⁶ Li	.00	.00	.00	.00	.00	.00	.00	⁴⁶ Ca	.29	.34	.00	.33	.28	.18	.07
⁷ Li	4.80	4.73	3.63	.00	2.09	2.28	2.53	⁴⁸ Ca	.00	.00	.00	.00	.00	.00	.00
⁹ Be	.01	.01	.00	.00	.01	.01	.01	⁴⁸ Sc	4.08	4.12	5.40	2.77	1.67	1.70	4.30
¹⁰ B	.00	.01	.00	.01	.01	.01	.01	⁴⁶ Ti	1.19	1.97	.88	.64	2.36	3.90	5.00
¹¹ B	13.76	11.22	9.54	18.49	16.75	10.17	8.25	⁴⁷ Ti	.46	.62	.45	.26	.28	.35	.56
¹² C	2.76	3.06	3.44	4.51	4.48	3.82	3.81	⁴⁸ Ti	6.85	4.91	5.77	4.33	5.23	5.45	6.63
¹³ C	.12	.13	.13	.14	.14	.14	.14	⁴⁹ Ti	2.65	4.97	2.72	2.67	3.51	3.78	3.27
¹⁴ N	.25	.31	.32	.31	.31	.31	.33	⁵⁰ Ti	.02	.03	.05	.08	.11	.08	.09
¹⁵ N	.30	.42	.91	.92	1.06	1.33	1.36	⁵⁰ V	.10	.175	.32	.67	1.36	1.29	1.54
¹⁶ O	1.42	2.57	4.26	6.31	8.77	11.05	13.08	⁵¹ V	1.35	4.50	2.23	2.94	4.20	4.35	3.01
¹⁷ O	.89	.84	.79	.66	.52	.50	.40	⁵⁰ Cr	.40	7.60	.83	1.45	2.09	2.18	1.78
¹⁸ O	.79	1.35	1.42	2.32	1.04	.24	.07	⁵² Cr	6.10	7.99	7.64	8.50	12.72	13.64	9.41
¹⁹ F	5.52	2.10	3.48	7.10	2.20	.84	.79	⁵³ Cr	2.70	7.44	3.93	4.62	6.29	6.72	4.67
²⁰ Ne	.70	2.22	3.39	7.75	3.27	1.11	1.19	⁵⁴ Cr	.05	.51	.12	.20	.23	.20	.16
²¹ Ne	1.46	1.50	2.77	2.20	1.37	.83	.42	⁵⁵ Mn	2.60	5.51	3.24	2.81	3.06	3.06	2.59
²² Ne	.98	.23	.31	.86	1.27	1.41	1.42	⁵⁴ Fe	.47	6.72	1.04	1.61	1.90	2.00	1.40
²³ Na	.32	1.04	1.41	3.49	.98	.32	.43	⁵⁶ Fe	14.25	13.18	12.35	7.19	5.82	5.37	7.68
²⁴ Mg	.99	2.79	3.10	9.23	5.51	1.68	2.56	⁵⁷ Fe	23.23	22.14	15.00	7.08	4.09	3.42	7.95
²⁵ Mg	.29	.52	.65	1.14	.94	.53	.51	⁵⁸ Fe	.26	.44	.30	.45	.41	.29	.28
²⁶ Mg	.21	.36	.50	.97	.91	.65	.68	⁵⁹ Co	10.98	13.05	7.11	2.95	.87	.63	2.65
²⁷ Al	.38	1.27	1.38	4.24	2.69	1.51	2.26	⁵⁸ Ni	15.64	22.63	5.67	1.89	5.4	.51	1.41
²⁸ Si	4.33	8.47	8.01	11.81	19.61	24.96	26.10	⁶⁰ Ni	24.72	18.16	18.15	8.67	4.01	2.86	10.86
²⁹ Si	.43	.83	.89	1.92	1.90	2.43	2.83	⁶¹ Ni	33.96	29.72	22.35	9.93	4.35	3.01	13.52
³⁰ Si	.38	1.44	1.37	3.60	2.20	2.24	3.37	⁶² Ni	50.11	59.14	21.61	7.53	1.85	1.51	8.11
³¹ P	.78	1.78	1.66	3.36	4.79	8.31	11.32	⁶⁴ Ni	.18	.28	.52	.77	1.25	.94	1.08
³² S	3.21	6.77	6.31	7.39	17.91	23.22	23.72	⁶⁵ Cu	2.38	2.21	1.69	1.09	.86	.60	1.30
³³ S	1.36	2.54	2.38	3.46	9.36	16.76	22.29	⁶⁸ Cu	.67	.68	.87	.93	1.23	1.33	1.78
³⁴ S	.54	.90	.96	1.75	3.46	10.20	10.84	⁶⁴ Zn	6.09	2.04	2.81	1.60	1.41	1.20	3.54
³⁶ S	.21	.24	.28	.37	.52	.62	.68	⁶⁶ Zn	5.24	5.71	2.72	1.33	1.07	1.88	3.23
³⁶ Cl	.71	1.72	1.24	2.04	8.59	21.13	32.52	⁶⁷ Zn	.13	.21	.41	.58	1.10	.70	.80
³⁷ Cl	.49	1.08	.86	1.12	5.06	10.38	14.96	⁶⁸ Zn	.10	.17	.39	.60	1.40	1.56	1.85
³⁸ Ar	3.49	6.68	6.31	7.04	17.78	25.77	28.33	⁷⁰ Zn	.10	.16	.33	.31	.61	.63	.44
³⁸ Ar	.24	.78	.50	.71	3.85	7.50	9.06	⁶⁹ Ga	.36	.46	1.13	1.38	2.31	4.70	6.14
⁴⁰ Ar	.44	.50	.61	.74	.97	1.02	1.26	⁷¹ Ga	.83	1.54	3.36	7.37	14.17	11.56	13.47
³⁹ K	.47	1.35	.74	.85	5.69	8.76	15.57	⁷⁰ Ge	.39	.70	1.66	2.69	4.89	17.11	24.23
⁴⁰ K	.35	.68	.79	1.24	8.12	14.03	25.26								
⁴¹ K	.58	1.20	.74	.71	6.06	7.01	11.09								

TABLE 11B
PRODUCTION FACTORS 30–40 M_{\odot} MODELS; $Z = 0.1 Z_{\odot}$

KE $_{\infty}$	P30A	P30B	P35A	P35B	P35C	P40A	P40B	P40C	P40A	P35C	P35B	P35A	P30B	P30A	P30B	P35A	P35B	P35C	P40A	P40B	P40C
¹ H	.59	.58	.61	.55	.53	.61	.53	.49	.61	.53	.55	.61	.58	.59	.58	.61	.55	.53	.61	.53	.49
² H	.12	.11	.12	.10	.10	.11	.10	.09	.11	.10	.10	.12	.11	.12	.11	.12	.10	.10	.11	.10	.09
³ He	1.11	1.08	1.20	1.07	1.03	1.19	1.04	.97	1.19	1.03	1.07	1.20	1.08	1.11	1.08	1.20	1.07	1.03	1.19	1.04	.97
⁴ He	1.39	1.35	1.53	1.37	1.32	1.63	1.42	1.33	1.63	1.32	1.37	1.53	1.35	1.39	1.35	1.53	1.37	1.32	1.63	1.42	1.33
⁶ Li	.00	.00	.00	.00	.00	.00	.00	.00	.00	.00	.00	.00	.00	.00	.00	.00	.00	.00	.00	.00	.00
⁷ Li	2.61	2.14	2.35	1.75	1.51	2.13	1.55	1.35	2.13	1.51	1.75	2.35	2.14	2.61	2.14	2.35	1.75	1.51	2.13	1.55	1.35
⁹ Be	.00	.00	.00	.00	.00	.00	.00	.00	.00	.00	.00	.00	.00	.00	.00	.00	.00	.00	.00	.00	.00
¹⁰ B	.00	.00	.00	.00	.00	.00	.00	.00	.00	.00	.00	.00	.00	.00	.00	.00	.00	.00	.00	.00	.00
¹¹ B	6.42	5.59	4.83	4.92	4.53	4.46	6.62	6.13	4.46	4.53	4.92	4.83	5.59	6.42	5.59	4.83	4.92	4.53	4.46	6.62	6.13
¹² C	3.66	3.56	3.70	3.46	3.31	3.58	3.68	3.45	3.58	3.31	3.46	3.70	3.56	3.66	3.56	3.70	3.46	3.31	3.58	3.68	3.45
¹³ C	.13	.12	.12	.11	.11	.14	.12	.11	.14	.11	.11	.12	.12	.13	.12	.12	.11	.11	.14	.12	.11
¹⁴ N	.36	.35	.41	.37	.35	.46	.40	.38	.46	.35	.37	.41	.36	.36	.35	.41	.37	.35	.46	.40	.38
¹⁵ N	1.14	1.17	.94	1.31	1.28	.92	1.19	1.31	.92	1.28	1.31	.94	1.14	1.14	1.17	.94	1.31	1.28	.92	1.19	1.31
¹⁶ O	15.63	16.35	11.35	18.93	18.79	9.14	18.22	19.52	9.14	18.79	18.93	11.35	16.35	15.63	16.35	11.35	18.93	18.79	9.14	18.22	19.52
¹⁷ O	.35	.35	.39	.35	.33	.39	.34	.32	.39	.33	.35	.39	.35	.35	.35	.39	.35	.33	.39	.34	.32
¹⁸ O	.14	.13	.02	.01	.01	.01	.01	.01	.01	.01	.01	.02	.13	.14	.13	.02	.01	.01	.01	.01	.01
¹⁹ F	7.40	6.55	5.76	8.03	7.32	5.67	13.61	12.27	5.67	7.32	8.03	5.76	6.55	7.40	6.55	5.76	8.03	7.32	5.67	13.61	12.27
²⁰ Ne	14.38	13.74	10.66	15.56	14.72	11.99	25.22	23.46	11.99	14.72	15.56	10.66	13.74	14.38	13.74	10.66	15.56	14.72	11.99	25.22	23.46
²¹ Ne	.94	.89	1.44	1.87	1.76	2.19	3.96	3.67	2.19	1.76	1.87	1.44	.89	.94	.89	1.44	1.87	1.76	2.19	3.96	3.67
²² Ne	1.41	1.37	1.48	1.33	1.27	1.40	1.23	1.15	1.40	1.27	1.33	1.48	1.37	1.41	1.37	1.48	1.33	1.27	1.40	1.23	1.15
²³ Ne	3.17	3.04	3.99	5.02	4.75	6.74	11.44	10.66	6.74	4.75	5.02	3.99	3.04	3.17	3.04	3.99	5.02	4.75	6.74	11.44	10.66
²⁴ Mg	22.69	23.20	9.90	21.09	20.38	4.84	14.47	16.63	4.84	20.38	21.09	9.90	23.20	22.69	23.20	9.90	21.09	20.38	4.84	14.47	16.63
²⁵ Mg	2.07	1.99	1.54	2.15	2.04	1.36	2.75	2.58	1.36	2.04	2.15	1.54	1.99	2.07	1.99	1.54	2.15	2.04	1.36	2.75	2.58
²⁶ Mg	2.14	2.06	1.77	2.36	2.24	1.56	3.11	2.90	1.56	2.24	2.36	1.77	2.06	2.14	2.06	1.77	2.36	2.24	1.56	3.11	2.90
²⁷ Al	10.66	10.79	5.02	10.41	10.04	2.65	7.52	8.25	2.65	10.04	10.41	5.02	10.66	10.66	10.79	5.02	10.41	10.04	2.65	7.52	8.25
²⁸ Si	4.02	11.19	1.31	5.10	16.44	.38	1.15	16.79	.38	16.44	5.10	1.31	4.02	4.02	11.19	1.31	5.10	16.44	.38	1.15	16.79
²⁹ Si	2.80	3.41	1.23	3.13	3.53	.39	1.55	2.72	.39	3.53	3.13	1.23	2.80	2.80	3.41	1.23	3.13	3.53	.39	1.55	2.72
³⁰ Si	6.17	7.15	2.33	6.94	7.06	4.5	2.11	3.96	4.5	7.06	6.94	2.33	6.17	6.17	7.15	2.33	6.94	7.06	4.5	2.11	3.96
³¹ P	4.48	5.60	1.74	4.79	5.72	.55	1.59	3.82	.55	5.72	4.79	1.74	4.48	4.48	5.60	1.74	4.79	5.72	.55	1.59	3.82
³² S	.26	.26	.16	.44	11.20	.13	.14	12.88	.13	11.20	.44	.16	.26	.26	.26	.16	.44	11.20	.13	.14	12.88
³³ S	.62	2.58	.19	1.47	3.50	.11	.22	3.28	.11	3.50	1.47	.19	.62	.62	2.58	.19	1.47	3.50	.11	.22	3.28
³⁴ S	.37	1.41	.14	.78	1.92	.05	.12	1.60	.05	1.92	.78	.14	.37	.37	1.41	.14	.78	1.92	.05	.12	1.60
³⁶ S	.62	.62	.61	1.26	2.66	.11	1.04	.99	.11	2.66	1.26	.61	.62	.62	.62	.61	1.26	2.66	.11	1.04	.99
³⁷ Cl	1.06	2.05	.36	.95	1.61	.84	1.20	1.83	.84	1.61	.95	.36	1.06	1.06	2.05	.36	.95	1.61	.84	1.20	1.83
³⁶ Ar	.14	5.70	.14	.19	11.17	.14	.12	12.87	.14	11.17	.19	.14	.14	.14	5.70	.14	.19	11.17	.14	.12	12.87
³⁸ Ar	.10	.58	.08	.13	.92	.08	.13	.79	.08	.92	.13	.08	.10	.10	.58	.08	.13	.92	.08	.13	.79
⁴⁰ Ar	1.47	1.42	1.51	1.91	1.82	1.54	2.75	2.56	1.54	1.82	1.91	1.51	1.47	1.47	1.42	1.51	1.91	1.82	1.54	2.75	2.56
³⁹ K	.20	.75	.13	.23	1.27	.10	.19	1.19	.10	1.27	.23	.13	.20	.20	.75	.13	.23	1.27	.10	.19	1.19
⁴⁰ K	3.38	3.45	2.82	3.78	3.88	2.66	4.79	4.73	2.66	3.88	3.78	2.82	3.38	3.38	3.45	2.82	3.78	3.88	2.66	4.79	4.73
⁴¹ K	.18	.65	.17	.19	1.01	.16	.21	.99	.16	1.01	.19	.17	.18	.18	.65	.17	.19	1.01	.16	.21	.99

TABLE 12A—Continued

Table with 14 columns: KE∞, T12A, T119A, T115A, T118A, T20A, T22A, T25A. It contains mass data for various isotopes from 55Co to 80Ar, with values in scientific notation (e.g., 2.46E-04, 3.79E-04).

TABLE 12B

EJECTED MASSES AT 2.5 × 10^4 SECONDS; 30-40 M_sun MODELS; Z = 0.01 Z_sun

Table with 14 columns: KE∞, T30A, T30B, T35A, T35B, T35C, T40A, T40B, T40C. It contains mass data for various isotopes from 1H to 40Ar, with values in scientific notation (e.g., 11.6, 1.28, 1.84).

TABLE 12B—Continued

KE _∞	T30A	T30B	T35A	T35B	T35C	T40A	T40B	T40C	T40C
KE _∞	1.28	1.84	1.23	2.03	2.47	1.21	2.00	2.54	2.54
³⁹ K	2.31E-06	6.44E-05	8.94E-07	6.48E-05	7.14E-05	5.91E-07	1.57E-06	9.88E-05	5.24E-11
⁴⁰ K	2.07E-08	5.67E-08	2.81E-08	6.69E-08	6.48E-08	2.36E-08	4.83E-08	8.39E-08	1.73E-03
⁴¹ K	2.65E-08	3.04E-08	3.78E-08	4.53E-08	4.50E-08	3.74E-08	4.64E-08	5.97E-08	1.32E-02
⁴⁰ Ca	9.80E-06	1.77E-02	1.06E-05	2.02E-02	2.11E-02	1.15E-05	1.19E-05	3.72E-02	1.54E-03
⁴¹ Ca	3.57E-08	5.29E-06	2.95E-08	5.07E-06	5.69E-06	3.48E-08	3.48E-08	6.39E-09	1.63E-08
⁴² Ca	7.17E-08	4.16E-06	6.90E-08	3.65E-06	4.46E-06	5.70E-08	1.12E-07	1.29E-07	1.92E-06
⁴⁸ Ca	1.17E-08	5.86E-08	1.89E-08	8.21E-08	5.87E-07	1.58E-08	3.31E-08	8.37E-07	2.55E-07
⁴⁴ Ca	8.24E-08	8.49E-08	1.09E-07	1.27E-07	1.32E-07	1.56E-07	1.56E-07	1.66E-07	2.64E-08
⁴⁵ Ca	1.26E-09	1.31E-09	2.78E-09	3.36E-09	3.36E-09	2.99E-09	5.66E-09	5.67E-09	2.30E-08
⁴⁶ Ca	1.93E-10	2.11E-10	5.94E-10	7.53E-10	7.57E-10	7.36E-10	1.54E-09	1.57E-09	4.64E-12
⁴⁷ Ca	4.66E-12	6.81E-12	9.01E-12	1.19E-11	1.30E-11	1.92E-11	3.57E-11	4.50E-11	1.87E-06
⁴⁸ Ca	1.58E-11	1.60E-11	1.83E-11	1.86E-11	1.88E-11	2.12E-11	2.55E-11	2.55E-11	6.44E-08
⁴³ Sc	2.05E-10	1.18E-07	1.19E-07	1.13E-07	7.17E-07	3.58E-11	2.59E-10	6.04E-07	1.89E-06
⁴⁵ Sc	1.73E-08	7.66E-07	2.04E-08	3.91E-07	8.47E-07	1.30E-08	3.29E-08	4.41E-07	4.37E-04
⁴⁴ Ti	2.70E-09	4.27E-05	2.78E-10	2.23E-05	2.01E-04	2.00E-11	1.18E-09	2.39E-04	1.69E-06
⁴⁶ Ti	3.30E-10	3.40E-07	5.53E-11	2.14E-07	2.10E-06	5.91E-12	2.52E-10	5.41E-07	6.19E-07
⁴⁶ Ti	6.03E-08	1.34E-06	3.45E-08	1.21E-06	2.51E-06	2.13E-08	5.52E-08	2.26E-06	7.25E-06
⁴⁷ Ti	1.57E-08	3.33E-07	1.33E-08	5.91E-07	2.27E-06	9.23E-09	2.20E-07	2.68E-06	3.06E-08
⁴⁸ Ti	1.62E-07	3.26E-07	1.83E-07	5.10E-07	4.08E-07	2.10E-07	5.90E-07	5.90E-07	3.24E-08
⁴⁹ Ti	2.14E-08	2.27E-08	3.13E-08	3.98E-08	3.67E-08	2.95E-08	4.60E-08	4.77E-08	1.27E-03
⁵⁰ Ti	4.89E-08	4.83E-08	6.06E-08	7.86E-08	7.79E-08	4.77E-08	1.03E-07	1.02E-07	3.13E-04
⁴⁷ V	2.81E-10	1.96E-07	5.71E-11	7.88E-08	8.59E-07	7.71E-12	3.50E-10	5.59E-09	1.01E-07
⁴⁸ V	1.11E-09	2.58E-05	2.07E-10	4.90E-05	3.99E-05	3.49E-11	6.67E-10	6.76E-05	8.80E-07
⁴⁹ V	1.35E-08	4.38E-06	5.84E-09	9.87E-06	6.60E-06	2.13E-09	9.71E-09	1.31E-05	7.32E-07
⁵⁰ V	3.29E-09	5.30E-09	3.47E-09	7.41E-09	7.10E-09	1.86E-09	5.82E-09	1.11E-08	1.01E-07
⁵¹ V	1.92E-08	6.59E-08	1.94E-08	1.53E-07	3.07E-08	1.78E-08	2.63E-08	4.31E-08	2.31E-06
⁴⁸ Cr	8.44E-11	2.26E-04	3.89E-12	2.54E-04	5.89E-04	1.73E-13	1.63E-10	7.65E-04	3.97E-08
⁴⁹ Cr	6.41E-11	4.91E-06	2.71E-12	2.48E-06	9.60E-06	2.10E-13	1.49E-10	1.29E-05	1.42E-03
⁵⁰ Cr	1.87E-08	9.25E-06	8.62E-09	1.16E-05	1.13E-05	8.32E-09	1.18E-08	2.88E-05	3.19E-06
⁵¹ Cr	6.71E-09	1.11E-05	9.79E-10	2.36E-05	8.48E-06	2.13E-10	2.27E-09	2.20E-05	3.33E-06
⁵² Cr	1.68E-06	1.63E-05	1.88E-06	4.17E-05	4.00E-06	2.06E-06	2.09E-06	6.26E-06	2.72E-09
⁵³ Cr	9.82E-08	9.98E-08	1.13E-07	1.17E-07	1.17E-07	1.23E-07	1.29E-07	1.32E-07	9.54E-09
⁵⁴ Cr	1.00E-07	1.00E-07	1.32E-07	1.63E-07	1.63E-07	1.17E-07	2.12E-07	2.12E-07	7.80E-07
⁵¹ Mn	5.19E-11	9.60E-06	2.32E-12	3.88E-06	1.94E-05	2.58E-13	7.51E-11	2.98E-05	1.04E-06
⁵² Mn	7.12E-10	7.82E-04	2.99E-11	2.01E-03	2.69E-04	2.65E-12	5.97E-10	6.05E-04	6.40E-13
⁵³ Mn	6.05E-09	1.50E-04	1.08E-09	2.35E-04	1.99E-04	2.96E-10	2.56E-09	4.05E-04	8.40E-08
⁵⁴ Mn	4.78E-09	3.65E-07	1.18E-09	4.09E-07	3.79E-07	2.54E-10	2.27E-09	1.10E-06	2.63E-05
⁵⁵ Mn	3.28E-07	3.42E-07	3.64E-07	3.96E-07	4.01E-07	3.86E-07	4.12E-07	4.50E-07	1.06E-07
⁵² Fe	4.01E-12	2.93E-02	5.09E-14	3.31E-03	5.61E-03	4.10E-15	1.18E-11	8.52E-03	1.24E-08
⁵³ Fe	4.54E-12	2.28E-05	5.11E-14	6.80E-06	4.50E-05	1.20E-14	9.75E-12	2.88E-05	9.80E-09
⁵⁴ Fe	6.01E-07	1.08E-03	6.72E-07	1.34E-03	1.34E-03	7.37E-07	7.33E-07	3.78E-03	4.47E-08
⁵⁵ Fe	2.67E-08	7.76E-05	1.36E-08	1.37E-04	1.44E-04	1.50E-08	2.05E-08	2.16E-04	1.24E-16
⁵⁶ Fe	1.07E-04	1.17E-04	1.21E-04	1.32E-04	1.35E-04	1.32E-04	1.33E-04	1.56E-04	3.74E-23
⁵⁷ Fe	4.39E-06	4.56E-06	5.12E-06	5.39E-06	5.62E-06	5.71E-06	6.03E-06	6.62E-06	1.08E-05
⁵⁸ Fe	3.27E-06	3.30E-06	3.74E-06	4.61E-06	4.62E-06	3.72E-06	6.00E-06	6.03E-06	7.41E-10
⁵⁹ Fe	1.16E-07	1.47E-07	1.56E-07	1.97E-07	2.16E-07	3.84E-07	5.26E-07	5.79E-07	4.79E-08
⁶⁰ Fe	1.46E-08	2.19E-08	2.14E-08	2.86E-08	3.30E-08	6.83E-08	1.01E-07	1.27E-07	1.21E-08
Mass	26.9	28.0	29.8	32.8	33.2	31.1	35.8	38.2	38.2

TABLE 13A
PRODUCTION FACTORS 12–25 M_{\odot} MODELS; $Z = 0.01 Z_{\odot}$

	T12A	T13A	T15A	T18A	T20A	T22A	T25A	T12A	T13A	T15A	T18A	T20A	T22A	T25A
¹ H	.84	.82	.78	.73	.71	.68	.63	4.10	7.04	7.98	10.06	16.94	16.09	13.94
² H	.17	.16	.14	.12	.12	.11	.10	.23	.21	.40	1.59	9.18	2.40	7.97
³ He	1.19	1.14	1.08	1.00	.97	.94	.88	.41	.41	.52	3.29	.81	.30	.87
⁴ He	1.33	1.34	1.37	1.38	1.33	1.36	1.37	4.04	3.86	4.70	2.10	.50	.52	3.38
⁶ Li	.00	.00	.00	.00	.00	.00	.00	.00	.03	.02	.01	.01	.01	.00
⁷ Li	5.01	3.82	3.05	2.53	1.56	1.79	2.15	.00	.00	.00	.00	.00	.00	.00
⁹ Be	.01	.00	.00	.00	.00	.00	.00	4.05	4.89	6.25	3.37	.94	.74	4.48
¹⁰ B	.00	.00	.00	.00	.00	.00	.00	.93	.74	.74	1.20	2.27	.78	2.23
¹¹ B	10.73	10.92	10.26	7.19	7.28	7.57	6.95	.39	.40	.54	.24	.21	.17	.42
¹² C	2.79	3.08	3.64	3.88	3.79	4.07	3.95	6.35	7.74	8.40	5.40	4.31	4.70	6.15
¹³ C	.02	.02	.03	.02	.03	.03	.04	2.24	2.95	3.14	2.69	2.92	2.98	2.55
¹⁴ N	.03	.03	.04	.03	.03	.04	.04	.00	.00	.00	.00	.00	.00	.00
¹⁵ N	.16	.22	.39	.68	1.20	1.15	1.29	.02	.04	.11	.33	.49	.36	.47
¹⁶ O	1.39	1.88	3.26	6.01	9.28	10.06	12.69	.00	.00	.12	2.74	3.48	3.39	2.08
¹⁷ O	.43	.37	.26	.18	.16	.13	.10	.91	1.89	2.12	2.74	3.48	3.39	2.08
¹⁸ O	.07	.11	.14	.22	.16	.05	.03	.15	.24	.51	1.30	1.13	.88	.68
¹⁹ F	.59	.46	.79	4.74	4.7	.28	.30	4.72	9.29	8.22	9.00	11.73	12.30	7.29
²⁰ Ne	.56	1.33	1.84	6.91	1.87	1.27	1.17	1.97	3.71	3.68	4.40	5.31	5.39	3.34
²¹ Ne	.24	.31	.42	1.10	1.16	.22	.16	1.86	2.61	2.62	2.37	2.11	2.07	1.87
²² Ne	.08	.02	.03	.12	.10	.14	.15	.18	.34	.61	1.14	1.03	.96	.59
²³ Ne	.14	.18	.26	2.12	.13	.26	.30	12.23	14.06	10.87	7.03	3.47	4.24	7.02
²⁴ Mg	1.06	1.78	3.05	4.22	1.79	5.55	3.31	18.60	18.90	14.76	7.23	1.42	2.10	7.61
²⁵ Mg	.07	.10	.18	.33	.11	.16	.12	.10	.09	.09	.03	.02	.03	.03
²⁶ Mg	.04	.04	.12	.27	.06	.12	.11	7.65	7.43	5.84	1.27	.07	.13	2.75
²⁷ Al	.21	.30	.94	1.02	1.01	2.68	2.09	9.79	8.93	6.12	.53	.26	.30	1.28
²⁸ Si	4.49	5.46	8.30	9.39	20.64	23.74	25.33	23.20	23.02	18.75	9.71	.38	1.42	10.91
²⁹ Si	.23	.32	.72	.52	1.64	2.00	2.18	28.22	28.83	23.59	9.98	.29	1.40	13.76
³⁰ Si	.09	.15	.76	.37	1.16	2.51	2.33	30.48	28.56	22.27	4.49	.06	.04	7.59
³¹ P	.45	.62	1.29	1.38	6.03	6.11	8.86	.01	.01	.03	.07	.05	.08	.07
³² S	3.32	4.74	6.47	8.59	20.64	18.62	22.22	1.83	1.95	2.43	.86	.06	.06	.89
³³ S	1.00	1.33	2.17	2.86	15.15	11.07	20.36	4.6	4.7	.50	.23	.06	.19	.36
³⁴ S	.14	.18	.57	.69	4.66	2.32	3.55	13.73	13.04	11.27	4.76	.17	1.38	3.54
³⁶ S	.01	.02	.03	.02	.21	.14	.21	3.50	3.35	2.77	.76	.13	.14	1.25
³⁶ Cl	.35	.46	.97	1.87	15.64	9.31	22.64	.04	.04	.06	.08	.04	.05	.07
³⁷ Cl	.24	.28	.46	1.22	11.37	5.05	14.43	.01	.01	.02	.07	.07	.12	.12
³⁸ Ar	3.42	5.37	6.66	8.89	26.29	18.41	27.77	.01	.01	.02	.01	.02	.03	.03
³⁸ Ar	.07	.09	.27	1.13	4.71	1.40	3.19	.02	.03	.07	.13	.19	.34	.50
⁴⁰ Ar	.01	.04	.04	.04	.34	.23	.44	.05	.08	.19	.75	.65	.91	1.05
³⁹ K	.29	.34	.57	1.54	9.01	4.62	12.98	.02	.05	.08	.05	.15	1.15	2.21
⁴⁰ K	.06	.09	.19	.69	12.08	7.79	16.16	.04	.05	.15	.28	1.23	1.15	2.21
⁴¹ K	.41	.43	.58	1.42	8.16	4.28	11.67							

TABLE 13B
PRODUCTION FACTORS 30-40 M_{\odot} MODELS; $Z = 0.01 Z_{\odot}$

KE $_{\infty}$	T30A	T30B	T35A	T35B	T35C	T40A	T40B	T40C	KE $_{\infty}$	T30A	T30B	T35A	T35B	T35C	T40A	T40B	T40C
¹ H	.61	.59	.61	.55	.55	.62	.54	.51	⁴⁰ Ca	.01	10.59	.01	10.31	10.62	.01	.01	16.27
² H	.09	.09	.09	.08	.08	.09	.08	.07	⁴² Ca	.01	.35	.01	.27	.32	.00	.01	.33
³ He	.86	.83	.88	.80	.79	.93	.81	.76	⁴³ Ca	.00	.07	.01	.07	.44	.01	.01	.43
⁴ He	1.39	1.34	1.47	1.33	1.32	1.62	1.41	1.33	⁴⁴ Ca	.00	1.08	.00	.48	4.25	.00	.00	4.39
⁶ Li	.00	.00	.00	.00	.00	.00	.00	.00	⁴⁶ Ca	.00	.00	.01	.01	.01	.01	.02	.01
⁷ Li	1.83	1.46	1.83	1.31	1.17	1.60	1.16	1.00	⁴⁸ Ca	.00	.00	.00	.00	.00	.00	.00	.00
⁹ Be	.00	.00	.00	.00	.00	.00	.00	.00	⁴⁵ Sc	.02	1.02	.02	.48	2.28	.01	.03	.66
¹⁰ B	.00	.00	.00	.00	.00	.00	.00	.00	⁴⁶ Ti	.01	.22	.01	.17	.34	.00	.01	.27
¹¹ B	5.40	4.83	4.54	4.39	4.17	3.64	5.29	4.86	⁴⁷ Ti	.00	.09	.00	.10	.45	.00	.00	.41
¹² C	3.86	3.72	3.79	3.55	3.50	3.60	3.58	3.36	⁴⁸ Ti	.00	4.19	.00	4.31	8.81	.00	.00	10.16
¹³ C	.03	.02	.03	.02	.02	.03	.02	.02	⁴⁹ Ti	.01	2.04	.01	2.31	2.99	.01	.01	4.17
¹⁴ N	.04	.04	.04	.04	.04	.05	.04	.04	⁵⁰ Ti	.01	.01	.01	.01	.01	.01	.02	.02
¹⁵ N	1.17	1.24	.65	1.18	1.12	.29	1.07	1.19	⁵¹ V	.13	.20	.13	.24	.23	.06	.18	.31
¹⁶ O	15.40	16.58	12.84	17.98	17.67	8.74	18.03	19.27	⁵² Cr	.00	1.97	.00	2.24	2.23	.00	.00	3.60
¹⁷ O	.08	.07	.06	.05	.05	.06	.05	.05	⁵³ Cr	.00	.45	.00	.48	.46	.00	.00	1.02
¹⁸ O	.01	.01	.01	.01	.01	.01	.01	.01	⁵⁴ Cr	.00	8.98	.00	11.02	11.91	.00	.00	16.09
¹⁹ F	2.34	2.04	4.96	5.54	5.24	3.48	7.80	7.00	⁵⁵ Cr	.00	3.61	.00	4.30	4.27	.00	.00	6.62
²⁰ Ne	8.19	7.75	14.75	17.68	17.24	10.55	22.70	21.05	⁵⁶ Cr	.01	.04	.01	.04	.04	.01	.01	.08
²¹ Ne	.73	.68	1.36	1.52	1.47	1.35	2.49	2.29	⁵⁵ Mn	.00	1.42	.00	1.49	2.68	.00	.00	3.84
²² Ne	.15	.14	.16	.15	.14	.16	.15	.14	⁵⁴ Fe	.00	.54	.00	.57	.57	.00	.00	1.39
²³ Ne	1.52	1.44	2.99	3.24	3.15	3.06	5.26	4.91	⁵⁶ Fe	.00	5.53	.00	4.84	15.35	.00	.00	15.88
²⁴ Mg	18.38	19.13	11.77	19.60	19.20	4.63	15.34	17.26	⁵⁷ Fe	.01	3.82	.01	2.77	16.16	.01	.01	15.83
²⁵ Mg	.48	.47	.74	.92	.89	.47	1.05	.99	⁵⁸ Fe	.03	.03	.03	.04	.06	.03	.05	.10
²⁶ Mg	.39	.37	.69	.83	.81	.42	.97	.90	⁵⁹ Co	.02	.42	.01	.41	.41	.01	.02	6.15
²⁷ Al	5.87	6.07	3.05	5.20	5.09	1.02	3.90	4.37	⁵⁸ Ni	.00	.40	.00	.34	3.66	.00	.00	5.97
²⁸ Si	6.62	16.87	.93	12.54	12.58	1.19	1.17	16.57	⁶⁰ Ni	.01	5.37	.01	2.69	22.51	.01	.01	20.99
²⁹ Si	.91	1.67	.41	1.43	1.42	.12	.56	1.49	⁶¹ Ni	.04	5.76	.04	2.68	24.99	.03	.05	22.87
³⁰ Si	3.29	3.75	.89	2.15	2.13	.15	1.08	1.68	⁶² Ni	.03	.05	.03	.73	16.18	.02	.04	20.77
³¹ P	3.08	4.23	.63	2.36	2.32	.11	.75	2.22	⁶⁴ Ni	.21	.20	.20	.25	.24	.14	.28	.26
³² S	.31	8.88	.02	8.53	8.58	.01	.03	13.05	⁶³ Cu	.05	.13	.06	.16	1.62	.04	.08	1.91
³³ S	.53	2.65	.03	2.16	2.30	.01	.12	2.52	⁶⁵ Cu	.25	.58	.19	.31	.59	.13	.27	.57
³⁴ S	.21	.88	.03	.57	.60	.00	.03	.62	⁶⁴ Zn	.02	6.39	.02	1.37	6.49	.01	.02	5.18
³⁶ S	.02	.03	.02	.03	.03	.02	.03	.04	⁶⁶ Zn	.16	.43	.12	.29	2.03	.08	.18	2.28
³⁵ Cl	1.02	2.08	.07	1.12	1.10	.01	.10	1.29	⁶⁷ Zn	.18	.17	.24	.29	.29	.16	.34	.34
³⁷ Cl	.06	.66	.03	.55	.57	.03	.04	.60	⁶⁸ Zn	.34	.33	.33	.41	.40	.23	.48	.46
³⁹ Ar	.01	8.87	.01	8.62	8.74	.01	.01	13.47	⁷⁰ Zn	.06	.05	.04	.06	.06	.03	.09	.09
³⁸ Ar	.01	.35	.00	.27	.28	.00	.01	.29	⁶⁹ Ga	.69	.72	.50	.73	.71	.36	.79	.84
⁴⁰ Ar	.05	.05	.07	.08	.08	.07	.10	.10	⁷¹ Ga	4.55	4.31	5.79	6.98	6.81	4.38	8.95	8.29
³⁹ K	.02	.66	.01	.57	.62	.01	.01	.75	⁷⁰ Ge	1.65	1.99	.66	1.53	1.53	.42	1.07	1.77
⁴⁰ K	.14	.37	.17	.37	.35	.14	.24	.40									
⁴¹ K	.01	.72	.01	.59	.66	.01	.01	.70									

TABLE 14B—Continued

KE _∞	U30A	U30B	U35A	U35B	U35C	U40A	U40B	U40C	U40B	U40C
KE _∞	1.30	2.02	1.18	1.86	2.44	1.33	1.97	2.53	1.97	2.53
³⁹ K	8.32E-07	5.09E-05	6.01E-11	7.39E-07	6.63E-05	6.88E-11	2.99E-07	8.17E-05	7.44E-13	1.03E-14
⁴⁰ K	2.50E-09	2.97E-08	1.74E-13	1.47E-09	2.87E-08	3.18E-13	4.49E-10	3.00E-08	1.67E-11	3.88E-13
⁴¹ K	2.26E-10	3.36E-09	5.78E-09	5.95E-09	9.07E-08	1.09E-11	7.25E-11	3.19E-09	1.48E-09	9.91E-14
⁴⁰ Ca	3.37E-07	1.60E-02	1.59E-08	9.28E-07	2.18E-02	1.84E-08	1.39E-07	3.42E-02	4.98E-10	8.39E-14
⁴¹ Ca	4.71E-09	4.69E-06	1.20E-12	1.02E-08	5.59E-06	1.31E-11	7.08E-10	5.90E-06	1.81E-08	2.47E-09
⁴² Ca	3.21E-09	2.97E-06	9.63E-06	3.90E-08	3.90E-06	1.74E-11	1.25E-09	4.27E-06	1.21E-09	3.88E-10
⁴³ Ca	1.45E-10	4.59E-08	2.50E-09	2.80E-09	4.66E-07	6.92E-12	7.37E-11	6.08E-07	1.09E-09	2.22E-11
⁴⁴ Ca	6.40E-10	3.69E-09	1.58E-08	1.59E-08	2.22E-08	4.00E-10	5.60E-10	7.60E-09	1.18E-13	6.73E-19
⁴⁵ Ca	1.48E-10	1.47E-10	9.64E-09	9.86E-09	9.83E-09	4.97E-12	1.87E-11	2.06E-11	2.01E-12	1.41E-12
⁴⁶ Ca	3.19E-10	3.18E-10	2.52E-08	2.59E-08	2.58E-08	2.66E-12	1.06E-11	1.12E-11	4.92E-08	5.25E-08
⁴⁷ Ca	1.19E-10	1.24E-10	9.20E-09	9.94E-09	1.02E-08	6.17E-14	1.39E-12	1.56E-12	1.96E-11	1.23E-10
⁴⁸ Ca	3.20E-10	3.33E-10	6.99E-08	7.26E-08	7.26E-08	6.76E-14	5.26E-13	5.88E-13	4.50E-08	1.93E-08
⁴³ Sc	1.51E-11	1.06E-07	3.26E-15	9.72E-11	8.02E-07	1.07E-17	6.72E-12	8.44E-07	1.11E-08	1.69E-09
⁴⁵ Sc	5.69E-11	9.29E-07	8.26E-11	1.66E-10	6.08E-07	1.91E-11	6.59E-11	2.46E-07	3.03E-04	3.12E-08
⁴⁴ Ti	2.40E-10	6.17E-05	9.46E-17	3.77E-10	2.04E-04	9.09E-19	7.88E-11	2.35E-04	5.42E-09	9.19E-10
⁴⁶ Ti	1.54E-11	9.18E-07	1.04E-16	2.23E-11	2.32E-06	7.06E-18	5.86E-12	8.97E-06	2.42E-09	7.63E-10
⁴⁶ Ti	1.44E-10	9.79E-07	6.34E-12	1.04E-09	2.22E-06	6.57E-12	8.53E-11	1.95E-06	9.77E-13	2.87E-16
⁴⁷ Ti	3.73E-11	2.49E-07	1.02E-09	1.12E-09	2.04E-06	6.47E-12	3.16E-11	2.42E-06	1.89E-11	2.16E-15
⁴⁸ Ti	7.73E-10	8.72E-08	2.84E-09	2.56E-09	1.49E-07	9.16E-10	9.51E-10	7.77E-08	2.90E-08	4.53E-17
⁴⁹ Ti	1.12E-10	4.73E-10	5.84E-09	5.92E-09	6.88E-09	1.15E-10	1.69E-10	1.09E-09	3.97E-09	9.16E-11
⁵⁰ Ti	2.60E-10	2.66E-10	2.63E-08	2.69E-08	2.67E-08	3.09E-11	2.94E-10	3.14E-10	4.63E-10	1.69E-13
⁴⁷ V	5.81E-13	2.34E-07	4.52E-16	5.21E-12	1.04E-06	3.94E-18	6.45E-13	8.39E-07	7.84E-09	1.15E-10
⁴⁸ V	1.79E-12	1.57E-05	3.09E-15	5.51E-12	2.93E-05	7.29E-17	1.24E-12	2.91E-05	4.13E-12	8.20E-15
⁴⁹ V	1.65E-11	2.60E-06	8.23E-14	4.89E-11	6.26E-06	7.02E-16	1.30E-11	1.13E-05	3.45E-19	1.10E-05
⁵⁰ V	4.69E-12	1.43E-09	2.64E-13	8.61E-12	1.71E-09	4.28E-15	7.84E-12	3.69E-09	9.94E-19	1.37E-08
⁵¹ V	6.77E-11	2.27E-09	3.03E-09	3.93E-09	1.04E-08	3.61E-11	7.69E-11	9.73E-09	4.10E-12	1.16E-03
⁴⁸ Cr	3.19E-13	2.40E-04	4.14E-20	4.83E-13	6.18E-04	1.69E-22	5.71E-13	7.88E-04	3.24E-07	1.06E-05
⁴⁹ Cr	2.12E-13	5.68E-06	1.70E-18	5.53E-13	1.01E-05	1.79E-18	3.91E-13	1.30E-05	5.04E-09	9.89E-10
⁵⁰ Cr	2.98E-11	6.72E-06	1.29E-11	2.54E-10	9.29E-06	1.44E-11	2.31E-11	2.04E-05	9.95E-10	1.76E-12
⁵¹ Cr	1.11E-11	4.03E-06	2.92E-13	7.01E-11	8.19E-06	3.47E-14	5.29E-12	1.87E-05	1.18E-08	2.75E-10
⁵² Cr	5.43E-09	9.78E-07	1.56E-08	1.62E-08	1.46E-06	6.57E-09	7.16E-09	1.48E-06	2.30E-09	3.29E-09
⁵³ Cr	3.00E-10	1.41E-09	1.89E-09	1.94E-09	3.17E-09	3.38E-10	4.50E-10	3.20E-09	4.47E-08	4.40E-08
⁵⁴ Cr	4.97E-10	7.54E-10	1.34E-08	1.42E-08	1.47E-08	1.20E-10	1.07E-09	1.90E-09	7.99E-09	9.36E-09
⁵¹ Mn	8.87E-14	1.18E-05	7.34E-16	3.36E-13	1.91E-05	5.86E-17	1.63E-13	2.80E-05	1.14E-15	7.02E-07
⁵² Mn	1.48E-12	1.28E-04	1.83E-14	3.35E-12	2.46E-04	9.12E-16	1.93E-12	4.63E-04	6.37E-14	7.56E-07
⁵³ Mn	4.03E-11	1.11E-04	3.97E-14	5.71E-11	2.00E-04	1.72E-15	2.06E-11	3.72E-04	9.51E-16	1.22E-05
⁵⁴ Mn	2.22E-11	2.52E-07	1.60E-13	1.93E-11	3.14E-07	2.02E-15	1.24E-11	8.12E-07	1.19E-10	2.85E-08
⁵⁵ Mn	1.31E-09	9.10E-09	3.91E-09	4.89E-09	2.78E-08	1.48E-09	1.75E-09	2.41E-08	3.03E-11	3.13E-11
⁵³ Fe	1.35E-14	3.01E-03	3.48E-20	2.80E-14	5.80E-03	1.83E-21	4.41E-14	8.46E-03	8.83E-10	9.46E-13
⁵⁴ Fe	2.31E-14	3.45E-05	3.56E-18	5.63E-14	4.48E-05	3.78E-18	4.33E-14	3.17E-05	5.11E-10	6.75E-10
⁵⁵ Fe	1.38E-09	8.10E-04	1.50E-09	1.75E-09	1.14E-03	1.69E-09	1.75E-09	2.85E-03	1.29E-22	2.49E-36
⁵⁶ Fe	8.94E-11	3.88E-05	1.00E-12	1.43E-10	1.21E-04	1.35E-11	6.93E-11	1.38E-04	1.09E-26	7.01E-18
⁵⁷ Fe	5.54E-07	6.42E-06	6.07E-07	6.34E-07	1.08E-05	6.89E-07	7.26E-07	8.95E-06	2.37E-06	2.05E-05
⁵⁸ Fe	2.86E-08	1.23E-07	2.36E-08	3.54E-08	2.70E-07	2.99E-08	4.79E-08	2.35E-07	5.80E-10	5.63E-09
⁵⁹ Fe	3.54E-08	3.47E-08	6.17E-09	5.01E-08	5.68E-08	1.05E-08	7.36E-08	9.69E-08	5.08E-11	3.97E-09
⁶⁰ Fe	9.15E-10	8.86E-10	5.76E-09	6.54E-09	6.52E-09	2.96E-09	1.14E-08	1.17E-08	1.58E-11	1.66E-11
⁶⁰ Fe	7.60E-09	7.44E-09	1.73E-08	1.80E-08	1.80E-08	1.23E-09	5.80E-09	6.17E-09	1.30E-07	1.28E-07
Mass										
		27.3	25.1	32.2	33.2	28.1	36.1	26.5		
										38.2

TABLE 15A
PRODUCTION FACTORS 12–25 M_{\odot} MODELS; $Z = 10^{-4} Z_{\odot}$

	U12A	U13A	U18A	U20A	U22A	U25A	U12A	U13A	U15A	U18A	U20A	U22A	U25A
¹ H	.84	.83	.80	.72	.70	.65	18.13	7.22	5.51	6.10	17.37	19.12	13.47
² H	.09	.08	.07	.06	.05	.05	5.17	1.19	.23	.37	5.29	3.26	2.21
³ He	.72	.69	.65	.55	.53	.49	.63	.23	.12	.35	.50	.35	.47
⁴ He	1.32	1.35	1.37	1.32	1.34	1.33	4.18	3.50	3.28	2.83	.52	.99	3.14
⁶ Li	.00	.00	.00	.00	.00	.00	.00	.00	.00	.00	.00	.00	.00
⁷ Li	4.84	4.53	1.89	1.50	2.31	2.13	3.69	3.28	.00	.00	.00	.00	.00
⁹ Be	.01	.01	.00	.00	.00	.00	4.24	3.28	20.33	5.20	1.67	1.28	3.64
¹⁰ B	.00	.00	.00	.00	.00	.00	.00	1.09	1.65	.49	1.67	.89	.74
¹¹ B	7.55	12.47	9.17	6.00	9.71	6.84	.34	.24	.56	.39	.20	.16	.34
¹² C	2.26	3.10	3.50	3.90	4.47	4.18	6.35	6.71	6.74	5.53	4.93	5.30	6.53
¹³ C	.02	.02	.02	.03	.03	.02	2.78	2.72	2.07	2.38	3.17	2.98	2.63
¹⁴ N	.00	.00	.00	.00	.00	.00	.00	.00	.00	.00	.00	.00	.00
¹⁵ N	.19	.18	.33	1.09	1.01	1.26	.48	.18	.05	.21	.41	.17	.27
¹⁶ O	1.41	1.62	2.97	8.71	8.96	12.47	1.56	1.96	1.09	2.22	3.75	3.12	2.26
¹⁷ O	.01	.01	.01	.01	.01	.01	2.24	.94	.24	.88	1.04	.70	.51
¹⁸ O	.00	.00	.00	.00	.00	.00	5.03	7.70	5.33	6.46	13.23	12.37	8.60
¹⁹ F	2.24	2.1	.62	5.98	.43	.49	2.95	3.62	2.34	3.29	5.78	5.16	3.70
²⁰ Ne	3.20	.55	1.56	2.01	2.00	2.17	.05	.05	.02	.07	.07	.04	.04
²¹ Ne	.27	.05	.14	.08	.17	.16	1.47	1.80	.90	2.53	2.27	1.85	1.91
²² Ne	.00	.00	.00	.00	.00	.00	.91	.83	.30	.99	1.02	.71	.54
²³ Na	1.18	.07	.13	2.82	.17	.33	4.33	6.58	4.05	8.38	4.27	5.26	7.61
²⁴ Mg	1.52	1.25	2.56	6.67	3.16	8.01	7.03	8.51	3.92	10.23	1.92	3.04	7.60
²⁵ Mg	.10	.03	.10	.05	.11	.15	.00	.00	.00	.02	.00	.00	.01
²⁶ Mg	.08	.02	.08	.01	.07	.10	1.43	1.07	.74	4.25	.09	.25	2.59
²⁷ Al	.39	.20	.74	2.19	1.13	3.17	.50	.51	1.21	2.18	.30	.44	1.37
²⁸ Si	8.55	6.85	5.94	20.33	21.25	23.63	10.50	11.89	7.38	13.60	.95	3.26	11.02
²⁹ Si	.23	.24	.55	1.60	1.14	1.77	10.69	11.65	8.18	15.80	.85	3.55	13.38
³⁰ Si	.05	.06	.56	1.34	.63	2.40	6.58	4.70	.28	11.39	.02	.01	6.53
³¹ P	1.43	.80	.91	1.72	4.02	6.05	.00	.00	.00	.00	.00	.00	.00
³² S	11.18	5.99	4.40	19.68	20.79	17.58	2.18	2.70	.88	1.21	.03	.04	.73
³³ S	3.71	1.92	1.62	12.86	10.58	12.00	.27	.32	.56	.20	.03	.20	.36
³⁴ S	.98	.50	.41	4.21	1.45	1.53	7.47	11.37	16.37	3.31	.78	3.59	5.28
³⁵ S	.02	.01	.01	.16	.07	.10	1.06	1.01	.67	1.38	.02	.13	.98
³⁶ Cl	3.76	1.21	.66	11.60	8.43	9.57	.01	.01	.01	.01	.00	.00	.01
³⁷ Cl	2.81	.84	.51	8.38	6.53	5.90	.00	.00	.00	.00	.00	.00	.00
³⁶ Ar	13.36	6.26	4.55	23.16	22.45	17.13	.00	.00	.00	.00	.00	.00	.00
³⁸ Ar	2.93	.85	.20	3.44	1.81	1.01	.00	.00	.00	.00	.00	.00	.00
⁴⁰ Ar	.03	.01	.00	.18	.12	.19	.00	.00	.00	.00	.00	.00	.00
³⁸ K	4.90	.98	.34	5.44	5.56	5.25	.00	.00	.00	.00	.00	.00	.00
⁴⁰ K	1.23	.35	.13	6.83	4.68	7.40	.00	.00	.00	.00	.00	.00	.00
⁴¹ K	4.63	.85	.54	5.97	5.96	6.69	.00	.00	.00	.00	.00	.00	.00

TABLE 15B
 PRODUCTION FACTORS 30–40 M_{\odot} MODELS; $Z = 10^{-4}$

KE $_{\infty}$	U30A	U30B	U35A	U35B	U35C	U40A	U40B	U40C	KE $_{\infty}$	U30A	U30B	U35A	U35B	U35C	U40A	U40B	U40C
¹ H	.62	.60	.74	.58	.56	.77	.56	.53	⁴⁰ Ca	.00	9.50	.00	.00	10.96	.00	.00	14.94
² H	.04	.04	.05	.04	.04	.05	.04	.04	⁴² Ca	.00	.25	.00	.00	.28	.00	.00	.27
³ He	.46	.45	.56	.44	.42	.57	.42	.40	⁴³ Ca	.00	.06	.00	.00	.43	.00	.00	.42
⁴ He	1.34	1.31	1.70	1.34	1.30	1.66	1.37	1.30	⁴⁴ Ca	.00	1.54	.00	.00	4.31	.00	.00	4.33
⁷ Li	2.02	2.00	2.62	2.18	2.31	2.93	2.52	2.65	⁴⁶ Ca	.00	.00	.36	.29	.28	.00	.00	.00
¹¹ B	5.34	4.63	2.20	4.34	3.93	1.63	5.31	4.82	⁴⁸ Ca	.00	.00	.02	.02	.02	.00	.00	.00
¹² C	4.03	3.91	2.15	3.68	3.55	.99	3.84	3.63	⁴⁸ Sc	.00	1.69	.01	.01	2.27	.00	.00	.77
¹³ C	.02	.02	.01	.01	.01	.00	.01	.01	⁴⁶ Ti	.00	.15	.00	.00	.30	.00	.00	.23
¹⁵ N	1.15	1.15	.00	1.18	1.12	.00	1.06	1.13	⁴⁷ Ti	.00	.08	.00	.00	.45	.00	.00	.41
¹⁶ O	15.54	16.13	.11	18.01	17.63	.03	17.89	18.70	⁴⁸ Ti	.00	4.25	.00	.00	9.07	.00	.00	9.96
¹⁹ F	3.11	2.66	.03	4.53	4.14	.00	6.98	6.31	⁴⁹ Ti	.00	1.80	.00	.00	3.00	.00	.00	3.89
²⁰ Ne	10.47	9.92	.00	15.91	15.18	.00	21.53	20.12	⁵⁰ V	.00	.05	.00	.00	.06	.00	.00	.10
²¹ Ne	.81	.75	.01	1.20	1.13	.00	2.19	2.03	⁵¹ V	.00	1.50	.00	.00	2.18	.00	.00	3.25
²² Ne	.01	.01	.00	.01	.01	.00	.02	.02	⁵⁰ Cr	.00	.32	.00	.00	.38	.00	.00	.72
²³ Ne	1.63	1.54	.00	2.31	2.20	.00	4.26	4.00	⁵² Cr	.00	7.53	.00	.00	12.25	.00	.00	15.72
²⁴ Ne	17.91	18.09	.00	19.77	18.99	.00	15.04	16.15	⁵³ Cr	.00	3.01	.00	.00	4.30	.00	.00	6.16
²⁵ Mg	.46	.44	.00	.73	.69	.00	.83	.79	⁵⁴ Cr	.00	.02	.00	.00	.02	.00	.00	.05
²⁶ Mg	.34	.33	.00	.61	.59	.00	.71	.67	⁵⁵ Mn	.00	1.24	.00	.00	2.57	.00	.00	3.51
²⁷ Mg	4.91	4.93	.00	4.77	4.64	.00	3.36	3.60	⁵⁴ Fe	.00	.40	.00	.00	.48	.00	.00	1.05
²⁸ Si	5.37	14.25	.00	4.51	12.41	.00	1.49	14.71	⁵⁶ Fe	.00	6.47	.00	.00	15.12	.00	.00	15.54
²⁸ Si	.72	1.29	.00	1.08	1.27	.00	.48	1.24	⁵⁷ Fe	.00	4.99	.00	.00	15.88	.00	.00	15.72
³⁰ Si	2.33	2.53	.00	1.93	1.90	.00	.92	1.26	⁵⁸ Fe	.00	.00	.00	.00	.03	.00	.00	.06
³¹ P	2.19	3.02	.00	1.59	2.17	.00	.69	1.83	⁵⁹ Co	.00	.58	.00	.00	5.87	.00	.00	6.19
³² S	.24	7.97	.00	.25	8.45	.00	.05	11.59	⁵⁸ Ni	.00	.54	.00	.00	3.64	.00	.00	6.42
³³ S	.56	2.29	.00	.71	2.17	.00	.24	2.28	⁶⁰ Ni	.00	8.08	.00	.00	22.09	.00	.00	20.76
³⁴ S	.14	.61	.00	.28	.51	.00	.03	.48	⁶¹ Ni	.00	8.66	.00	.00	24.72	.00	.00	22.65
³⁶ S	.03	.04	.23	.19	.19	.00	.00	.01	⁶² Ni	.00	.03	.00	.00	16.03	.00	.00	21.86
³⁵ Cl	.62	1.42	.00	.33	1.03	.00	.10	1.05	⁶³ Cu	.00	.13	.00	.00	1.55	.00	.00	1.86
³⁷ Cl	.03	.55	.00	.04	.52	.00	.01	.49	⁶⁵ Cu	.00	.44	.00	.00	.35	.00	.00	.29
³⁶ Ar	.04	8.01	.00	.04	8.82	.00	.01	12.14	⁶⁴ Zn	.00	9.89	.00	.00	6.52	.00	.00	5.01
³⁸ Ar	.00	.25	.00	.01	.23	.00	.00	.23	⁶⁶ Zn	.00	.41	.00	.00	1.85	.00	.00	2.16
⁴⁰ Ar	.00	.01	.07	.06	.06	.00	.00	.00	⁶⁷ Zn	.00	.00	.00	.00	.01	.00	.00	.02
³⁸ K	.01	.52	.00	.01	.58	.00	.01	.62	⁶⁹ Ga	.01	.01	.01	.02	.02	.00	.00	.00
⁴⁰ K	.02	.19	.00	.01	.16	.00	.00	.14	⁷¹ Ga	.06	.06	.19	.15	.15	.00	.01	.01
⁴¹ K	.00	.63	.00	.00	.64	.00	.00	.59	⁷⁰ Ge	.00	.00	.01	.01	.01	.00	.00	.00

TABLE 16A
EJECTED MASSES AT 2.5×10^4 s, 1.2 – $2.5 M_{\odot}$ MODELS; $Z = 0$

KE $_{\infty}$	Z12A	Z13A	Z15A	Z18A	Z20A	Z22A	Z25A	Z25B	Z25C
¹ H	6.39	6.83	7.69	8.85	9.56	10.2	11.4	11.4	11.4
⁴ He	4.08	4.42	4.90	5.70	6.32	7.10	7.33	7.33	7.33
² H	1.14E-05	1.00E-06	9.94E-06	8.57E-06	7.29E-06	7.29E-06	7.29E-06	7.29E-06	7.29E-06
³ He	7.39E-05	7.80E-05	8.12E-05	8.78E-05	9.37E-05	9.63E-05	1.02E-04	1.02E-04	1.02E-04
⁷ Li	1.00E-07	8.14E-08	1.10E-08	1.88E-09	2.43E-08	2.43E-08	5.64E-09	5.64E-09	5.64E-09
⁷ Be	1.59E-07	2.89E-07	1.14E-06	1.95E-06	2.88E-06	2.88E-06	2.27E-06	2.27E-06	2.27E-06
⁹ Be	5.35E-13	9.92E-13	8.83E-14	1.13E-15	5.18E-16	4.62E-14	1.61E-16	1.61E-16	1.61E-16
¹⁰ B	1.42E-12	3.33E-12	6.82E-12	2.69E-11	2.68E-11	1.23E-11	6.92E-12	6.92E-12	6.92E-12
¹¹ B	1.84E-07	3.87E-07	5.02E-07	9.16E-08	8.80E-08	4.99E-07	1.57E-07	1.57E-07	1.57E-07
¹¹ C	3.05E-08	2.80E-08	4.45E-08	1.28E-08	1.14E-08	1.21E-07	9.96E-09	9.96E-09	9.96E-09
¹² C	4.30E-02	6.84E-02	1.45E-01	1.10E-01	8.98E-02	2.77E-01	8.31E-02	8.31E-02	8.31E-02
¹³ C	8.36E-05	6.25E-06	9.89E-06	4.79E-06	4.58E-06	2.44E-05	2.23E-05	2.23E-05	2.23E-05
¹⁴ C	1.80E-05	2.89E-07	4.11E-07	4.36E-07	4.04E-07	3.90E-07	7.53E-07	7.53E-07	7.53E-07
¹⁵ N	1.33E-07	1.07E-07	2.25E-07	1.51E-07	1.19E-07	8.10E-07	4.67E-08	4.67E-08	4.67E-08
¹⁴ N	2.18E-06	2.37E-06	3.63E-06	1.93E-06	1.68E-06	1.10E-05	2.17E-04	2.17E-04	2.17E-04
¹⁵ N	3.23E-06	7.63E-06	2.10E-05	2.05E-05	8.09E-08	7.29E-05	2.23E-05	2.23E-05	2.23E-05
¹⁶ O	6.67E-02	1.37E-01	4.00E-01	3.00E-02	9.21E-03	1.85	9.67E-03	9.67E-03	9.67E-03
¹⁷ O	1.02E-06	4.75E-08	1.62E-07	1.08E-09	6.71E-10	2.49E-07	5.24E-07	5.24E-07	5.24E-07
¹⁸ O	5.07E-08	4.80E-08	8.99E-08	7.39E-08	6.15E-08	1.97E-07	8.54E-08	8.54E-08	8.54E-08
¹⁹ F	2.21E-07	4.17E-06	1.51E-05	1.88E-08	4.75E-09	8.36E-05	3.03E-07	3.03E-07	3.03E-07
²⁰ Ne	2.55E-03	3.04E-02	9.28E-02	7.71E-04	2.11E-04	5.57E-01	1.30E-07	1.30E-07	1.30E-07
²¹ Ne	1.07E-05	6.88E-06	2.24E-05	1.29E-06	8.66E-07	1.71E-04	5.13E-09	5.13E-09	5.13E-09
²² Ne	4.97E-05	1.49E-02	3.34E-02	1.31E-03	1.09E-03	1.01E-05	4.44E-07	4.44E-07	4.44E-07
²² Na	5.25E-08	3.03E-07	9.49E-07	1.09E-09	9.49E-10	8.19E-06	9.35E-13	9.35E-13	9.35E-13
²³ Na	9.83E-06	1.90E-04	5.68E-04	9.57E-10	1.01E-09	3.90E-03	1.04E-08	1.04E-08	1.04E-08
²⁴ Mg	3.84E-03	1.49E-02	3.34E-02	4.76E-06	2.00E-06	9.31E-02	7.08E-09	7.08E-09	7.08E-09
²⁵ Mg	1.56E-05	9.09E-05	3.09E-04	3.68E-08	3.62E-08	1.00E-03	3.81E-08	3.81E-08	3.81E-08
²⁶ Mg	2.09E-05	8.93E-05	3.73E-04	6.22E-09	3.02E-09	1.01E-03	4.52E-08	4.52E-08	4.52E-08
²⁶ Al	2.82E-06	1.11E-05	2.58E-05	3.79E-11	5.70E-11	3.42E-05	3.38E-13	3.38E-13	3.38E-13
²⁷ Al	7.19E-05	5.55E-04	1.31E-03	1.47E-10	1.09E-10	2.43E-03	1.88E-03	1.88E-03	1.88E-03
²⁸ Si	2.49E-02	3.37E-02	6.81E-02	2.50E-09	1.58E-09	1.65E-01	1.54E-09	1.54E-09	1.54E-09
²⁹ Si	7.92E-05	1.95E-04	4.03E-04	6.70E-11	8.00E-11	3.93E-04	3.69E-10	3.69E-10	3.69E-10
³⁰ Si	9.27E-05	2.45E-04	4.33E-04	2.28E-10	3.10E-10	2.20E-04	8.24E-10	8.24E-10	8.24E-10
³¹ P	4.16E-05	7.91E-05	1.62E-04	8.34E-11	1.10E-10	3.51E-04	1.43E-09	1.43E-09	1.43E-09
³² S	8.52E-03	1.34E-02	2.58E-02	8.48E-12	1.08E-11	1.09E-01	1.26E-10	1.26E-10	1.26E-10
³³ S	2.94E-05	4.03E-05	9.02E-05	2.66E-13	3.48E-13	2.87E-04	1.62E-11	1.62E-11	1.62E-11
³⁴ S	1.15E-04	1.06E-04	2.26E-04	4.94E-11	5.66E-11	4.54E-04	3.84E-10	3.84E-10	3.84E-10
³⁵ S	1.29E-07	4.65E-08	1.05E-07	1.04E-11	1.52E-11	2.65E-07	2.25E-10	2.25E-10	2.25E-10
³⁶ S	8.96E-07	5.45E-09	1.10E-08	5.95E-11	2.10E-11	1.08E-08	1.54E-09	1.54E-09	1.54E-09
³⁶ Cl	9.82E-06	1.17E-05	3.47E-05	4.57E-13	6.40E-13	2.01E-04	2.06E-11	2.06E-11	2.06E-11
³⁶ Cl	7.92E-08	1.25E-07	2.93E-07	1.61E-14	2.14E-14	1.71E-06	8.42E-13	8.42E-13	8.42E-13
³⁷ Cl	1.79E-07	3.09E-08	1.34E-07	5.68E-10	7.21E-10	9.31E-07	1.83E-10	1.83E-10	1.83E-10
³⁶ Ar	1.56E-03	2.91E-03	4.81E-03	1.76E-09	2.44E-09	2.40E-02	3.27E-06	3.27E-06	3.27E-06
³⁷ Ar	1.92E-06	8.27E-07	4.35E-06	3.35E-12	4.44E-12	4.90E-05	5.27E-13	5.27E-13	5.27E-13
³⁸ Ar	3.72E-05	7.92E-06	7.13E-05	2.17E-10	1.69E-10	9.89E-04	1.50E-10	1.50E-10	1.50E-10
⁴⁰ Ar	5.21E-08	4.80E-11	1.03E-10	4.23E-12	5.62E-12	1.03E-09	1.08E-10	1.08E-10	1.08E-10

TABLE 16B—Continued

KE _∞	Z30A	Z30B	Z35A	Z35B	Z35C	Z40A	Z40B	Z40C	Z40C
	1.18	2.06	1.26	1.94	2.49	1.31	1.92	3.01	3.01
³⁹ K	5.85E-13	3.14E-08	1.50E-18	5.50E-10	4.78E-08	1.31E-22	6.86E-11	7.21E-05	6.81E-46
⁴⁰ K	6.09E-14	1.16E-08	1.72E-22	2.87E-11	1.92E-05	1.10E-22	7.38E-12	2.51E-08	9.29E-46
⁴¹ K	3.80E-10	1.71E-09	8.90E-26	3.91E-10	2.60E-09	3.33E-26	1.29E-11	2.64E-09	1.98E-49
⁴⁰ Ca	1.38E-15	8.59E-03	1.17E-17	2.64E-11	1.75E-02	1.17E-17	1.30E-15	3.08E-02	2.23E-52
⁴¹ Ca	7.01E-15	2.64E-06	7.72E-22	2.55E-12	4.22E-06	4.36E-22	1.04E-15	5.51E-06	8.21E-10
⁴² Ca	5.23E-10	2.13E-06	8.52E-26	4.70E-10	2.58E-06	2.72E-26	1.74E-11	3.87E-06	1.59E-53
⁴³ Ca	1.35E-10	3.90E-07	4.04E-27	1.14E-10	7.57E-07	9.38E-27	5.35E-12	2.19E-07	2.70E-57
⁴⁴ Ca	9.66E-10	8.68E-09	1.58E-27	6.02E-10	1.11E-08	3.38E-28	3.43E-11	4.00E-09	5.79E-01
⁴⁵ Ca	4.35E-10	4.73E-10	1.67E-31	3.29E-10	3.23E-10	2.05E-32	4.91E-13	1.47E-11	7.83E-56
⁴⁶ Ca	1.40E-09	1.48E-09	1.51E-33	8.73E-10	8.48E-10	1.20E-34	8.49E-14	3.45E-12	6.12E-03
⁴⁷ Ca	4.37E-11	6.24E-11	6.30E-38	4.42E-10	4.37E-10	2.92E-39	7.98E-15	5.45E-14	5.21E-56
⁴⁸ Ca	2.72E-09	2.88E-09	7.40E-38	2.95E-09	2.97E-09	4.11E-38	1.66E-15	3.94E-15	1.27E-02
⁴⁸ Sc	2.54E-16	1.18E-06	6.81E-30	3.92E-14	3.95E-07	6.80E-32	2.85E-17	1.27E-06	4.33E-04
⁴⁵ Sc	3.83E-11	6.61E-07	4.02E-26	1.92E-11	3.14E-06	1.29E-26	2.89E-12	2.10E-07	4.82E-04
⁴⁴ Ti	4.63E-17	1.88E-04	9.29E-33	1.21E-14	1.88E-04	1.35E-33	1.68E-17	2.44E-04	1.10E-10
⁴⁶ Ti	1.10E-16	6.28E-06	5.93E-32	4.09E-15	2.10E-06	1.41E-32	3.91E-16	1.54E-06	1.73E-68
⁴⁷ Ti	1.09E-11	2.87E-06	1.19E-26	3.16E-11	2.18E-06	1.19E-26	1.18E-11	2.45E-06	3.00E-61
⁴⁷ Ti	1.42E-10	1.35E-06	3.35E-11	3.35E-11	3.42E-07	8.08E-30	4.76E-12	2.05E-06	3.92E-04
⁴⁸ Ti	3.25E-10	3.34E-08	4.73E-30	5.38E-11	3.49E-07	2.25E-30	1.11E-11	1.41E-08	3.70E-69
⁴⁹ Ti	4.99E-10	9.93E-10	1.30E-27	2.65E-10	2.13E-09	1.40E-27	1.54E-11	4.43E-10	8.39E-67
⁵⁰ Ti	2.38E-09	2.88E-09	3.73E-31	9.64E-10	1.09E-09	1.15E-31	9.87E-11	1.09E-09	3.33E-70
⁴⁷ V	5.21E-17	1.48E-06	4.93E-34	1.71E-15	3.14E-07	3.75E-36	1.06E-17	1.44E-06	2.49E-04
⁴⁸ V	5.68E-16	9.36E-06	3.99E-34	3.96E-14	5.55E-05	3.88E-35	9.79E-17	1.47E-05	5.51E-14
⁴⁹ V	7.76E-15	4.14E-06	4.07E-33	3.06E-12	6.73E-06	1.27E-33	1.23E-15	8.25E-06	4.32E-06
⁵⁰ V	2.08E-14	1.38E-09	2.46E-28	2.88E-12	1.35E-09	3.69E-28	3.43E-15	2.45E-09	4.91E-09
⁵¹ V	2.07E-10	4.35E-09	9.45E-30	2.54E-10	9.58E-09	1.55E-29	9.25E-12	3.73E-09	7.42E-04
⁵¹ Cr	4.87E-21	4.66E-04	1.50E-39	7.88E-17	5.27E-04	1.14E-39	3.48E-21	7.56E-04	5.65E-07
⁵⁰ Cr	2.24E-21	7.87E-06	1.46E-38	7.81E-17	7.88E-06	1.31E-38	1.97E-21	1.33E-05	1.28E-71
⁵¹ Cr	4.73E-16	6.91E-06	1.62E-32	1.77E-13	7.79E-06	2.71E-32	8.41E-17	1.53E-05	1.19E-75
⁵² Cr	2.66E-14	5.25E-06	1.70E-35	1.63E-13	7.65E-06	1.38E-35	5.17E-15	1.16E-05	2.39E-77
⁵³ Cr	8.88E-10	4.60E-07	5.47E-31	3.66E-10	3.16E-06	9.17E-31	4.17E-11	5.95E-07	1.36E-82
⁵⁴ Cr	1.45E-10	1.06E-09	1.03E-33	5.72E-11	1.05E-09	1.64E-33	7.03E-12	1.85E-09	1.73E-09
⁵¹ Mn	6.51E-17	1.10E-05	2.16E-38	9.87E-17	1.63E-05	2.21E-38	1.57E-17	2.27E-05	2.40E-85
⁵² Mn	1.94E-15	1.15E-04	2.83E-37	1.68E-15	3.08E-04	2.94E-37	4.47E-16	3.04E-04	1.68E-82
⁵³ Mn	3.41E-15	1.21E-04	2.00E-33	2.31E-13	1.89E-04	3.50E-33	6.84E-16	2.88E-04	1.63E-85
⁵⁴ Mn	1.44E-14	2.47E-07	1.07E-36	1.19E-13	2.63E-07	1.18E-36	3.04E-15	4.73E-07	5.67E-89
⁵⁵ Mn	1.77E-10	1.57E-08	5.78E-38	3.08E-08	3.08E-08	9.84E-38	9.82E-12	1.76E-08	2.88E-08
⁵² Fe	3.58E-21	2.97E-03	2.29E-40	2.27E-18	5.25E-03	2.46E-40	3.83E-21	7.36E-03	1.29E-09
⁵³ Fe	2.13E-23	2.56E-05	7.93E-42	3.00E-19	4.03E-05	7.53E-42	5.11E-17	1.94E-05	6.70E-11
⁵⁴ Fe	2.34E-16	8.06E-04	6.56E-36	4.80E-15	1.00E-03	1.16E-35	7.89E-41	5.82E-34	2.29E-13
⁵⁵ Fe	1.48E-14	5.73E-05	1.49E-39	6.68E-14	1.65E-04	1.67E-39	3.15E-15	9.81E-05	1.96E-05
⁵⁶ Fe	5.67E-10	4.80E-06	3.32E-40	1.59E-10	2.00E-05	6.07E-40	3.03E-11	6.42E-06	5.22E-13
⁵⁷ Fe	1.91E-10	2.73E-07	1.33E-43	1.22E-10	5.78E-07	2.29E-43	1.05E-11	6.71E-08	2.00E-09
⁵⁸ Fe	5.67E-10	7.74E-08	1.01E-46	2.55E-10	7.61E-09	1.73E-46	2.93E-11	8.45E-09	0.00E+00
⁵⁹ Fe	2.23E-10	2.68E-10	8.19E-51	2.65E-10	2.55E-10	8.49E-51	5.35E-13	1.90E-11	3.16E-18
⁶⁰ Fe	1.28E-09	1.35E-09	8.44E-55	9.78E-10	9.50E-10	5.45E-55	5.90E-14	9.60E-13	6.29E-10
Mass									

TABLE 17A
PRODUCTION FACTORS 12-25 M_{\odot} MODELS; $Z = 0$

KE $_{\infty}$	Z12A	Z13A	Z15A	Z18A	Z20A	Z22A	Z25A	Z25B	Z25A	Z22A	Z20A	Z18A	Z15A	Z13A	Z12A	KE $_{\infty}$	Z12A	Z13A	Z15A	Z18A	Z20A	Z22A	Z25A	Z25B	
1H	.85	.82	.80	.85	.85	.70	.86	.69	.86	.70	.85	.85	.80	.82	.85	40Ca	2.22	4.26	5.16	.00	.00	1.15	1.26	1.22	1.83
2H	.02	.02	.02	.01	.01	.01	.01	.01	.01	.01	.01	.01	.01	.01	.01	42Ca	.47	.24	.44	.00	.00	.00	.00	.00	12.59
3He	.24	.23	.20	.20	.20	.16	.19	.15	.19	.16	.20	.20	.20	.23	.24	44Ca	.30	.80	.47	.00	.00	.00	.00	.00	.69
4He	1.38	1.36	1.31	1.41	1.44	1.25	1.42	1.22	1.42	1.25	1.44	1.41	1.31	1.36	1.38	46Ca	3.90	3.69	3.87	.00	.00	.00	.00	.00	.25
7Li	2.59	3.36	9.12	14.18	19.30	6.54	12.96	13.69	12.96	6.54	19.30	14.18	9.12	3.36	2.59	48Ca	.49	.00	.00	.00	.00	.00	.00	.00	2.10
11B	4.22	7.44	8.53	1.50	1.31	6.35	1.88	13.02	1.88	6.35	1.31	1.50	8.53	7.44	4.22	50Ca	.04	.00	.00	.00	.00	.00	.00	.00	.00
12C	1.32	1.91	3.54	2.46	1.85	4.43	1.46	6.00	1.46	4.43	1.85	2.46	3.54	1.91	1.32	46Sc	2.00	3.47	5.75	.00	.00	.00	.00	.00	3.68
13C	.21	.01	.02	.01	.01	.03	.03	.05	.03	.03	.01	.01	.02	.01	.21	48Ti	1.28	1.16	.87	.00	.00	.00	.00	.00	.59
15N	.07	.15	.35	.00	.00	.81	.27	1.19	.27	.81	.00	.00	.35	.07	.07	47Ti	.33	.52	.48	.00	.00	.00	.00	.00	.26
16O	.65	1.21	3.08	.21	.06	9.37	.05	10.47	.05	9.37	.06	.21	3.08	1.21	.65	48Ti	5.82	6.58	6.40	.00	.00	.00	.00	.00	6.89
19F	.05	.87	2.75	.00	.00	10.01	.04	6.04	.04	10.01	.00	.00	2.75	.87	.05	49Ti	2.27	3.08	2.50	.00	.00	.00	.00	.00	3.52
20Ne	.15	1.59	4.23	.03	.01	16.68	.00	13.55	.00	16.68	.01	.03	4.23	1.59	.15	50V	.06	.07	.14	.00	.00	.00	.00	.00	.26
21Ne	.24	.14	.40	.02	.01	2.01	.00	1.64	.00	2.01	.01	.02	.40	.14	.24	51V	.83	1.64	1.51	.00	.00	.00	.00	.00	3.45
22Ne	.04	.00	.00	.00	.00	.02	.00	.02	.00	.02	.00	.00	.00	.00	.04	50Cr	.44	.46	.72	.00	.00	.00	.00	.00	1.47
23Na	.03	.48	1.26	.00	.00	5.66	.00	3.68	.00	5.66	.00	.00	1.26	.48	.03	52Cr	3.63	6.91	5.13	.00	.00	.00	.00	.00	12.64
24Mg	.70	2.45	4.79	.00	.00	8.77	.00	7.73	.00	8.77	.00	.00	4.79	2.45	.70	53Cr	2.05	3.43	2.65	.00	.00	.00	.00	.00	5.88
25Mg	.02	.11	.34	.00	.00	.72	.00	.42	.00	.72	.00	.00	.34	.11	.02	54Cr	.02	.03	.05	.00	.00	.00	.00	.00	.09
26Mg	.03	.11	.38	.00	.00	.65	.00	.37	.00	.65	.00	.00	.38	.11	.03	55Mn	1.32	3.00	2.26	.00	.00	.00	.00	.00	3.21
27Al	.12	.81	1.67	.00	.00	2.03	.00	1.40	.00	2.03	.00	.00	1.67	.81	.12	54Fe	.44	.64	.77	.00	.00	.00	.00	.00	1.62
28Si	3.56	4.38	7.69	.00	.00	12.23	.00	15.20	.00	12.23	.00	.00	7.69	4.38	3.56	56Fe	6.50	13.99	10.20	.00	.00	.00	.00	.00	10.72
29Si	.22	.48	.87	.00	.00	.56	.00	.83	.00	.56	.00	.00	.87	.48	.22	57Fe	11.79	27.29	14.37	.00	.00	.00	.00	.00	10.14
30Si	.37	.88	1.36	.00	.00	.45	.00	.57	.00	.45	.00	.00	1.36	.88	.37	58Fe	.04	.33	.04	.00	.00	.00	.00	.00	.01
31P	.48	.82	1.47	.00	.00	2.09	.00	1.71	.00	2.09	.00	.00	1.47	.82	.48	59Co	5.01	15.67	5.87	.00	.00	.00	.00	.00	2.59
32S	2.01	2.86	4.82	.00	.00	13.38	.00	11.51	.00	13.38	.00	.00	4.82	2.86	2.01	56Ni	4.80	35.41	4.36	.00	.00	.00	.00	.00	1.36
33S	.74	1.06	2.07	.00	.00	4.32	.00	2.98	.00	4.32	.00	.00	2.07	1.06	.74	60Ni	14.27	22.39	18.75	.00	.00	.00	.00	.00	13.50
34S	.58	.48	.89	.00	.00	1.18	.00	1.20	.00	1.18	.00	.00	.89	.48	.58	61Ni	17.04	41.63	22.33	.00	.00	.00	.00	.00	13.82
36S	.89	.01	.01	.00	.00	.02	.00	.01	.00	.02	.00	.00	.01	.01	.89	62Ni	20.88	98.11	20.59	.00	.00	.00	.00	.00	8.16
36Cl	.37	.39	1.01	.00	.00	3.85	.00	1.79	.00	3.85	.00	.00	1.01	.39	.37	63Cu	1.12	2.76	1.48	.00	.00	.00	.00	.00	.84
36Ar	1.88	3.19	4.58	.00	.00	15.04	.00	11.10	.00	15.04	.00	.00	4.58	3.19	1.88	64Zn	3.73	3.82	4.77	.00	.00	.00	.00	.00	4.36
38Ar	.23	.04	.34	.00	.00	3.12	.00	.75	.00	3.12	.00	.00	.34	.04	.23	67Zn	2.25	9.61	2.46	.00	.00	.00	.00	.00	1.05
40Ar	.19	.00	.00	.00	.00	.04	.00	.01	.00	.04	.00	.00	.00	.00	.19	67Zn	.03	.09	.02	.00	.00	.00	.00	.00	.01
39K	.32	.29	.52	.00	.00	4.71	.00	.96	.00	4.71	.00	.00	.52	.29	.32	70Zn	.02	.00	.00	.00	.00	.00	.00	.00	.00
40K	.06	.02	.02	.00	.00	1.46	.00	.31	.00	1.46	.00	.00	.02	.02	.06	68Ga	.08	.00	.00	.00	.00	.00	.00	.00	.00
41K	.40	.37	.46	.00	.00	4.38	.00	.78	.00	4.38	.00	.00	.46	.37	.40	71Ga	.11	.00	.00	.00	.00	.00	.00	.00	.00
																70Ge	.06	.00	.00	.00	.00	.00	.00	.00	.00

TABLE 17B
PRODUCTION FACTORS 30-40 M_{\odot} MODELS; $Z = 0$

	Z30A	Z30B	Z35A	Z35B	Z35C	Z40A	Z40B	Z40C	KE $_{\infty}$	Z30A	Z30B	Z35A	Z35B	Z35C	Z40A	Z40B	Z40C
KE $_{\infty}$	1.18	2.06	1.26	1.94	2.49	1.31	1.92	3.01		1.18	2.06	1.26	1.94	2.49	1.31	1.92	3.01
¹ H	.82	.63	.90	.73	.61	.90	.77	.56	40Ca	.00	5.01	.00	.00	8.77	.00	.00	13.43
³ He	.17	.13	.19	.19	.13	.19	.16	.12	42Ca	.00	.18	.00	.00	.18	.00	.00	.24
⁴ He	1.50	1.18	1.33	1.40	1.16	1.33	1.55	1.14	43Ca	.00	.61	.00	.00	.39	.00	.00	.43
⁷ Li	4.78	4.75	10.58	21.40	19.50	1.39	25.85	20.70	44Ca	.00	4.61	.00	.00	3.95	.00	.00	4.47
¹¹ B	2.19	4.82	.00	2.44	4.51	.00	.74	6.78	46Ca	.02	.02	.00	.01	.01	.00	.00	.00
¹² C	1.63	4.01	.00	4.17	3.99	.00	3.35	4.16	46Sc	.00	6.23	.00	.00	4.03	.00	.00	1.17
¹³ C	.12	.11	.00	.02	.02	.00	.01	.01	46Ti	.00	.45	.00	.00	.29	.00	.00	.29
¹⁴ N	.15	.11	.00	.00	.00	.00	.00	.00	47Ti	.00	.47	.00	.00	.39	.00	.00	.44
¹⁵ N	.38	1.72	.00	.45	1.25	.00	.02	1.06	48Ti	.00	7.73	.00	.00	8.14	.00	.00	9.39
¹⁶ O	.13	15.85	.00	7.25	17.46	.00	2.15	19.79	48Ti	.00	2.56	.00	.00	2.68	.00	.00	3.45
¹⁷ O	.68	.52	.00	.00	.00	.00	.00	.00	50V	.00	.05	.00	.00	.04	.00	.00	.07
¹⁹ F	.28	8.05	.00	3.24	8.28	.00	.05	8.09	51V	.00	1.50	.00	.00	1.91	.00	.00	2.39
²⁰ Ne	.00	22.47	.00	8.42	22.50	.00	.24	25.60	50Cr	.00	.33	.00	.00	.31	.00	.00	.54
²¹ Ne	.00	1.54	.00	.90	2.28	.00	.03	2.88	52Cr	.00	7.26	.00	.00	11.23	.00	.00	13.50
²² Ne	.00	.01	.00	.01	.02	.00	.00	.03	53Cr	.00	2.99	.00	.00	4.00	.00	.00	5.03
²³ Na	.00	4.06	.00	2.02	4.73	.00	.00	6.13	54Cr	.00	.02	.00	.00	.02	.00	.00	.03
²⁴ Mg	.00	16.62	.00	3.34	13.69	.00	.02	14.07	55Mn	.00	1.85	.00	.00	2.35	.00	.00	2.85
²⁵ Mg	.00	.93	.00	.28	.83	.00	.00	.85	54Fe	.00	.40	.00	.00	.42	.00	.00	.71
²⁶ Mg	.00	.83	.00	.24	.74	.00	.00	.75	56Fe	.00	9.73	.00	.00	15.12	.00	.00	16.24
²⁷ Al	.00	3.54	.00	.55	2.62	.00	.00	2.55	57Fe	.00	13.97	.00	.00	15.32	.00	.00	17.05
²⁸ Si	.00	6.59	.00	.09	9.61	.00	.00	13.71	58Fe	.00	.26	.00	.00	.02	.00	.00	.07
²⁹ Si	.00	.82	.00	.05	.90	.00	.00	1.00	59Co	.00	7.59	.00	.00	5.20	.00	.00	6.28
³⁰ Si	.00	.93	.00	.05	.71	.00	.00	.71	58Ni	.00	17.90	.00	.00	3.71	.00	.00	6.74
³¹ P	.00	1.11	.00	.03	1.15	.00	.00	1.39	60Ni	.00	16.00	.00	.00	21.96	.00	.00	22.58
³² S	.00	4.02	.00	.00	6.79	.00	.00	10.68	61Ni	.00	23.61	.00	.00	24.68	.00	.00	24.00
³³ S	.00	1.44	.00	.00	1.90	.00	.00	2.19	62Ni	.00	43.61	.00	.00	13.47	.00	.00	23.56
³⁴ S	.00	.25	.00	.00	.36	.00	.00	.43	65Cu	.00	2.67	.00	.00	1.09	.00	.00	1.97
³⁶ S	.02	.02	.00	.02	.02	.00	.00	.01	65Cu	.00	.87	.00	.00	.55	.00	.00	.90
³⁵ Cl	.00	.49	.00	.00	.69	.00	.00	.91	64Zn	.00	16.79	.00	.00	10.87	.00	.00	5.77
³⁷ Cl	.00	.27	.00	.00	.40	.00	.00	.46	66Zn	.00	4.83	.00	.00	1.74	.00	.00	2.34
³⁶ Ar	.00	4.08	.00	.00	7.04	.00	.00	11.04	67Zn	.00	.12	.00	.00	.01	.00	.00	.02
³⁸ Ar	.00	.10	.00	.00	.15	.00	.00	.21	68Zn	.00	.04	.00	.00	.00	.00	.00	.00
³⁹ K	.00	.32	.00	.00	.41	.00	.00	.54	71Ga	.02	.01	.00	.00	.01	.00	.00	.00
⁴⁰ K	.00	.07	.00	.00	.10	.00	.00	.12									
⁴¹ K	.00	.35	.00	.00	.48	.00	.00	.55									

supernovae, which otherwise have relatively normal light curves. The distinguishing characteristics of these light curves, if any, would be slower than typical velocity and, in most cases where a black hole is formed, lack of a radioactive tail from ^{56}Co decay. Caution must be used here until multidimensional calculations are carried out. The same decreasing ρr^3 that slows the shock also causes mixing.

The loss of substantial heavy elements to black holes along with the ejection of helium by these massive stars may require re-evaluation of “cutoff” masses based upon Galactic chemical evolution and dY/dZ , the change in helium abundance divided by the change in metallicity (Paper III).

The abundances of elements lighter than silicon are, with rare exceptions, unmodified by the explosion. The nuclei that are ejected are the same ones present in the presupernova star. The rare exceptions chiefly involve the neutrino process (Table 4). Elements from silicon to scandium are, at least in a $25 M_{\odot}$ model, ejected in quantities similar to what existed in the presupernova star and their synthesis is relatively insensitive to details of the explosion mechanism (§ 4.5; Weaver & Woosley 1993; Tables 7 and 8). However, the agreement is partly fortuitous. Intermediate mass elements are destroyed (burned to the iron group) following shock passage, but nearly equal amounts are created by explosive oxygen burning. Elements in the iron group and ^{44}Ca (^{44}Ti) are much more sensitive to the explosion mechanism, whereby we mean chiefly the location of the final mass separation and the energy. The iron yield (i.e., ^{56}Ni) that we calculate could easily be in error by a factor of 2 for any individual supernova or for the entire ensemble. This must eventually lead to some ambiguity when assigning the relative roles of Type Ia and Type II/Ib supernovae in making the Galactic abundance of iron (Paper III). Other nuclei due to the α -rich freeze out, e.g., ^{44}Ti , are even more uncertain.

It is frequently assumed that the synthesis of major elements, especially those having $Z = N$ and heavier than nitrogen, should be independent of the initial stellar metallicity. That is, the nucleosynthesis should be governed by the mass of the helium core, at least for those isotopes that do not require a neutron excess for their synthesis, and little else. A scan of the tables shows that this is true in a general way, especially for oxygen. But in some cases, e.g., ^{20}Ne in Tables 6A and 10A), it is not. There are several reasons for this. One is the non-negligible level of chaos that exists in the final yields from stars of very similar mass (Paper I). We have repeatedly verified that two stars of identical initial composition, mass, and parameterized explosion give virtually identical results (when the symmetry is broken by zoning or time step criteria or simply running the calculations on different machines). But stars of slightly different mass can end up with substantially different final structures and abundances owing to the complicated interplay of convective shells that occurs during the late stages of evolution. Changing the metallicity changes slightly the conditions under which hydrogen burns; it changes the initial stages of helium burning [$^{14}\text{N}(\alpha, \gamma)^{18}\text{F}$ generates appreciable energy]; and most importantly, especially as one goes from solar to 0.1 solar metallicity, it changes the initial helium abundance (since the sum of mass fractions must be one) and this does affect the helium core mass. The stars of *zero* initial metallicity are a special case. There the final structure is *markedly*

different from a solar metallicity star of the same mass. Not only is the low-metallicity star a blue supergiant (as are all the other very low-metallicity stars; Paper I), but the interior structure is different as well. The need to burn a trace of helium before igniting on the main sequence forever alters the entropy in the core. For zero metallicity stars one ends up with more compact mantles that are more difficult to explode and more likely to leave black hole remnants and all that implies.

While we have not explicitly followed the synthesis of very heavy elements by neutron capture, our calculations do show evidence of the s -process for $A \lesssim 64$ and indicators from which the neutron exposure history can be extracted have been provided (§ 4.8, Fig. 26). Similarly we are able to examine the temperature profile experienced following shock passage (Fig. 9) in our stars and estimate the yield of p -process nuclei. We find (§ 4.9) that the total yields are approximately what is required, but caution that the pre-explosive processing of the s -process seeds during oxygen burning must be considered carefully in any realistic calculation. Finally, though we do observe rapid neutron addition at the base of the helium shell following shock passage, the “ r -process” there is severely limited both in strength and extent (§ 4.10). The major r -process responsible for the solar abundances should come from the neutrino driven wind which was not considered here (Woosley et al. 1994).

The other major effort of which we are aware to model nucleosynthesis in massive stars in commensurate detail to what we have reported here is the ongoing work of Thielemann, Nomoto, Hashimoto, and colleagues. Over the last decade their work (and ours) have been reported in numerous papers and conference proceedings of which Nomoto & Hashimoto (1988) and Thielemann, Nomoto, & Hashimoto (1990, 1994) are representative. Their work is best summarized in a preprint (Thielemann, Nomoto, & Hashimoto 1995, hereafter TNH95) which arrived while we were writing up our work. Table 18 gives a representative comparison of their yields and ours for the four stars which they consider. Both the similarities and differences warrant discussion. The yields of the most abundant isotopes are not very different, especially oxygen where we differ by at most 40% ($15 M_{\odot}$). The iron core masses and ^{56}Ni produced in the explosions are also qualitatively similar.

However, there are systematic differences that can be traced to the different physics employed by the two groups. (1) TNH95 use the Caughlan et al. (1985) rate for $^{12}\text{C}(\alpha, \gamma)^{16}\text{O}$; we use a value 1.7 times Caughlan & Fowler (1988). That is our rate for this critical reaction is about 74% that of TNH95 (§ 2.2). This results in more carbon being created in our calculations (Table 18). For the lighter stars studied this also translates into more carbon burning products—neon, magnesium, etc. For the more massive stars the extent of convective shells changes this pattern. (2) TNH95 use the Schwarzschild theory for convection; we use the Ledoux criterion with modifications for semiconvection. In general, their convective shells have greater extent than ours (though sometimes we may have multiple shells where they have one). (3) We follow the composition in each zone from the main sequence through explosion using the same 200 isotope network; TNH95 use a larger network for the explosion, but do not follow the presupernova

TABLE 18
COMPARISON WITH THIELEMANN, NOMOTO, & HASHIMOTO (1995)

Species	13 M_{\odot}	13 M_{\odot}	15 M_{\odot}	15 M_{\odot}
	TNH95	This paper	TNH95	This paper
M_{cut}/M_{\odot}	1.27	1.46	1.33	1.43
M_{Fe}/M_{\odot}	1.18	1.41	1.28	1.32
^{12}C	0.059	0.11	0.083	0.16
^{16}O	0.21	0.27	0.42	0.68
^{20}Ne	0.025	0.045	0.028	0.11
^{24}Mg	0.0096	0.016	0.042	0.027
^{28}Si	0.048	0.059	0.065	0.11
^{32}S	0.024	0.026	0.022	0.063
^{36}Ar	0.0045	0.0045	0.0035	0.013
^{40}Ca	0.0043	0.0036	0.0030	0.011
^{56}Ni	0.15	0.13	0.130	0.12

Species	20 M_{\odot}	20 M_{\odot}	25 M_{\odot}	25 M_{\odot}
	TNH95	This paper	TNH95	This paper
M_{cut}/M_{\odot}	1.62	2.06	1.77	2.07
M_{Fe}/M_{\odot}	1.40	1.74	1.61	1.78
^{12}C	0.11	0.21	0.15	0.32
^{16}O	1.48	1.94	2.99	3.25
^{20}Ne	0.23	0.11	0.59	0.39
^{24}Mg	0.15	0.031	0.16	0.11
^{28}Si	0.083	0.29	0.10	0.32
^{32}S	0.024	0.15	0.038	0.14
^{36}Ar	0.0042	0.026	0.0067	0.022
^{40}Ca	0.0037	0.014	0.0061	0.017
^{56}Ni	0.074	0.088	0.052	0.13

evolution in such detail and, in particular, do not couple the large network to time-dependent convection. (4) TNH95 use different explosion energies, 1.0×10^{51} ergs for all their models; we use 1.2×10^{51} ergs. We simulate explosion with a piston. They deposit energy. (5) TNH95 do not include the neutrino process. (6) TNH95 consider only stars of solar (and occasionally LMC) composition and have not modeled Galactic chemical evolution to obtain consistent starting compositions for low-metallicity stars. (7) TNH95 have evolved helium cores. We have evolved entire stars. Moreover, TNH95 assume that a certain relation exists between the helium core mass and the main sequence mass, 8 and 25 M_{\odot} , for example. Our relation, one that is actually calculated in a self consistent way, is different. For example our 25 M_{\odot} star (actually a 25.14 M_{\odot} , or 5×10^{34} g star) has a helium core mass of 9.21 M_{\odot} . Our larger helium core masses are probably a consequence of using the Anders & Grevesse (1989) helium mass fraction (0.275). A larger helium abundance leads to larger helium cores.

Because of these differences: (1) We make more carbon, by about a factor of 2. As noted above this is a consequence of their larger rate for $^{12}\text{C}(\alpha, \gamma)^{16}\text{O}$. (2) The iron core masses of TNH95 are smaller. They do not allow the Y_e discontinuity at the outer boundary of the silicon shell to inhibit the growth of the convective silicon shell. Their iron cores thus grow to the effective Chandrasekhar mass more readily, while we must occasionally go through additional stages of silicon shell burning leading to a tendency to overshoot M_{CH} . Small iron cores may also indicate a lower entropy and steeper density gradient in the material just outside the iron core of TNH95. Their entropy could be lower because of more extensive convection and greater neutrino losses, but we are unable to ascertain this level of detail from what has been published. Also, our helium cores are larger (see difference [7] above). (3) We tend to make

more intermediate mass elements, silicon through calcium, especially in the more massive stars. In part this is because of our larger oxygen abundance [$^{12}\text{C}(\alpha, \gamma)^{16}\text{O}$ again] and larger helium cores, but may also indicate lower entropy and steeper density gradients in the region around the iron core where explosive nucleosynthesis occurs. (4) We make many orders of magnitude more of certain trace isotopes like ^{60}Fe . Our calculations of ^{26}Al production also differs markedly. The synthesis of these isotopes is sensitive to following the composition of the *presupernova* star very carefully, especially the coupling of the large network to convection during the last few hours of neon and oxygen burning. (5) Because we evolve the entire star, we can make predictions regarding the synthesis of species in the hydrogen envelope, e.g., ^{17}O , that TNH95 cannot.

We certainly agree with TNH95 that the explosion mechanism, and in particular the mass cut, remains a major uncertainty in both our models, but all in all, with the exception of trace isotopes alluded to above, the agreement between our two studies is not too bad.

Many processes and sites have been discussed in this paper for the synthesis of the elements lighter than zinc. As a road map for the reader, we provide Table 19 giving our best current estimate of where the various isotopes are predominantly made. When more than one entry is given, a priority ranking has been attempted. Here “BB” stands for the big bang (e.g., Walker et al. 1991); “L*” is low-mass stars ($M \lesssim 8 M_{\odot}$; e.g., Renzini & Voli 1981) or in some cases AGB stars (Sackmann & Boothroyd 1992); “CR” is cosmic-ray spallation (e.g., Prantzos et al. 1993); “Nova” indicates classical novae (e.g., Woosley 1986); “ ν ” is the neutrino process (Woosley et al. 1990); and “Ia” is Type Ia supernovae (Nomoto, Thielemann, & Yokoi 1984 for ordinary Ia’s which are assumed to ignite at the Chandrasekhar mass; Woosley & Eastman 1995 for the in-

TABLE 19
THE ORIGIN OF THE LIGHT AND INTERMEDIATE-MASS ELEMENTS

Species	Origin	Species	Origin	Species	Origin
¹ H	BB	²⁹ Si	Ne,xNe	⁵⁰ Ti	nse-Ia-MCh
² H	BB	³⁰ Si	Ne,xNe	⁵⁰ V	Ne,xNe,xO
³ He	BB,L*	³¹ P	Ne,xNe	⁵¹ V	α,Ia-det,xSi,xO,ν
⁴ He	BB,L*,H	³² S	xO,O	⁵⁰ Cr	xSi,xO,α,Ia-det
⁶ Li	CR	³³ S	xO,xNe	⁵² Cr	xSi,α,Ia-det
⁷ Li	BB,ν,L*,CR	³⁴ S	xO,O	⁵³ Cr	xO,xSi
⁹ Be	CR	³⁶ S	Ne,xNe	⁵⁴ Cr	nse-Ia-MCh
¹⁰ B	CR	³⁵ Cl	xO,xNe,ν	⁵⁵ Mn	Ia, xSi, ν
¹¹ B	ν	³⁷ Cl	xO,xNe	⁵⁴ Fe	Ia,xSi
¹² C	L*,He	³⁶ Ar	xO,O	⁵⁶ Fe	xSi,Ia
¹³ C	L*,H	³⁸ Ar	xO,O	⁵⁷ Fe	xSi,Ia
¹⁴ N	L*,H	⁴⁰ Ar	C,Ne	⁵⁸ Fe	He(s),nse-Ia-MCh
¹⁵ N	Nova,ν	³⁹ K	xO,O,ν	⁵⁹ Co	He(s),α,Ia,ν
¹⁶ O	He	⁴⁰ K	C,Ne	⁵⁸ Ni	α,Ia
¹⁷ O	H	⁴¹ K	xO	⁶⁰ Ni	α, He(s)
¹⁸ O	He	⁴⁰ Ca	xO,O	⁶¹ Ni	α,Ia-det,He(s)
¹⁹ F	ν,He	⁴² Ca	xO	⁶² Ni	α,He(s)
²⁰ Ne	C	⁴³ Ca	C,Ne	⁶⁴ Ni	He(s)
²¹ Ne	C,He(s)	⁴⁴ Ca	α,Ia-det	⁶³ Cu	He(s), α
²² Ne	He	⁴⁶ Ca	C,Ne	⁶⁵ Cu	He(s)
²³ Na	C,He(s),H	⁴⁸ Ca	nse-Ia-MCh	⁶⁴ Zn	He(s),α
²⁴ Mg	C,Ne	⁴⁵ Sc	α,C,Ne,ν	⁶⁶ Zn	He(s),α,nse-Ia-MCh
²⁵ Mg	C,Ne,He(s)	⁴⁶ Ti	xO, Ia-det	⁶⁷ Zn	He(s)
²⁶ Mg	C,Ne,He(s)	⁴⁷ Ti	xO, xSi, Ia-det	⁶⁸ Zn	He(s)
²⁷ Al	C,Ne	⁴⁸ Ti	xSi,Ia-det		
²⁸ Si	xO,O	⁴⁹ Ti	xSi,He(s)		

ner neutron-rich regions of ordinary Ia's—here called “nse-Ia-MCh”; Woosley & Weaver 1994 for sub-Chandrasekhar detonation models “Ia-He-det”). All other entries refer to the burning process in the massive stars considered here—H, He, C, Ne, O, and Si—responsible for producing the isotope, with a prefix “x” indicating explosive nucleosynthesis.

In the Paper III of this series (Timmes et al. 1995a), which through inevitable variability in human schedules, was submitted before this one, we consider the outcome of Galactic chemical evolution when the nucleosynthetic yields presented here are combined with those from lower mass stars and Type Ia supernovae. We defer conclusions relating the yields calculated here to solar abundances to that paper.

This work has been supported by the National Science Foundation (AST-9115367), the NASA Theory Program (NAGW-2525), and, at Livermore, by the Department of Energy (W-7405-ENG-48). The authors are grateful for assistance with the nuclear reaction network and rates provided by Rob Hoffman and Frank Timmes and numerous educational conversations with Marc Herant regarding supernova hydrodynamics. They are also grateful for numerous educational conversations with Willy Fowler regarding nucleosynthesis in stars and with Hans Bethe regarding shock propagation in supernovae. Finally they appreciate critical readings of the manuscript by Roberto Gallino and the referee, M. Hashimoto.

REFERENCES

- Anders, E., & Grevesse, N. 1989, *Geochim. Cosmochim. Acta*, 53, 197
 Arnett, W. D. 1974, *ApJ*, 193, 169
 ———. 1994, *ApJ*, 427, 932
 Arnett, W. D., & Thielemann, F.-K. 1985, *ApJ*, 295, 589
 Arnett, W. D., & Truran, J. W. 1969, *ApJ*, 157, 339
 Arnould, M. 1976, *A&A*, 46, 117
 Azuma, R. E., et al. 1994, *Phys. Rev. C*, 50, 1194
 Bao, Z. Y., & Käppeler, F. 1986, *At. Data Nucl. Data Tables*, 36, 411
 Baraffe, I., El Eid, M., & Prantzos, N. 1992, *A&A*, 258, 357
 Barnes, C. A. 1995, In *Proc. Symp. Physics of Unstable Nuclei*, (Amsterdam: Elsevier), in press
 Bazan, G., & Arnett, W. D. 1994, *ApJ*, 433, L41
 Bethe, H. A. 1990, *Rev. Mod. Phys.*, 62, 801
 Bodenheimer, P., & Woosley, S. E. 1983, *ApJ*, 269, 281
 Brown, G. 1988, *Nature*, 336, 519
 Brown, G., & Bethe, H. A. 1994, *ApJ*, 423, 659
 Brown, G., Bruenn, S., & Wheeler, J. C. 1992, *Comm. Astrophys.*, 16, 153
 Burbidge, E. M., Burbidge, G. R., Fowler, W. A., & Hoyle, F. 1957, *Rev. Mod. Phys.*, 29, 547
 Caughlan, G. R., & Fowler, W. A. 1988, *At. Data Nucl. Data Tables*, 40, 283
 Caughlan, G. R., Fowler, W. A., Harris, M. J., & Zimmerman, B. A. 1985, *At. Data Nucl. Data Tables*, 32, 197
 Chevalier, R. A., & Klein, R. I. 1978, *ApJ*, 219, 994
 Clayton, D. D. 1971, *Nature*, 234, 291
 Dearborn, D. S. P., Schramm, W., Steigman, G., & Truran, J. 1989, *ApJ*, 347, 455
 Fowler, W. A., & Hoyle, F. 1964, *ApJS*, 9, 201
 Fryxell, B. A., Arnett, W. D., & Müller, E. 1991, *ApJ*, 367, 619
 Fuller, G. M., Fowler, W. A., & Newman, M. 1980, *ApJS*, 42, 447
 ———. 1982, *ApJS*, 48, 279
 ———. 1985, *ApJ*, 293, 1
 Hachisu, I., Matsuda, T., Nomoto, K., & Shigeyama, T. 1990, *ApJ*, 358, L57
 ———. 1992, *ApJ*, 390, 230
 Hartmann, D. H., Woosley, S. E., & El Eid, M. 1985, *ApJ*, 297, 837
 Helfand, D., & Becker, R. H. 1984, *Nature*, 307, 215
 Herant, M., & Benz, W. 1992, *ApJ*, 387, 294
 Herant, M., & Woosley, S. E. 1994, 425, 814
 Hoffman, R. D. 1994, unpublished
 Hoffman, R. D., Woosley, S. E., Fuller, G. F., & Qian, Y. Z. 1995, in preparation
 Howard, W. M., & Woosley, S. E. 1995, in preparation
 Hoyle, F. 1946, *MNRAS*, 106, 343
 Kaspi, V. M., Taylor, J. H., & Ryba, M. F. 1994, *ApJ*, 428, 713
 Malaney, R. A. 1992, *ApJ*, 398, L45

- Malaney, R. A., & Fowler, W. A. 1989, *ApJ*, 345, L5
- Maeder, A. 1992, *A&A*, 264, 105
- . 1993, *A&A*, 268, 833
- Meynet, G., & Arnould, M. 1993, in *Nuclei in the Cosmos*, Proc. 2d Symposium, ed. F. Käppeler & K. Wisshak (Bristol: Inst. of Phys.), 503
- Mohr, P., Kölle, V., Wilmes, S., Atzrott, U., Hoyler, F., Engelmann, C., Staudt, G., & Oberhummer, H. 1995, in *Nuclei in the Cosmos 3*, ed. R. Busso & R. Gallino (New York: AIP), in press
- Nomoto, K., & Hashimoto, M. 1988, *Phys. Rep.*, 163, 13
- Nomoto, K., Thielemann, F. K., & Yokoi, Y. 1984, *A&A*, 286, 644
- Okabe, S. 1994, poster paper presented at Clusters 1994 (Strasbourg)
- Olive, K. A., Prantzos, N., Scully, S., & Vangioni-Flam, E. 1993, *ApJ*, 424, 666
- Prantzos, N., Casse, M., & Vangioni-Flam, E. 1993, *ApJ*, 403, 630
- Prantzos, N., Hashimoto, M., Rayet, M., & Arnould, M. 1990, *A&A*, 238, 455
- Rayet, M., Arnould, M., Hashimoto, M., Prantzos, N., & Nomoto, K. 1995, *A&A*, in press
- Rayet, M., Prantzos, N., & Arnould, M. 1990, *A&A*, 227, 271
- Reeves, H. 1994, *Rev. Mod. Phys.*, 66, 193
- Renzini, A., & Voli, M. 1981, *A&A*, 94, 175
- Sackmann, I. J., & Boothroyd, A. I. 1992, *ApJ*, L71
- Sargood, D. G. 1982, *Phys. Rep.*, 93, 61
- Thielemann, F.-K., & Arnett, W. D. 1985, *ApJ*, 295, 589
- Thielemann, F.-K., Hashimoto, M., & Nomoto, K. 1990, *ApJ*, 349, 222
- Thielemann, F.-K., Nomoto, K., & Hashimoto, M. 1993, in *Origin and Distribution of the Elements*, ed. N. Prantzos, E. Vangioni-Flam, & M. Casse (Cambridge: Cambridge Univ. Press), 297
- . 1994, in *Supernovae: Les Houches 1990, Session LIV*, ed. S. Bludman, R. Mochkovitch, & J. Zinn-Justin (Amsterdam: North-Holland), 629
- . 1995, *ApJ*, submitted (TNH95)
- Timmes, F. X., Woosley, S. E., Hartmann, D. H., Hoffman, R. D., Weaver, T. A., & Matteucci, F. 1995c, *ApJ*, 449, 204
- Timmes, F. X., Woosley, S. E., & Weaver, T. A. 1995a, *ApJS*, 98, 617 (Paper III)
- . 1995b, *ApJ*, submitted
- Twarog, B. A., & Wheeler, J. C. 1982, *ApJ*, 261, 636
- . 1987, *ApJ*, 316, 153
- Walker, T. P., Steigman, G., Schramm, D. N., Olive, K. A., & Kang, H. 1991, *ApJ*, 376, 51
- Weaver, T. A., & Woosley, S. E. 1980, in *Ann. NY Acad. Sci.*, 336, Ninth Texas Symp. on Relativistic Astrophysics, ed. J. Ehlers, J. Perry, & M. Walker, 335
- . 1993, *Phys. Rep.*, 227, 65
- . 1995, *ApJS*, in press (Paper I)
- Weaver, T. A., Zimmerman, G. B., & Woosley, S. E. 1978, *ApJ*, 225, 1021
- Wheeler, J. C., Sneden, C., & Truran, J. W. 1989, *ARA&A*, 27, 279
- Wilson, J. R., Mayle, R., Woosley, S. E., & Weaver, T. A. 1986, in *Ann. NY Acad. Sci.* 470, Proc. 12th Texas Rel. Astrophys. Symposium, ed. M. Livio & G. Shaviv, 267
- Woosley, S. E. 1986, in *Nucleosynthesis and Chemical Evolution*, 16th Advanced Course Swiss Society of Astrophysics and Astronomy, ed. B. Hauck, A. Maeder, & G. Meynet (Geneva: Geneva Obs.), 74
- . 1988, *ApJ*, 330, 218
- Woosley, S. E., Arnett, W. D., & Clayton, D. D. 1973, *ApJS*, 26, 231
- Woosley, S. E., & Eastman, R. E. 1995, in *Type I Supernovae*, Proc. 1993 Menorca Summer School, ed. E. Bravo, I. Ibanez, & J. Isern (Singapore: World Scientific), in press
- Woosley, S. E., Fowler, W. A., Holmes, J. A., & Zimmerman, B. A. 1978, *Atomic Data Nucl. Data Tables*, 22, 371
- Woosley, S. E., Garcia, D., Blinnikov, S., Sasorov, P., Niemeyer, J., & Hillebrandt, W. 1995, in *Proc. 17th Texas Symp. on Rel. Astrophys.*, in press
- Woosley, S. E., Hartmann, D., Hoffman, R., & Haxton, W. 1990, *ApJ*, 356, 272
- Woosley, S. E., & Haxton, W. 1988, *Nature*, 334, 45
- Woosley, S. E., & Hoffman, R. D. 1992, *ApJ*, 395, 202
- Woosley, S. E., & Howard, W. M. 1978, *ApJS*, 36, 285
- Woosley, S. E., Langer, N., & Weaver, T. A. 1993, *ApJ*, 411, 823
- . 1995, *ApJ*, 448, 315
- Woosley, S. E., Taam, R. E., & Weaver, T. A. 1986, *ApJ*, 301, 601
- Woosley, S. E., & Weaver, T. A. 1982, in *Essays in Nuclear Astrophysics*, ed. C. Barnes, D. Clayton, & D. Schramm (Cambridge: Cambridge Univ. Press), 377
- . 1986, *ARA&A*, 24, 205
- . 1988, *Phys. Rep.*, 163, 79
- . 1994, *ApJ*, 423, 371
- Woosley, S. E., Wilson, J. R., Mathews, G. J., Hoffman, R. D., & Meyer, B. S. 1994, *ApJ*, 433, 229